STM studies of ABP molecules - towards molecular latching for dangling-bond wire circuits

Dipl. Phys. Anja Nickel

Dissertation

zur Erlangung des akademischen Grades

Doktoringenieurin (Dr.-Ing.)

Erstgutachter
Prof. Dr. Gianaurelio Cuniberti
Zweitgutachter
Prof. Dr. Lukas Eng

Eingereicht am: 17.08.2015
Verteidigt am: 29.10.2015

Zusammenfassung

Das Ziel der vorliegenden Arbeit ist es ein Molekül zu finden und mittels hochauflösender Techniken zu untersuchen, das auf passivierten Halbleiteroberflächen als Schalter in atomaren Schaltkreisen wirken kann. Für diesen Zweck stehen Moleküle zur Verfügung, die aus mindestens einem aromatischen Ring und einer Ankergruppe bestehen, die kovalent auf Silizium bindet. Um einzelne Moleküle auf leitenden Substraten zu untersuchen, hat sich die Nutzung eines Tieftemperatur-Rastertunnelmikroskops (low-temperature scanning tunneling microscope, LT-STM) als geeignetes Werkzeug erwiesen. Zum Einen ist damit die topographische und spektroskopische Charakterisierung von leitenden Proben auf atomarer Ebene möglich, zum Anderen können einzelne Moleküle und Nanostrukturen hochpräzise bewegt oder elektrisch angesprochen werden.

Atomare Schaltkreise können besonders präzise auf passivierten Halbleiteroberflächen hergestellt werden. So ist es zum Beispiel möglich, eine Reihe Wasserstoffatome gezielt mit Hilfe einer STM-Spitze von der Oberfläche zu desorbieren. Durch die Überlappung der dann freien Orbitale entstehen, je nach Richtung auf der Oberfläche, atomare Drähte mit unterschiedlichen elektrischen Eigenschaften. Da die Drähte empfindlich hinsichtlich ihrer chemischen Umgebung sind, können diese auch als logische Schaltelemente verwendet werden. Dafür werden die Drähte mit einzelnen Molekülen angesteuert.

Geeignete Schaltmoleküle wurden zunächst auf der Au(111)-Oberfläche getestet. Dabei konnten grundlegende und interessante Eigenschaften von selbst-assemblierten Strukturen untersucht werden. Am Modellsystem von nicht-kovalent gebundenen 4-Acetylbiphenyl-Nanostrukturen auf Gold (111) wurde eine neue Methode entwickelt diese Molekülgruppen behutsam zu bewegen. Durch Anlegen eines Spannungspulses auf den Nanostrukturen konnten diese auf der Oberfläche über weite Strecken gezielt und ohne Beeinflussung der internen Struktur positioniert werden.

Um Moleküle für zukünftige elektronische Anwendungen zu untersuchen wurde zunächst das Verfahren zur Präparation von sauberen Siliziumoberflächen in die hier verwendeten Anlage implementiert. Es konnten reproduzierbar saubere, (2×1) rekonstruierte Si(100)-Oberflächen präpariert und charakterisiert werden.

Nach der erfolgreichen Präparation von Silizium-Oberflächen und der Entwicklung geeigneter Präparationsrezepte für das Schalter-Molekül 4-Acetylbiphenyl (ABP) wurden beide Systeme vereint. Das Molekül konnte erfolgreich auf die Silizium(100)-Oberfläche aufgebracht und die native Adsorptionskonfiguration durch das Anlegen von Spannungspulsen geändert werden. Das Schalten zwischen zwei Konfigurationen ist reproduzierbar und umkehrbar. ABP ist somit der erste umkehrbare molekulare Schalter, der jemals auf Silizium realisiert werden konnte.

Bei der Untersuchung technomimetischer Moleküle in Radachsen-Form konnte bisher die

Rollbewegung nur anhand der Analyse der Manipulationskurven nachvollzogen und belegt werden. In dieser Arbeit wurde das Rollen eines Nano-Radmoleküls bewiesen. Dazu wurde bei der Synthese in einem Teil der Subphthalocyanin-Räder eine Markierung in Form eines Stickstoffatoms gesetzt. Bei der lateralen Manipulation der Räder auf Gold(111) konnte dann durch Vergleich der STM-Bilder die Markierung verfolgt und darauf geschlossen werden, ob das Rad gerollt oder verschoben wurde.

Abstract

The aim of this thesis is the investigation of switching properties of single organic molecules, which can be used as molecular latches on a passivated silicon surface. Suitable molecules should be composed of an anchor group that can bind covalently to the silicon surface as well as an aromatic ring for the latching effect. For the imaging as well as the manipulation of single molecules on conductive substrates, a low-temperature scanning tunneling microscope, LT-STM, is a versatile and powerful tool. On the one hand, STM provides topographical and spectroscopic characterization of single molecules on conductive surfaces at the atomic level. On the other hand, under the tip of a STM single molecules and nanostructures can be moved with atomic precision or can be addressed by voltage pulses.

Moreover, by STM it is possible to build atomic-scale circuits on passivated semiconducting surfaces as silicon (100). The STM tip is used to extract single hydrogen atoms from the surface to built atomic wires. As the orbitals of the depassivated dangling bonds of the silicon surface overlap differently depending on the direction of the wire in reference to the surface reconstruction, the electrical properties of the wires differ. Moreover, the properties of the wires vary depending on the chemical environment. Taking advantage of these characteristics, the atomic wires can be used as atomic-scale logic elements. However, to bring the input signal to a single logic element, latches are required to controllably passivate and depassivate single dangling-bond pairs.

During preliminary studies on possible molecular latches, interesting experiments could be performed on 4-acetylbiphenyl (ABP) on Au(111). The molecules self assemble in non-covalently bond groups of three or four molecules. These groups can be moved controllably by applying voltage pulses on top of the supramolecular structure. The manipulation is possible over long ranges and without losing the internal structure of the assemblies.

For the investigation of promising candidates for future molecular electronics on silicon, a preparation procedure tailored to the used UHV machine was developed. During this process, clean (2×1) reconstructed Si(100) surfaces could be prepared reproducibly and were characterized by means of STM imaging and spectroscopy.

Switches are essential for electronic circuitry, on macroscopic as well as microscopic level. For the implementation of molecular devices on silicon, ABP is a promising candidate for a latch. In this thesis, ABP was successfully deposited on Si(100) and was switched by applying voltage pulses on top of the molecule. Two stable conformations were found and switching was realized reproducibly and reversibly.

In the last part of this work, the rolling of a double-wheel technomimetic molecule was demonstrated. This thesis shows the rolling of a nanowheel on Au(111) as opposed to pushing, pulling or sliding. For this, the subphthalocyanine wheels were tagged by nitrogen during their synthesis. As this tag has different electronic properties than the rest of the

wheel, it can be monitored in the STM images. By comparing the images before and after the manipulation the position of the tag proves the actual rolling.

Selbstständigkeitserklärung

Hiermit versichere ich, dass ich die vorliegende Arbeit ohne unzulässige Hilfe Dritter und ohne Benutzung anderer als der angegebenen Hilfsmittel angefertigt habe. Die aus fremden Quellen direkt oder indirekt übernommenen Gedanken sind als solche kenntlich gemacht. Bei der Auswahl und Auswertung des Materials sowie der Herstellung des Manuskipts habe ich Unterstützung von folgenden Personen erhalten:

Prof. Dr. G. Cuniberti

PD Dr. F. Moresco

Dr. R. Ohmann

Dr. F. Nickel

Dipl. Phys. J. Meyer

M. Sc. J. Krüger

Weitere Personen waren an der geistigen Herstellung der vorliegenden Arbeit nicht beteiligt. Insbesondere habe ich nicht die Hilfe eines kommerziellen Promotionsberaters in Anspruch genommen. Dritte haben von mir keine geldwerten Leistungen für Arbeiten erhalten, die im Zusammenhang mit dem Inhalt der vorgelegten Dissertation stehen.

Die Arbeit wurde bisher weder im Inland noch im Ausland in gleicher oder ähnlicher Form einer anderen Prüfungsbehörde vorgelegt und ist auch noch nicht veröffentlicht worden.

Die Promotionsordnung der Fakultät Maschinenwesen der Technischen Universität Dresden erkenne ich an.

Dresden, 17.08.2015

Dipl. Phys. Anja Nickel

Contents

Contents

1 Introduction

With the ongoing miniaturization, the semiconductor industry is reaching a fundamental scaling limit for complementary metal-oxide semiconductor (CMOS) devices. Some problems, among others, are due to physical issues as leakage between devices or between the interconnects, source-drain resistance and muon-induced errors, or thermodynamic issues like the limited switching energy in today's transistors [1, 2]. The decrease of the lateral feature size (e.g. gate length) down to sub-nanometer scale will, moreover, challenge design rules and technologies used for fabrication. Therefore, new approaches and solutions are needed to allow a growing density of devices in information technology, most probably by stretching the boundaries beyond conventional electronics. Possible solutions can be optical computing, where photons and photonic crystals are used instead of electrons and semiconductors [3], or quantum computing, where calculations no longer follow the binary codex but are based on quantum mechanical phenomena [4].

While complex issues as the physical support and connectivity are already realized in present integrated circuits, it would be an attractive solution to further develop the existing semiconductor platform to accommodate new hybrid organic molecule-silicon devices.

As it was proposed in 1974 in the seminal work of Aviram and Ratner, single molecules can perform basic functions of digital electronics like rectification [5], amplification or storage. Based on this idea, the field of molecular electronics was developed, where molecular films like self-assembled monolayers (SAM) [6, 7] or single molecules [8–10] can be used as electronic devices. The monomolecular approach describes how elementary functions and interconnections can be integrated within one molecule. For the experimental realization of such molecular-scale devices, single-molecule manipulation as well as atomic-scale characterization are of essential importance. The atomic resolution of scanning probe techniques (SPM), namely scanning tunneling microscopy (STM) and atomic force microscopy (AFM), allow a surface to be imaged with picometer resolution and to understand the electronic behavior of a single molecule by contacting it individually with the tip.

Within the last decade, innovative techniques widened the field of molecular devices by improving spectroscopic measurements and tip modifications. One example is the identification of the local chemical composition of an alloy surface by dynamic force microscopy [11]. With this procedure chemical identification of single atoms was enabled. Another example is the sub-molecular resolution of organic molecules by modifying the SPM tip with a CO molecule [12, 13]. This atomically well-defined tip termination allows both the observation of the chemical structure of a molecule when applied to the tip of a non-contact AFM and the high-resolution imaging of the highest occupied molecular orbital (HOMO) and lowest unoccupied molecular orbital (LUMO) of a molecule when applied to a STM tip.

The ability of SPM to contact single molecules with the tip as an electrode on the one

side and the substrate as the second electrode allows also to experimentally measure the molecular conductance. Other methods for conductance measurements, like break junction experiments [14], provide statistical information on the conductance [15]. The tunneling conductance can also be measured in a controlled way by picking up single molecules from the surface with a STM tip [16]. The main problem of connecting single molecules for application to electrodes is that each contact alters the molecular characteristics [17]. Another limitation of this approach for technological application is the low transconductance of single molecular devices yielding a very low gain [18].

An alternative solution can be to create circuits on hydrogen-passivated semiconducting surfaces using dangling-bond rows as atomic wires and molecules as active elements [19]. In this case, the conductance of the surface atomic wire can be controlled by changing the position of one atom, *i. e.* one dangling bond [20].

This thesis follows this last approach. Its goal is to find a molecular latch that passivates and de-passivates the dangling bonds of a silicon surface. With a reversible chemical saturation and de-saturation of two silicon dangling bonds it should be possible to build atomic-scale logic gates [21]. To reach the ultimate goal of demonstrating a molecular latch on Si(100), 4-acetylbiphenyl (ABP) molecules were investigated in this work. This thesis is structured as described in the following:

Chapter 2 introduces dangling-bond atomic-wire circuits as well as atomic logic gates. Theoretically, the characteristics of dangling-bond wires are dependent on their orientation with respect to the surface reconstruction. Wires parallel to the reconstruction rows have metal-like features and could act as atomic-scale interconnects. On the contrary, wires perpendicular to the reconstruction are strongly dependent on their chemical surroundings and could therefore act as atomic-scale logic gates. The chapter proposes a possible concept to built atomic-wire circuits and also how to connect them to the macroscopic world.

Chapter 3 gives an introduction to the theoretical background of scanning tunneling microscopy and spectroscopy. Moreover, the possible modes of lateral manipulation are defined. This comprises both classical manipulation using direct tip molecule interaction and current and field induced manipulation.

Chapter 4 specifies the ultra-high vacuum chamber and STM unit. Furthermore, the typical metal sample preparation is described. There is also a description of the used molecular evaporator.

In Chapter 5 preliminary experiments on Au(111) are presented. A novel method to manipulate non-covalently bonded molecular assemblies is shown. The model system of ABP on Au(111) was used here to demonstrate voltage pulse induced positioning of nanostructures. The molecules assemble in groups of three or four molecules forming different shaped groups. These groups move during a voltage pulse on top of one of the molecules away from the tip apex or towards the tip apex depending on the polarity of the voltage. Using positive voltages, the structures can be moved over large distances while following the tip. The movement is explained by spectroscopic analysis as well as statistical evaluation of rate and yield dependency.

Chapter 6 describes the development of a preparation procedure to obtain clean (2×1) reconstructed Si(100) surfaces. The cleaning procedure is necessary to perform controlled switching experiments and is therefore described in detail. The characterization of the Si(100) surface is completed by STM imaging and spectroscopy.

In Chapter 7 the realization of the first bifunctional molecular switch on Si(100) is presented. This switch is composed of one ABP molecule on Si(100) anchored by the acetyl unit. By applying voltage pulses on top of the molecule, it changes its conformation by breaking or forming the bond between one of the phenyl rings and the substrate.

Chapter 8 shows a different path for molecular-scale devices, namely the design of mechanical molecular machines, by proving the rolling of double-wheel molecules on Au(111). The nanowheels consist of two subphthalocyanine, bowl-shaped wheels linked by an alkyne axis. Each wheel is tagged during the synthesis by a nitrogen atom, which can be followed during STM imaging. In this way, it is possible to precisely follow the rotation of the single wheels. This is the major advantage of this molecule in comparison to earlier experiments, where the regime of movement had to be extracted solely from the manipulation curves.

Chapter 9 summarizes the work done within this thesis. It also gives an outlook for future experiments and developments.
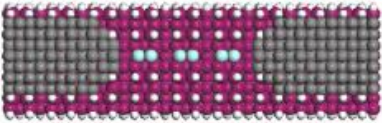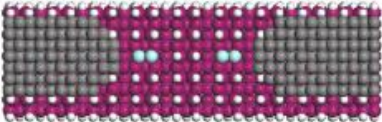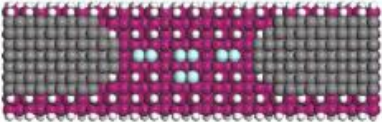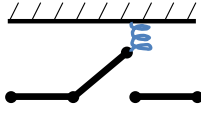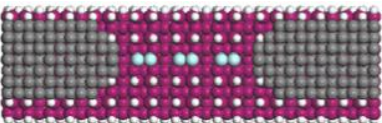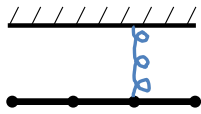
2 Dangling-bond atomic circuits

One alternative possibility to break the physical limitations of today's integrated circuits based on silicon is to follow bottom-up approaches by building atomic wires, switches, and logic gates atom by atom on hydrogen-terminated semiconducting surfaces. The idea is to manipulate single atoms on a surface by STM to form a conductive line, *i.e.* a wire. By changing the position of one or a few atoms along the wire, it is possible to change the conductance of the whole wire [22]. Therefore, the position of a few atoms can define the ON and the OFF state of a switch. Such atomic-scale circuits can be implemented fully planar and are expected to have a very fast intrinsic operating speed [20, 23].

2.1 Dangling-bond wires

A way to construct a single-atomic wire can be the alignment of single-atom dangling bonds (DB) on a passivated semiconducting or insulating surface. Experimentally, DB wires have been shown on hydrogen-terminated surfaces like Si(100)(2×1) [24–26] or germanium [27] as well as on semiconductors as MoS_2 [28]. Theoretically, DB wires can also be built on diamond [29]. To fabricate such a wire on hydrogen-passivated surfaces, single hydrogen atoms are extracted from the surface by applying voltage pulses using a STM tip. Due to their technical relevance, the protocols for the DB wire construction on Si(100)(2×1)-H are elaborated both for the fabrication of wires parallel and perpendicular to the reconstruction [24].

The electronic properties of DB wires are theoretically thoroughly investigated [22, 30, 31]. When Si surface atoms are de-passivated, the electronic DB states are introduced within the valence-conduction surface band gap. This means that a long line of DBs creates a conducting wire with states at the FERMI level. Density functional theory (DFT) calculations show a strong dependence of the electronic properties of the wires on their direction with respect to the surface reconstruction (see Fig. 6.3 in Chapter 6). The electronic states of DB wires parallel to the dimer rows are strongly localized around the DBs, while in wires perpendicular to the reconstruction they are much more delocalized [32]. Because of the constant overlap of the DB states within the DB wire parallel to the reconstruction, there are conduction channels at the FERMI energy. The dispersion of the DB band of the parallel wire is large, allowing an effective electron transport and a one-dimensional metallic character. On the contrary, DB wires perpendicular to the surface reconstruction contain two DB per unit cell where the intra-dimer overlap is large and the inter-dimer overlap is rather small. This leads to two bands within the surface band gap of Si(100)(2×1)-H originated from this DB direction. The dispersion between these two bands is smaller than the one of the parallel

	IN	OUT	Atomic structure	Classical structure
Inverter	0	ON	(a)	
	1	OFF	(b)	
Follower	0	OFF	(c)	
	1	ON	(d)	

Si   Si with DB   Au   H   Add two H atoms

Figure 2.1 – The table shows the atomic structures of two possible atomic switches, namely an inverter and a follower, created on Si(100)(2×1)-H as well as the classical equivalent of an electro-mechanical spring switch for each case. (a)+(b) By adding two hydrogen atoms to the central dimer in (a), leading to structure (b), a logic "1" input is encoded, giving an inverter switch. The classical structure shows that the circuit is closed ("ON") when the logic input is "0" (a) and open ("OFF") when the logic input is "1", corresponding to an inverter. (c)+(d) By adding two hydrogen atoms to the sidewise dimer of the "0" state (c) also a logic "1" is encoded (d). But in this case the circuit is switched from an "OFF" position to an "ON" position, corresponding to a follower. In the classical device this matches an open latch in the "OFF" state, which pulls on the spring of the elctro-mechanical switch to get in "ON" state. Taken from [21].

wires, because the inter-dimer coupling is small [22].

Parallel wires not only have a quasi one-dimensional metallic character, but they are also not influenced by local surface changes, as the conduction happens mainly trough p_y subsurface states and p_z surface states. This makes them suitable candidates for surface atomic scale interconnections [22].

2.2 Dangling-bond logic gates

Dangling-bond wires perpendicular to the dimer rows of the Si(100)(2×1) reconstruction show a large dependence on local surface changes [22]. The conductance changes drastically and abruptly by altering the position of a few atoms and the wire can therefore act as an atomic switch.

To build an atomic switch out of an atomic wire, it is crucial to know which atomic positions need to be changed in order to encode an ON or an OFF. It is also essential to understand

where to put metallic pads for the switch control in order to minimize the surface leakage current and to optimize the wire conductance. As a ballistic electron transport through the atomic device is preferred, the mean free path of an electron in silicon should be at least by an order of magnitude larger than the device, leading to a maximum lateral size of about 10 nm [33].

Starting from these general requirements, Kawai et *al.* proposed an inverter and a follower where the passivation of two DBs by hydrogen atoms encodes in each case a logical input "1" [21]. In Figure 2.1 the atomic structure of an inverter and a follower as well as the classical electrical equivalent for each switching position is shown. The inverter starts from a perpendicular DB wire consisting of three DB pairs in ON position (Figure 2.1(a)). By adding two H atoms to the central DB dimer, encoding "1", the output is switched OFF (Figure 2.1(b)). The classical structure of the electro-mechanical switch illustrates the switching from the closed to the open position.

In the case of a follower, the starting structure of the DB wire consists of three DB dimers and a dimer sideways from the central DB pair (Figure 2.1(c)). Such a DB arrangement corresponds to an open classical switch. By passivating the sideways dimer with H atoms, thus encoding a "1", the atomic switch is changed to the ON position (Figure 2.1(d)). Notice that the encoding convention can also be changed by encoding "1" with a de-passivation of DBs, meaning removing H atoms.

As the proposed switching devices can reach ON/OFF ratios of up to 2000, it is possible to build Boolean logic gates with two inputs and one output. According to KIRCHHOFFs law, an AND gate can be constructed by two consecutive followers, whereas a NAND gate can be built by two consecutive inverters [34].

2.3 Molecular latches

For the experimental realization of such switches and logic gates, a STM tip can be used to passivate and de-passivate the DB dimers. While DBs on Si(100)(2×1)-H can be created exactly and reproducible using a STM tip for de-passivation [35], the passivation is not possible in a reliable and reproducible way. However, there is an ultimate method to passivate and de-passivate two DBs, that is using aromatic molecules like benzene or biphenyl, which are known to chemisorb in so-called butterfly conformations on Si(100) [36]. For such a molecule to work as a reliable device to saturate and unsaturate DBs, additional groups need to be attached that work as an anchor for the whole molecule. In this case, the molecule will stay at its desired position, the aromatic rings can reversibly couple and decouple to the DBs, and the molecule acts as a latch quite similar to the classic case.

While it is favorable for the experimental handling to use a molecule for passivation and de-passivation of DBs, it could limit the performance of the switching device. From the theoretical point of view, it is possible that the molecule interacts with the surface DB states of the Si(100)(2×1)-H by introducing additional tunneling paths. These additional states could interfere with the states of the atomic-scale circuit and may affect the ON/OFF ratio of the device.
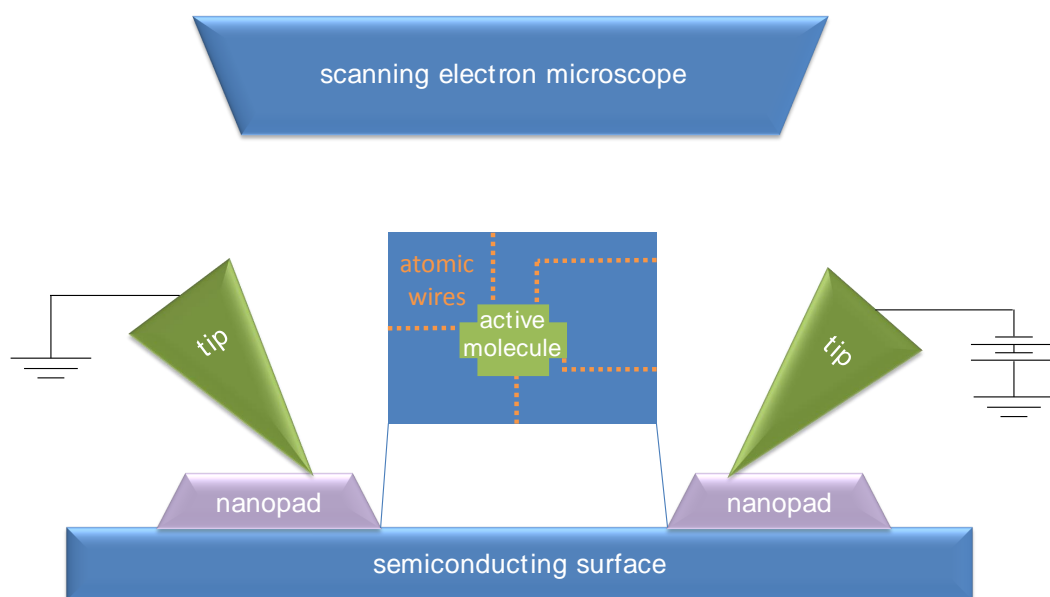
Figure 2.2 – Scheme of a typical setup of an interconnection machine for small-band gap materials. The interconnection between the atomic scale active elements (*e.g.* molecules) on a semiconducting surface follows a particular sequence of atomic wires, metallic nanopads and sharp metallic tips. For navigation of the nanopads and metallic tips, the whole setup is positioned under a scanning electron microscope.

2.4 Possible technical realization - interconnection machines

Regardless of which atomic-scale approach is followed, *e.g.* atomic-wire switch, atomic-wire molecular hybrid system, or single-molecule approach, atomic-scale mechanics and electronics require a large number of information and energy access channels with atomic precision and cleanliness. Furthermore, the circuits must be accessible from the macroscopic world. For this technological problem a multistage interconnection process was proposed by Joachim et *al.* [37].

For the interconnection process, a few flagship UHV machines were developed, which are specialized on interconnecting atomic level active elements to macroscopic contacts. Depending on the surface band gap of the supporting substrate the interconnection process varies. Here, the setup for a low-band gap material as silicon is presented.

Interconnection machines follow a particular sequence of interconnects from picometer scale to macroscopic world (see Figure 2.2):

(1) atomically clean surface with well-prepared atomic-scale circuitry and active elements (atomic scale)

(2) atomic wires of atomic-scale logic gates are connected to N metallic nanopads (nanometer scale)

(3) metallic nanopads are contacted by atomically sharp metallic tips (micrometer scale)

The whole atomic-scale production, *e.g.* atomic-scale circuitry as well as the contacting of molecules to the atomic wires (inset in Figure 2.2), can be produced using a STM. Subsequently, the sample is transferred to the interconnection machine to position the metallic nanopads as well as the atomically sharp tips on the nanopads. For navigation, a far-field microscope like a scanning electron microscope is used.

Metallic nanoclusters on surfaces can be formed by de-wetting of metallic films at elevated temperatures. As passivated semiconducting surfaces are not thermally stable, hydrogen desorbs from the silicon surface at about 400 K [38], the nanopads could be transferred to the surface by contact printing and then manipulated to contact the atomic wires. Flat nanopads can be formed by self-assembly, for example gold on MoS_2 forms triangular structures [39]. For the contacting of the nanopads, metallic nanotips can be produced from electrochemically etched tungsten tips. As the etched tips have normally radii of about 100 nm and the proposed nanopads have a lateral dimension of about 30 nm, the tips need to be sharpened, *e.g.* by an electric field-assisted technique within a field-ion microscope [40, 41].

Once all active elements are connected to micrometer scale, the sample can be electrically tested and characterized. For an out-of-vacuum use, the top-contacting of the nanopads is no longer practical. For this, a solution with backside interconnects was proposed [42]. The sample can then be capped with another wafer and transferred out of vacuum [43].

3 Scanning tunneling microscopy

In the 5th century BC in ancient Greek two philosophers, Leucippus and Democritus, developed a theory of atomism based on the idea of matter being composed entirely of various imperishable and indivisible elements, so called atoms [44]. Since then great efforts were spent that mankind may perceive whatever holds the world together. It took over 2000 years until the invention of the optical microscope by Zacharias Jansen in 1590 [44], which of course was - due to the wavelength of light - insufficient in terms of resolution to observe atoms, but paved the way for a variety of experimental real space imaging techniques existing today in coexistence. A significant milestone towards the atomic scale was reached by not imaging matter with lenses but with help of a probe scanning the surface by piezo-electric elements, a technique named Topografiner presented by Young et *al.* in the 1970s [45]. This principle was brought to perfection by IBM exploiting the tunneling effect between a specimen and a tip. This represents the invention of the scanning tunneling microscope (STM) [46], a state-of-the-art and ultra-sensitive method of measuring changes of the topography between sample and probe. Now the door to the atomic world was wide opened. The breakthrough of the technique was the atomic resolution of the long standing problem of the $(7{\times}7)$ reconstruction of the Si(111) surface [47]. This and the promise of an entirely new field for the study of the structure of matter culminated in the Nobel Prize for Gerd Binning and Heinrich Rohrer in 1986 [48].

The basic principle of a STM is shown in Figure 3.1. A sharp metallic tip is positioned a few Ångströms above the sample. When a voltage is applied between tip and sample, a current will flow caused by the tunneling of electrons through the vacuum gap. This current is amplified and then used to hold the distance z between tip and sample constant with the help of a feedback control. A piezoelectric element moves the tip over the sample in x and y direction. The signal of the tunneling current and the feedback control is measured at each point of the xy matrix and then processed and displayed with a PC.

In the beginning of STM, the direct tip-surface interaction, or tip-adsorbate interaction, was highly undesired, because it basically degraded the tip quality. However, only a few years after its invention, this interaction was used to move single particles with high precision [49]. Nowadays, not only single atoms can be manipulated, but also more complex molecules and nanostructures [50–52]. Continuing this path, a wide range of experiments and prototype applications could be achieved. A few main trends will be discussed in the following.

The possibility to manipulate single molecules on surfaces spurred the synthesis of molecules that mimic macroscopic building elements [53]. Such technomimetic molecules have been built to work as gears [54, 55], motors [56, 57] or more complex nanocars [58–60]. These molecules prove that mechanical laws are as true on the nanoscale as in the macroscopic world if the molecules are rigid enough. With the control of the nanomachines comes a better
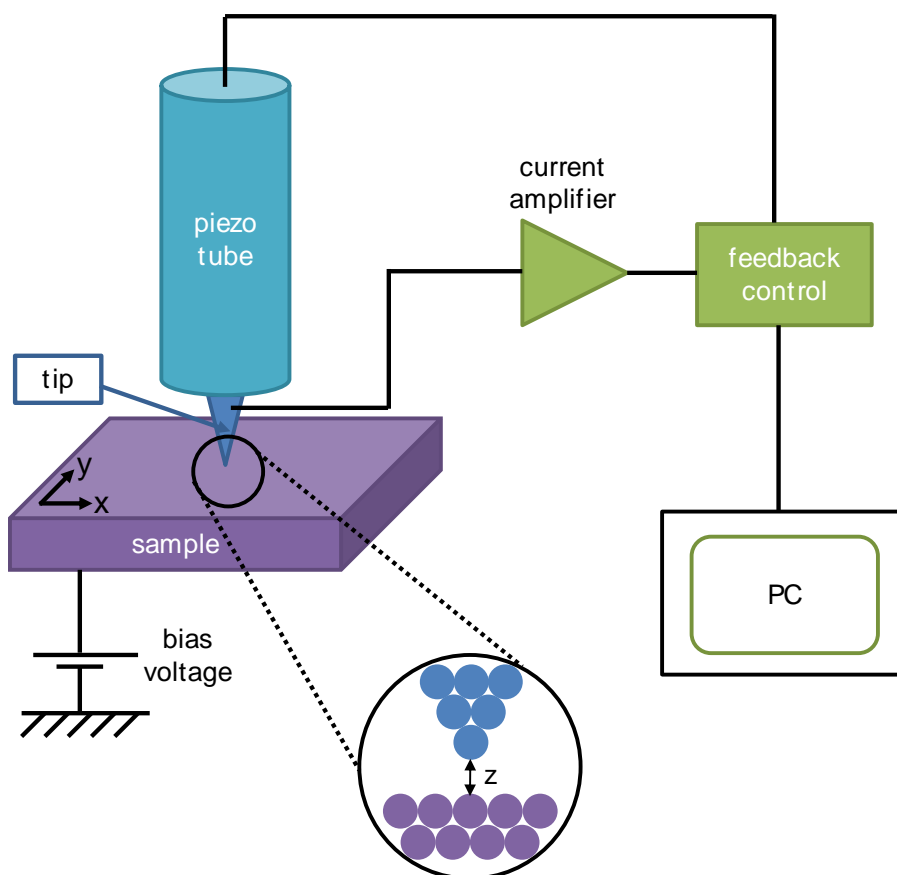
Figure 3.1 – Scheme of a STM. A sharp metallic tip is moved over the sample in a small distance z by a piezoelectric tube. When a voltage is applied between tip and sample a tunneling current will flow, which needs to be amplified. The current signal is used to keep the tip-sample distance constant by a feedback loop. A PC processes and displays the tunneling and feedback signals.

understanding for the transport of a nanocargo with the ultimate goal of enzyme-like directed assembly [60].

Another interesting field is the nanopatterning of surfaces. Next to top-down techniques like electron-beam lithography [61], the bottom-up approach of self-assembled networks is widely used. Especially on-surface synthesis of 2D molecular patterns is a strong developing field where the shape and characteristics of the network is controlled by careful selection of the precursors [62–64]. These networks are usually extended over the surface and are optimally hundreds of nanometer well ordered. Sometimes this is not favorable, especially for applications in sensor development, or nanoplasmonic devices. Here, small well-ordered structures on predefined positions are preferred. In this case, STM manipulation can help by moving small, self assembled, well ordered structures to the predestined position [65, 66].

As described, STM is since its invention an important tool for real space surface analysis. For the interpretation of the recorded images, understanding the theoretical background

of the technique is mandatory. In this chapter, the one-dimensional tunneling effect will be explained. Moreover, the theoretical principle of scanning tunneling spectroscopy and manipulation techniques, as they are needed for this work, will be illustrated.

3.1 Tunneling effect

The tunneling effect cannot be explained in classical physics with the picture of electrons being particles. It is necessary to go a step further and consider quantum mechanics. In quantum mechanics, a particle has a probability distribution expressed mathematically as a complex wave function

$$\psi(\vec{r}) = Ae^{i\vec{k}\vec{r}} \, . \tag{3.1}$$

In this equation $\vec{k}$ is the wave vector and $\vec{r}$ the position vector.

For basic understanding of the tunneling effect, it is sufficient to stay in one dimension. Therefore, a finite potential barrier with the height V_0 and a thickness d should be considered. In the classical case, a particle with an energy lower than V_0 will be reflected on the barrier. In case of quantum mechanics the particle is thought to be a wave function $\psi(z)$, which is able to penetrate and pass the potential barrier with a certain probability, so called tunneling. The probability of the wave function to tunnel through the barrier can be determined by solving the time-independent SCHRÖDINGER equation

$$\left(-\frac{\hbar^2}{2m}\frac{d^2}{dz^2} + V_0(z) \right) \psi(z) = E\psi(z) \, . \tag{3.2}$$

Here, $\hbar$ is PLANCK constant divided by 2π, m is the mass of an electron and z is the direction of propagation of the wave. Figure 3.2 illustrates the tunneling of the wave function through a finite barrier. In area I and III the wave functions of the electron correspond to plain waves.

$$\psi_I(z) = Ae^{ikz} + Be^{-ikz} \tag{3.3}$$
$$\psi_{III}(z) = Ce^{ikz} \tag{3.4}$$

with $k^2 = \frac{2mE}{\hbar^2}$ the wave number.

The first term in equation 3.3 describes the incoming plain wave, whereas the second term is due to the reflected part of the wave.

Within the barrier the wave function experiences an exponential decay given by

$$\psi_{II}(z) = De^{\kappa z} + Ee^{-\kappa z} \tag{3.5}$$

with $\kappa^2 = \frac{2m(V_0 - E)}{\hbar^2}$.

In a first approximation, the current in such a setup can be directly compared to the transmission coefficient T for the barrier, defined as the ratio between transmitted and incoming
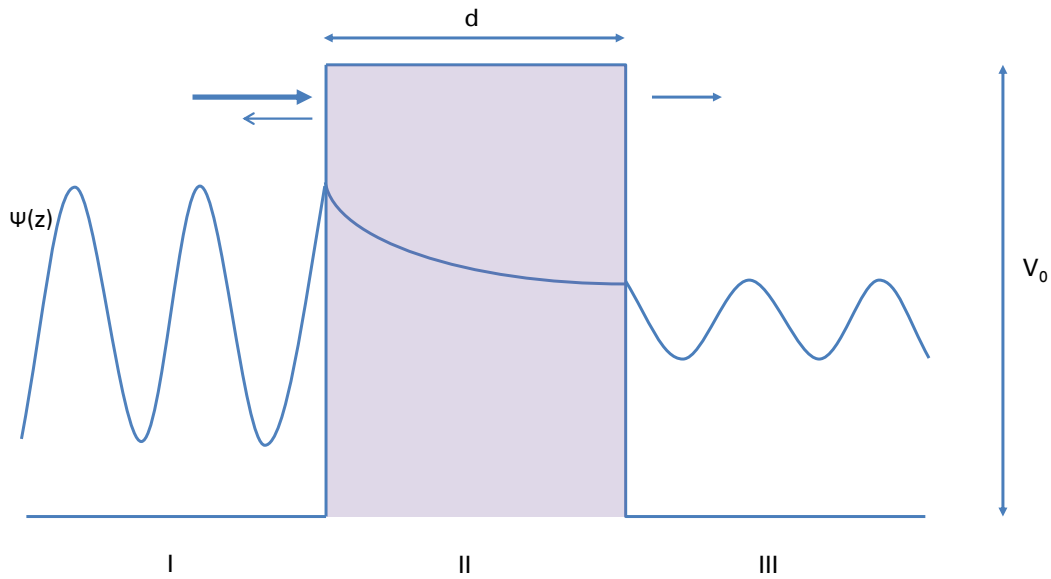
Figure 3.2 – Schematic process of quantum mechanical tunneling. The plain wave $\psi(z)$ is partially reflected when impinging on a potential barrier with height V_0 and thickness d. The other part penetrates the barrier while experiencing an exponential decay. For a not too broad potential wall the wave propagates partially through the barrier.

amplitude of the wave function.

$$T = \frac{|C|^2}{|A|^2} \tag{3.6}$$

If the barrier height is considered to be high and the barrier is not too thin ($\kappa d >> 1$) the transmission coefficient has the solution [67]

$$T = \frac{16k^2\kappa^2}{(k^2 + \kappa^2)^2} e^{-2\kappa d} \, . \tag{3.7}$$

3.2 Scanning tunneling microscopy

With the considerations of the previous section, the understanding of the high vertical and lateral resolution of a scanning tunneling microscope is straightforward.

The two sides of the potential barrier are represented by two electrodes, namely the tip and the sample. When no voltage is applied, the FERMI level of the electrodes will be equal, but the work functions are different, ϕ_T and ϕ_S, respectively (Figure 3.3). This results in an electric field depending on the difference $\phi_T - \phi_S$. The difference in case of metallic electrodes is a few electron-volt and the potential barrier is much higher than kT, with k the BOLTZMANN constant and T the temperature. A consequence of the work-function difference is that the electrons can tunnel only from the sample to the tip, or vice versa.

Nevertheless, there will be no net current unless a voltage, which is called the bias voltage, is applied between the electrodes. With typical STM parameters and equation 3.7, the
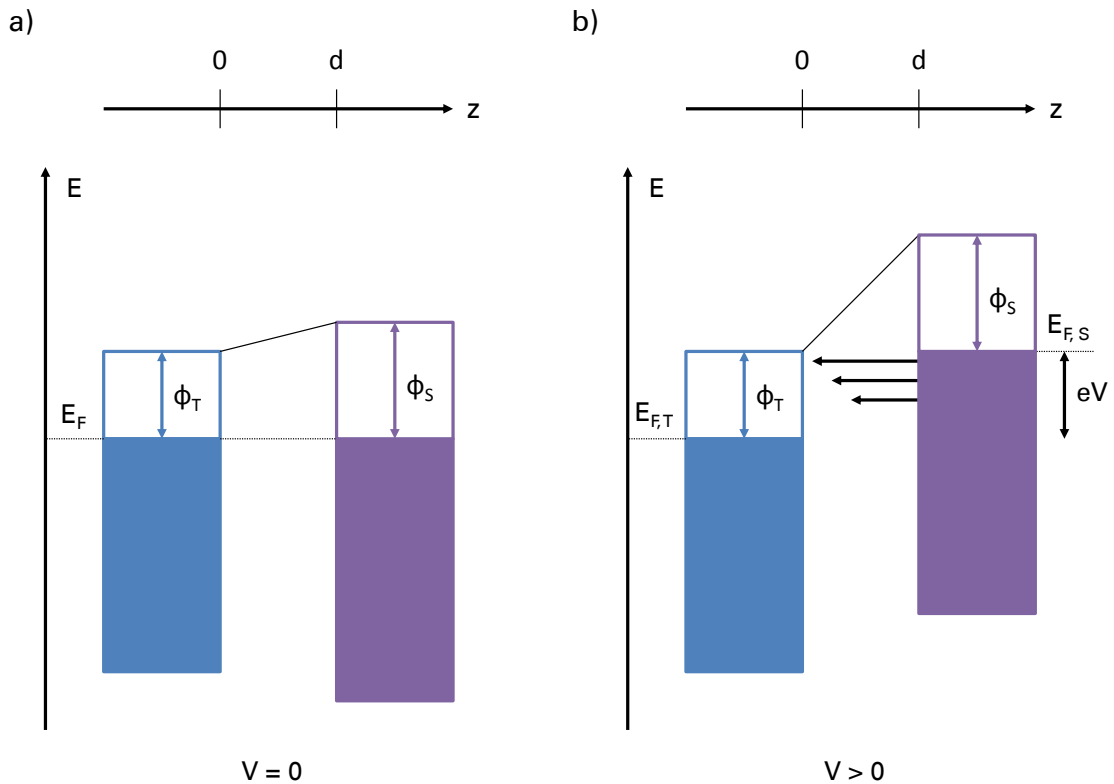
Figure 3.3 – Tunnel junction of an STM experiment. ϕ are the work functions, E_F the FERMI energies and d the distance between the electrodes. The indices T and S correspond to the tip and the sample, respectively. a) Junction without applied voltage. b) A bias voltage V is applied to the junction and a net current can flow from sample to tip. The decreasing length of the arrows indicates the exponential decay of the current with the thickness of the barrier.

sensitivity of the STM becomes apparent. With

$$\sqrt{\phi_{eff}} = \sqrt{V_0 - E} \approx 5eV \tag{3.8}$$

and d around 5 Å an increase in thickness of the barrier of about 1 Å leads to a decrease of the tunneling current of about one order of magnitude. Because the measurement of currents in the picoampere regime can be conveniently performed with modern electronics, very small changes in topography in the order of picometer can be measured.

Even with the very rough approximation of one-dimensional tunneling effect, the basic advantage of the STM could be shown. For a more realistic picture, one has to go a step further, especially for calculating tunneling currents and understanding images.

The basic ideas for solving this problem have been developed by BARDEEN [68] following the time-dependent perturbation approach for two electrodes separated by an insulating layer. In this approach, wave functions and the electronic structure of the electrodes are calculated assuming no interaction among themselves. TERSOFF and HAMANN [69] fit the theory to the system of a tip separated by a vacuum gap from the sample. For low temperatures and
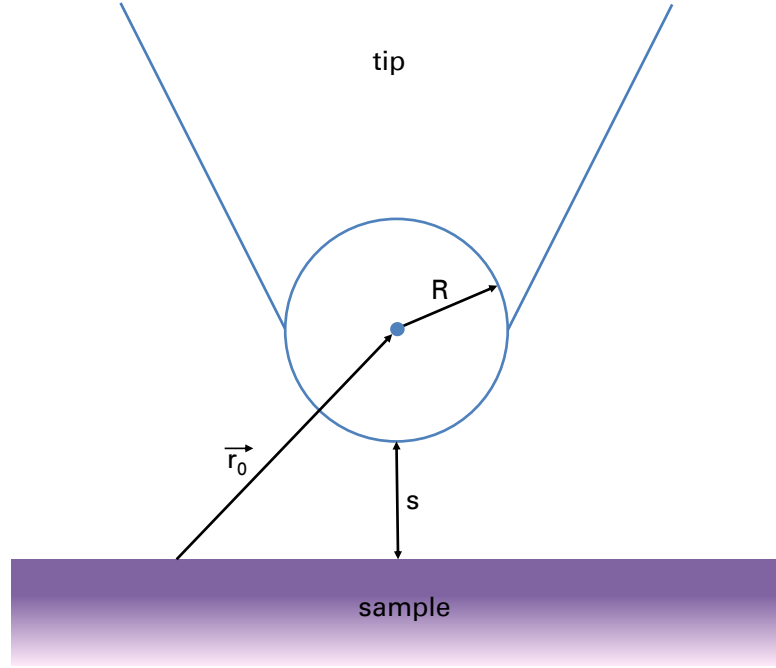
Figure 3.4 – Tip geometry as proposed by TERSOFF and HAMANN [69]. R is the radius of the spherical tip, s is the distance between sample and tip and $\vec{r}_0$ is the position of the tip.

sufficiently small voltages the tunneling current can be written as

$$I = \frac{2\pi}{\hbar} e^2 V \sum_{\tau,\sigma} |\mathbf{M}_{\tau\sigma}|^2 \delta\left(E_\tau - E_F\right)\left(E_\sigma - E_F\right) \; . \tag{3.9}$$

In this equation e is the elementary charge, V the applied bias and E_F the common FERMI level of tip and sample. The indices τ and σ indicate the tip and the sample, respectively. The δ-function shows that only elastically tunneled electrons will be counted. In order to calculate the tunneling current, the main challenge remains in solving the tunneling matrix $\mathbf{M}_{\tau\sigma}$. The latter describes the transition of the electron states ψ_σ before the tunneling in the sample to the states ψ_τ after the tunneling to the tip. According to BARDEEN, $\mathbf{M}_{\tau\sigma}$ depends on the wave functions of the electron and the energy levels of the tip and is given as

$$\mathbf{M}_{\tau\sigma} = \frac{\hbar^2}{2m} \int d\vec{S} \left(\psi_\tau^* \vec{\nabla} \psi_\sigma - \psi_\sigma \vec{\nabla} \psi_\tau^* \right) \; . \tag{3.10}$$

Experimentally, the geometrical and electronic structure of the tip electrode is unknown, due to ex-situ fabrication and changes during the measurements. This prohibits an analytical solution of equation 3.10.

TERSOFF and HAMANN provided a solution based on a simple tip geometry as sketched in Figure 3.4 [69]. At the point of measurement, the tip has a perfect spherical shape with the radius R and a distance s from the surface. The center of the sphere, which means the position of the tip, over a certain point of the sample is believed to be $\vec{r}_0$. Moreover, the tunneling process should only take part in form of s waves in the tip wave functions. Including

this assumptions equation 3.9 can be modified to

$$I \sim V \rho_T e^{2\kappa R} \sum_{\sigma} |\psi_\sigma|^2 \delta \left(E_\sigma - E_F \right) \ .$$

(3.11)

Here, ρ_T is the local density of states (LDOS) of the tip at position $\vec{r}_0$ and at the FERMI level. The sum function $\sum_{\sigma} |\psi_\sigma|^2 \delta \left(E_\sigma - E_F \right)$ is the LDOS of the sample at the FERMI level. Equation 3.11 gives rise to the assumption that maps of the surface scanned in constant-current mode equal maps of constant local density of states. As long as topographic features dominate over the electronic structure of the sample, STM images can be interpreted as topography images revealing the details of the surface structure.

This rough approximation is particularly no longer true in case of atomic resolution where the orbital character of the wave functions play an important role. A typical example is the CO molecule on metallic surfaces. As long as the tip can be considered to tunnel through s waves, the CO adsorbate seems to be a depression. When the tip is functionalized and tunneling happens trough p waves, *e.g.* with another CO molecule on the tip, the molecule seems to protrude [50]. This means, in the interpretation of STM images more parameters than just the topography play an important role. That is complicating the analysis, but opens also new possibilities of surface investigation.

More detailed theories, where the atomic form of the tip is taken into account, were developed later and are applied to simulate STM images with high precision [70].

3.3 Scanning tunneling spectroscopy

As described in the previous section, the dependence of the tunneling current on the samples local density of states is complicating the interpretation of STM images. On the other hand, this fact offers the possibility to probe the electronic characteristics of the surface with high resolution.

By transferring the LDOS of the sample into an integral, equation 3.11 yields

$$I \sim \int_0^{eV} \rho_T \left(\vec{r_0}, E - eV \right) \rho_S \left(\vec{r_0}, E \right) T \left(E, eV, d, \phi \right)$$

(3.12)

with the position of the tip over the sample surface $\vec{r}_0$ and the transmission probability T. The latter depends on the energetic states involved in the tunneling process, the applied bias voltage, the distance between tip and sample, and the height of the tunneling barrier, which is related to the work functions of tip and sample.

Consequently, the tunneling process depends, for a given energy, on three interrelated parameters: The tunneling current I, the bias voltage V , and the tip to sample distance d. In scanning tunneling spectroscopy one of the parameters is kept constant while the relation between the other two is measured. The three following modes are experimentally available:

- I-z curves, where the bias voltage is constant and the variation of the tunneling current with the tip-sample separation is measured,

- I-V curves, where the distance between tip and sample is fixed and the variation of the tunneling current with the bias is recorded, and

- V-z curves where the tunneling current is fixed and the variations in the tip-sample distance are measured as a function of bias voltage.

In I(V) spectroscopy the local density of states of the sample can be probed directly and is therefore most commonly used.

In order to calculate the LDOS with help of an experimentally determined set of tunneling current vs. voltage data points, equation 3.12 has to be differentiated with respect to the bias voltage:

$$
\begin{aligned}
\frac{dI}{dV} \sim\ & \rho_T(0)\rho_S(eV)T\left(E, eV, d, \phi\right) \\
& + \int_0^{eV} \rho_T(E - eV)\rho_S(E)\frac{dT\left(E, eV, d, \phi\right)}{dV}dE \\
& + \int_0^{eV} \rho_S(E)\frac{d\rho_T(e - eV)}{dV}T\left(E, eV, d, \phi\right)dE \ .
\end{aligned}
\tag{3.13}
$$

Assuming the density of states of the tip to be constant during the measurement procedure, as well as the transmission coefficient to be constant in the voltage regime, equation 3.13 can then be written as

$$
\frac{dI}{dV} \sim \rho_T(0)\rho_S(eV)T\left(E, eV, d, \phi\right) \ .
\tag{3.14}
$$

This relation serves as a sufficient approximation to experimentally determine the density of states of the surface at an energy eV.

For experimental realization, different methods can be used to obtain dI/dV spectra. The simplest way is to place the tip on a desired position over the surface and switch off the feedback circuit to hold the distance between tip and sample constant. Then the voltage is ramped over the wanted range and the tunneling current is recorded. The I-V curves are afterwards differentiated numerically.

It is also possible to detect the dI/dV signal directly by using a lock-in amplifier. A sinusoidal voltage modulation, $V_0 \sin(\omega t)$, is superimposed between tip and sample resulting in an in-phase current modulation, which is also detected by the lock-in. If the modulation signal is small, as in the experiments performed in this work, the modulated current can be developed in a FOURIER series on the applied modulation frequency ω

$$
\begin{aligned}
I(V_{Bias}, t) =\ & I(V_{Bias}) + \frac{dI(V_{Bias})}{dV}V_{mod}\sin(\omega t) \\
& + \frac{d^2I(V_{Bias})}{dV^2}\frac{V_{mod}^2}{4}\sin(2\omega t) + \cdots \ .
\end{aligned}
\tag{3.15}
$$

Thus, the first harmonic is proportional to the wanted dI/dV signal and is recorded by lock-in detection.

In comparison with other surface spectroscopic techniques at the FERMI level, like ultra-violet photoelectron spectroscopy, scanning tunneling spectroscopy has the highest spatial resolu-

tion. No other surface technique can probe the density of states of predefined adsorption sites or molecular binding sites. Next to the probing of the LDOS on one point, the spatial distribution of the states can also be measured in a 2D map during constant-current imaging.

3.4 Modes of manipulation

When surfaces and adsorbates are imaged, the direct interaction of the tip and the sample should be avoided. Moreover, for comparison of spectra it is highly recommended to keep the tip states comparable. In the beginning of STM experiments, it was soon realized that it is possible to make use of the tip-surface interaction to manipulate ensembles of atoms and molecules yielding complex nanostructures [49, 71].

Generally, it can be distinguished between lateral and vertical manipulation. In the latter case, the adsorbate is picked up from the surface. Then the tip is moved to the desired place and the adsorbate is released. As this mode changes the tip modification dramatically, it is used less often. An alternative method without influencing the tip is transferring the adsorbate by lateral manipulation, where the adsorbate is moved by the tip without losing the contact to the surface. In both cases the underlying mechanisms for moving the adsorbates are either atomic forces, the electric field or the tunneling current between tip and sample.

In all cases the mechanism has to be strong enough to overcome the hopping barrier of the particle to the next adsorption side on the surface. The force will be maximal in the immediate vicinity of the tip apex as described in the previous section. Moreover, for a controlled manipulation thermal diffusion has to be kept at minimum. Therefore, low sample temperatures below 10 K are necessary.

As in this work sensible molecules and molecular structures should be moved, only lateral manipulation is used, because of the less extensive interaction. This technique will be explained in detail in this section.

3.4.1 Lateral manipulation using atomic forces

In order to manipulate single adsorbates using lateral manipulation, short range forces between tip and sample are necessary [72]. In most cases this will be van-der-Waals forces. These can be attractive or repulsive resulting in different manipulation modes. In all cases, for the manipulation the distance between the tip and the adsorbate is varied in order to tune the force. Typical distances are between 3 Å and 5 Å. The standard procedure includes moving the tip to the desired particle in imaging distance (about 10 Å), then decrease the distance and move the tip with the adsorbate to the desired place and subsequently increase the distance to lose contact. During the process the tip height is recorded. From this curves, different modes of manipulation can be deflected.

The different modes and corresponding curves are illustrated in Figure 3.5 [50]. In the pushing scenario, repulsive forces are used to push the adsorbate in front of the tip across the surface. The tip is moved over the adparticle until a threshold is reached which induces hoping of the adsorbate away from the tip. In this moment the tip height decreases, before it increases again and the process is repeated. Most of the times, a jumping distance that
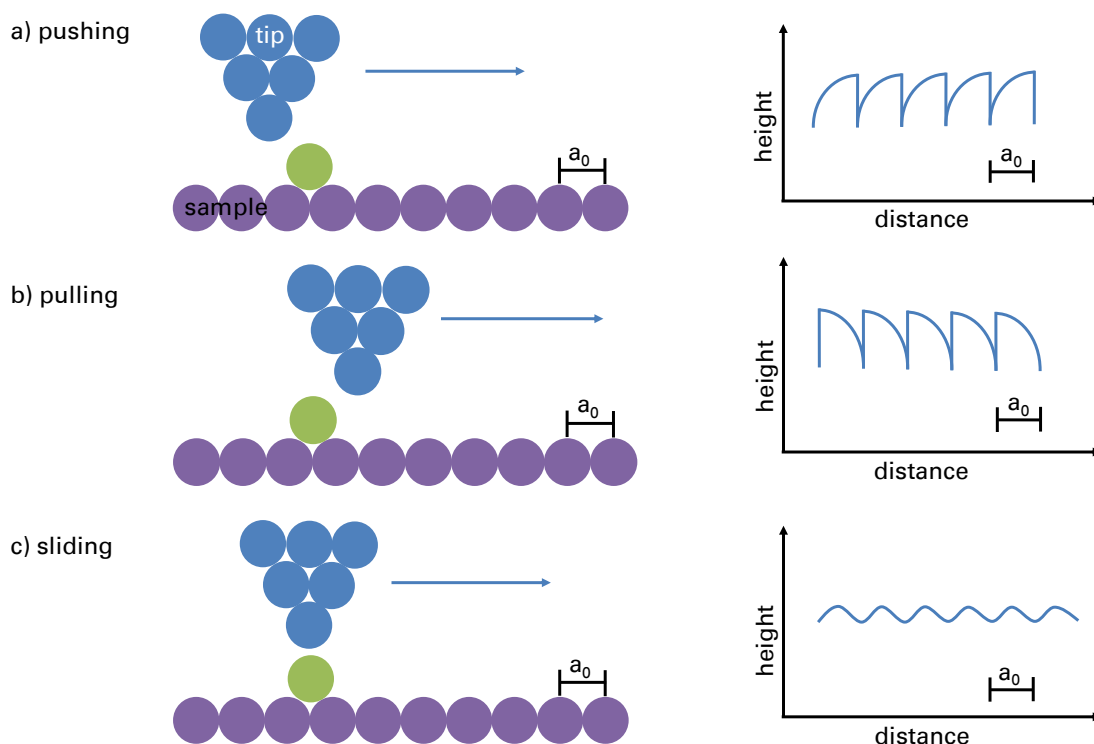
Figure 3.5 – Three modes of lateral manipulation using atomic forces. a) pushing, b) pulling, and c) sliding. The arrows indicate the manipulation direction. On the right side the corresponding tip-height traces for the different modes are sketched.

corresponds to the lattice parameter a_0 can be observed. This can be explained by the lattice symmetry of the surface. Within one lattice constant an energetically equivalent adsorption site can be found.

The pulling and sliding scenario make use of attractive forces between tip and adsorbate to perform the manipulation. In the pulling mode the adparticle jumps to the tip, which is why the tip height increases. When the tip is moved further the height decreases until a threshold is reached and the adsorbate jumps below the tip increasing the height again.

In the sliding mode adsorbates are moved continuously across the surface. To achieve this mode the force between tip and adparticle has to be significantly higher than in the pulling mode. The adsorbate can stays under the tip and does not jump to the energetically favored positions on the surface. The corrugation in the corresponding tip-height trace is due to the atoms on the surface.

3.4.2 Lateral manipulation using field or current

In the manipulation modes described in the previous subsection, the interaction of the tip and the adsorbate is high. This can cause problems when the adparticle is sensitive like in case of hydrogen-bond groups of molecules or when a conformational change should be achieved. The molecular structures can be destroyed or changed due to the strong tip interaction. In these cases, it is more convenient or necessary to use other techniques.
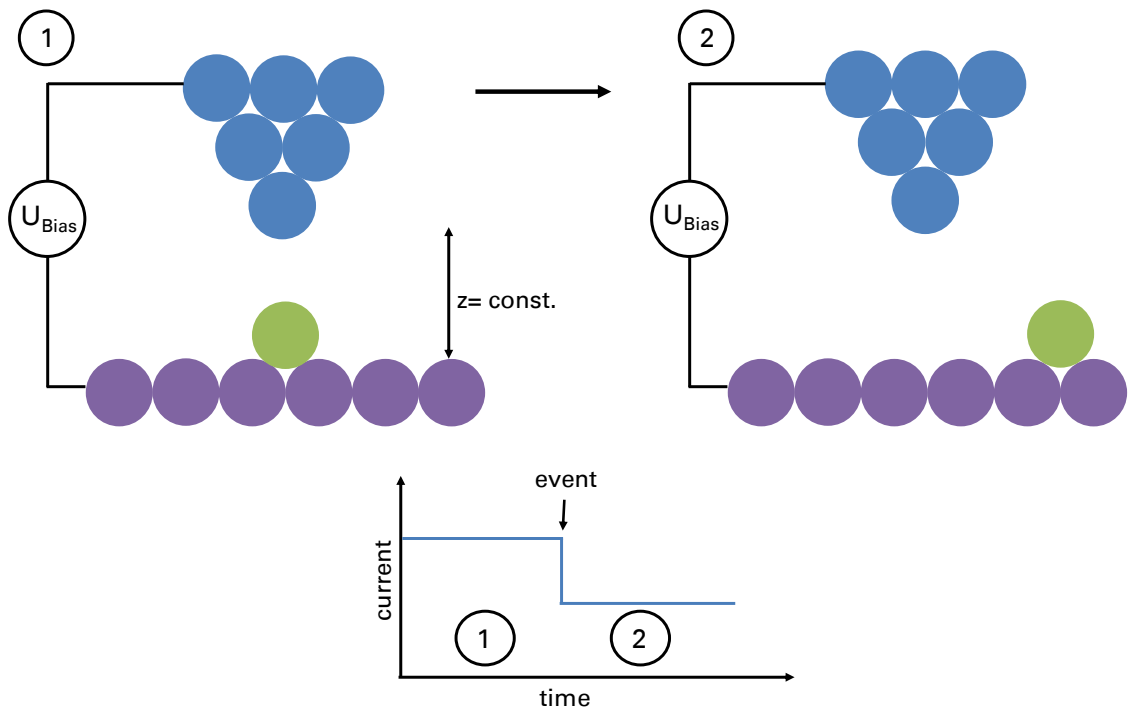
Figure 3.6 – Schematic process of field induced manipulation. During the manipulation the field is held constant. There is a successful event, when a jump in the current trace occurs.

If the adsorbate is charged, electric-field assisted diffusion is possible. Fields of 10^7 V/cm and higher are needed to overcome the diffusion barriers of the adparticles depending on their size. A scheme of the process is shown in Figure 3.6. The tip apex is brought over the adsorbate and the bias voltage is increased, whereas the height is held constant. The tunneling current is recorded during the procedure. If the manipulation is possible and the field is high enough, a jump in the tunneling current will occur. In the manipulation experiment illustrated in Figure 3.6 the decreased current shows that the adsorbate jumped away from the tip.

An optional method is the manipulation of a particle with high tunneling currents. In this scenario the current is held constant, and the tip height is recorded. Again, a sudden jump in the tip height will show a successful manipulation event.

The underlying process cannot be explained with the elastic tunneling of electrons from the tip to the sample, where the electrons do not lose energy. In fact, if the bias voltage eU is higher than a phonon resonance $h\nu$, the tunneling electrons can lose energy to this resonance. This is called inelastic tunneling (IET). Usually, the current originated from the elastic tunneling dominates the inelastic current by a few orders of magnitude. However, the rather small fraction of electrons is enough to excite states in the adparticle. The IET current is caused mainly by two mechanisms, namely dipole coupling and resonance coupling [73]. In the first case, the electric field of the tunneling electrons couples to a dipole moment of the adsorbate via COULOMB interaction. In case of resonance coupling, the tunneling

electrons are trapped for a traversal time within a resonance of the adsorbate. In this time, the adparticle will be in a vibrational excited state and thus be easier to move than in ground state. More often, the energy transfer from one single electron will not be enough to overcome the diffusion or potential barrier (hopping) of the adsorbate [74]. The movement can be achieved anyhow, if the energy quanta are summed up. This effect is called vibrationally assisted ladder climbing [75].

4 Experimental methods

The principle of scanning tunneling microscopy described in chapter 3 is a well understood and established technique in the field of nanotechnology. In this chapter, the particular microscope used in this work is specified, as well as sample preparation methods and routines.

4.1 Scanning tunneling microscope and vacuum system

The experiments performed in this thesis were carried out in a low-temperature microscope by SPS CreaTec GmbH operated at 5 K. A technical drawing is shown in Figure 4.1. The base pressure of the ultra-high vacuum system is below $7 \cdot 10^{-11}$ mbar.
The main parts of the three-chamber vacuum system are the load lock, the preparation chamber and the microscopy chamber (see Figure 4.2). The chambers are separated by all-metal valves and the samples or the evaporator can be transferred by a transfer stick or the manipulator. The main features of the chambers are the following:

- The load lock acts as a gate for the samples into the vacuum. Since it is bakeable to 120°C and equipped with a turbo molecular pump, it guarantees a fast and clean sample entry.

- In the preparation chamber, which is pumped by a combined ion-getter pump and titan-sublimation pump, standard preparation tools like a sputter gun and evaporation units can be found next to analysis tools like a mass spectrometer and a quartz microbalance. For sample heating, the sample is mounted on a ceramic bottom heater. The contacts can be applied by counter contacts on the manipulator. The sample can also be cooled by a flow-through cryostat included in the manipulator. This is necessary to avoid overheating of the sample holder during high-temperature preparations or to pre-cool the sample when it is transferred to the microscope.

- The microscopy chamber contains the microscope with the two cooling shields and the liquid-helium bath cryostat.

In the used microscopy system, the sample stays fixed in a so-called Besocke beetle-type measuring unit and only the tip is moved [76]. The basic components are shown in Figure 4.3. The rough movement in z direction is achieved by rotating the ramp (Figure 4.3(b)) with the tip by bending the piezoelectric tubes in the so-called slip-slide mode. When the sample is scanned during the measurement the tip is solely moved by the z piezo in z direction whereas the x-y direction is achieved by moving the ramp. By splitting the movement in z
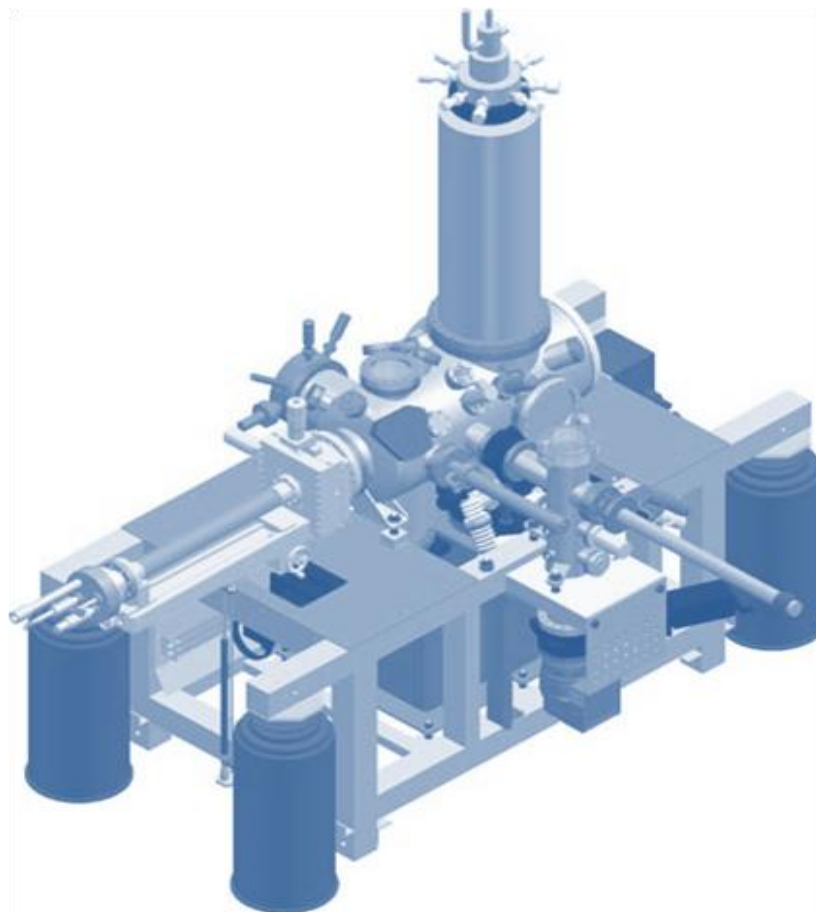
Figure 4.1 – Technical drawing of the UHV system that houses the STM. Prominent features are the cryostat for the liquid gases as well as the four dampers for vibration isolation.
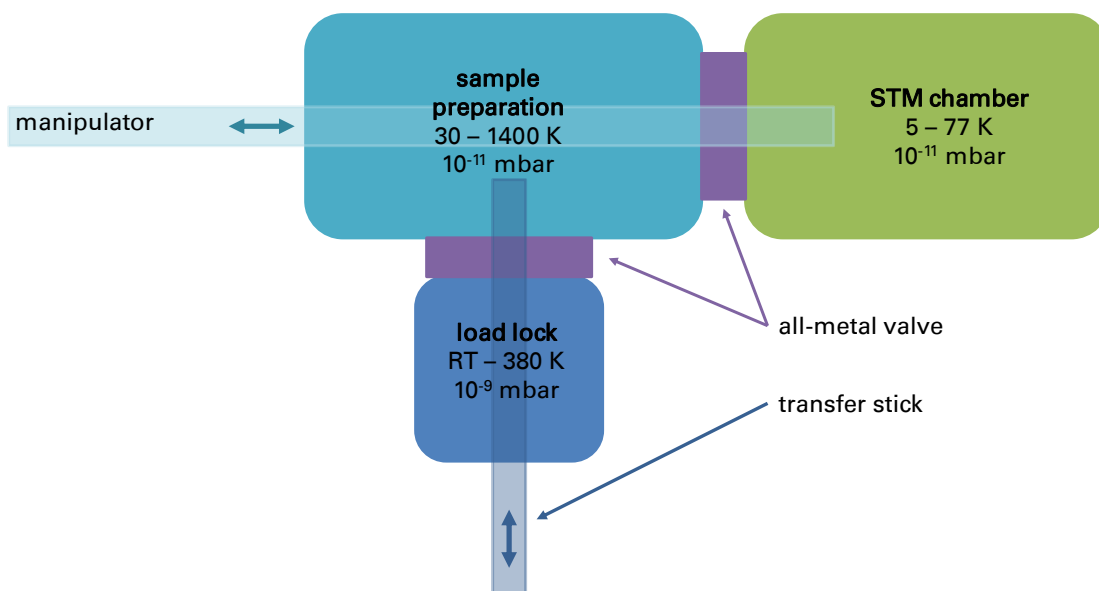

Figure 4.2 – Scheme of the ultra-high vacuum system. All sections can be locked by all-metal valves. The sample can be transferred by a transfer stick and the multi-purpose manipulator to access preparation tools and measurement positions.
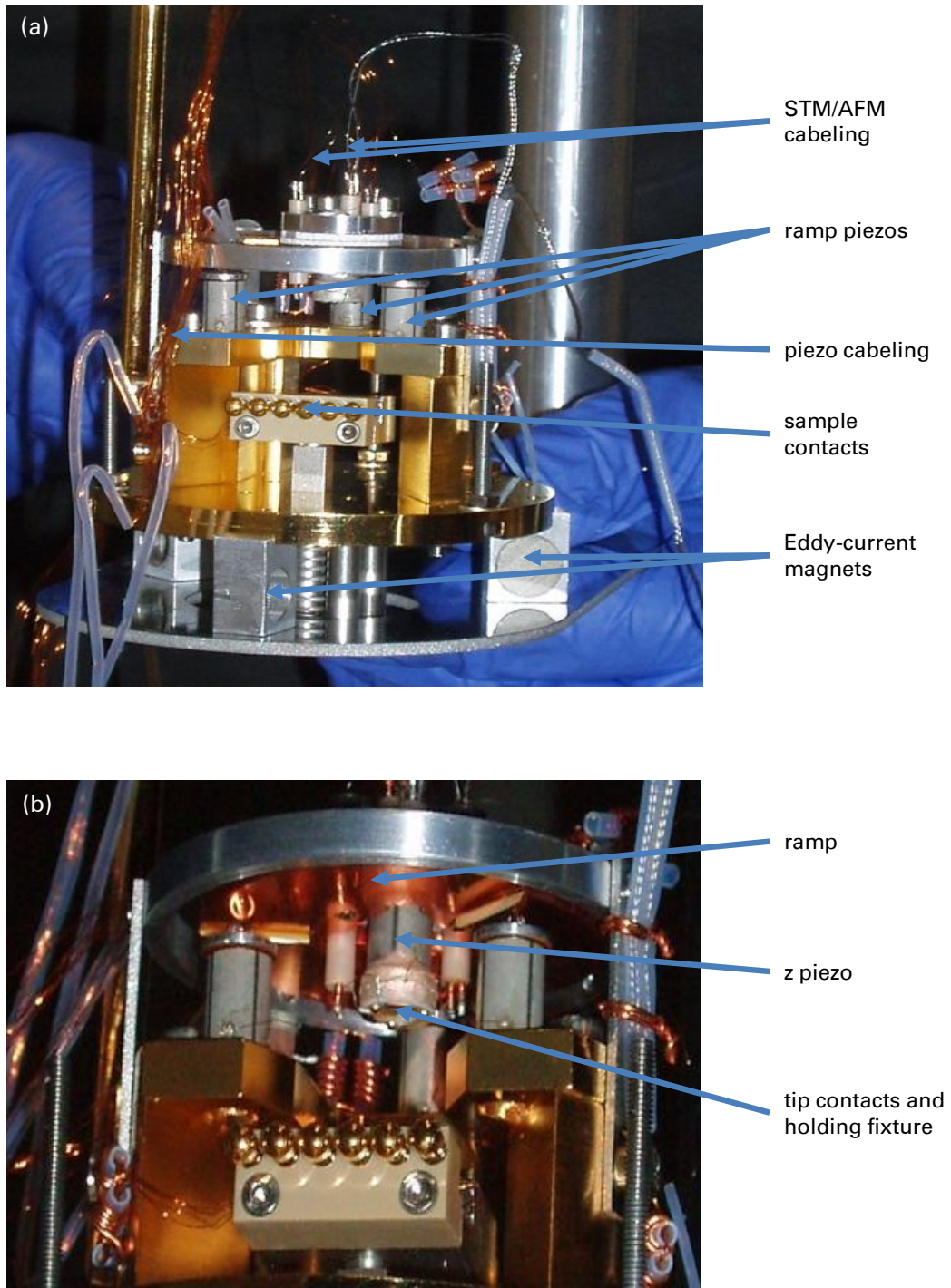
Figure 4.3 – Besocke-type scanner of the microscope. (a) Whole scanner head including Eddy-current damping system. (b) Zoom-in of the z piezo and tip contacts.
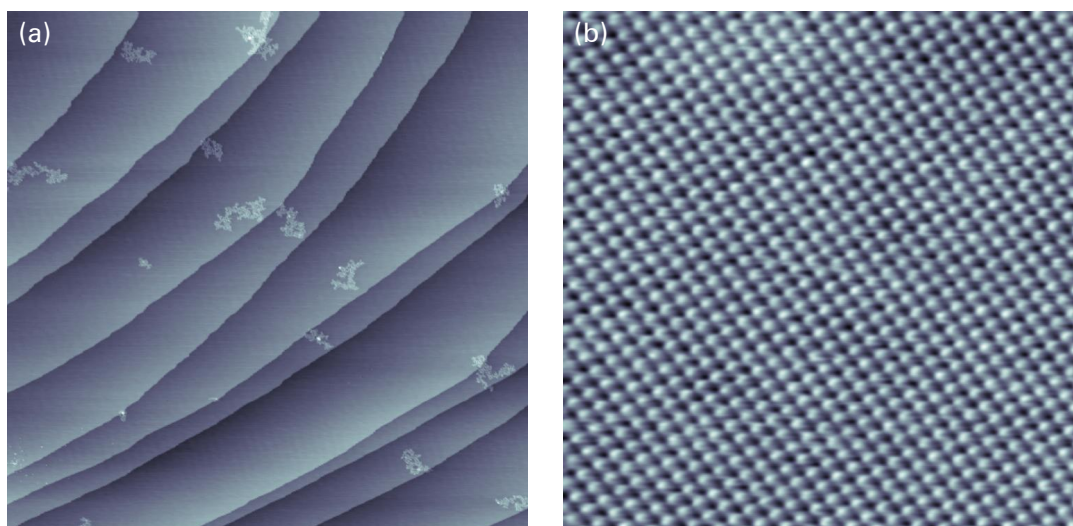
Figure 4.4 – Image of the Ag(100) surface topography to test the performance of the low-temperature STM at 77 K. (a) Overview image. $V_{sample} = 1.14$ V, $I = 26$ pA, Image size $= 320 \times 320$ nm^2. (b) Demonstration of atomic resolution. The Ag lattice crystal structure is well resolved. $V_{sample} = -1.17$ V, $I = 198$ pA, Image size $= 10 \times 10$ nm^2.

direction from the lateral movement the noise level can be reduced considerably.

The voltage between tip and sample is applied with reference to the sample. If not said otherwise, the images are recorded in constant-current regime. To achieve this, the piezo actuator which controls the movement in the z axis is connected to the feedback control. In this case, any departure from the set value of the tunneling current causes the tunneling gap to change in such a way to restore the set current.

The STM was only delivered in the beginning of this thesis. After the installation, the whole system had to be tested and commissioned. This includes the set up of the UHV lab with all the mechanical tools, a soldering station, as well as electrical equipment. Especially for the experiments on silicon, compatible equipment as a different sample holder or a pyrometer for non-contact temperature measurements had to be purchased as described in detail in Chapter 6.

The low-temperature STM was acquired to image and manipulate single molecules with picometer resolution. The first test of the STM incorporated therefore the imaging of a metal sample with atomic resolution. In Figure 4.4 images of the silver (100) surface in general and atomic resolution taken at 77 K are shown. The overview image shows various, well-resolved step edges of the single crystal. The bright structures adsorbed on the surface are crystallized water as the sample was not heated before the measurement. In the atomic resolved image the symmetry and lattice geometry of the silver face-centered cubic crystal is apparent. The measured lattice constant of 0.48 nm is in agreement with the literature value of 0.41 nm [77].

4.2 Sample preparation
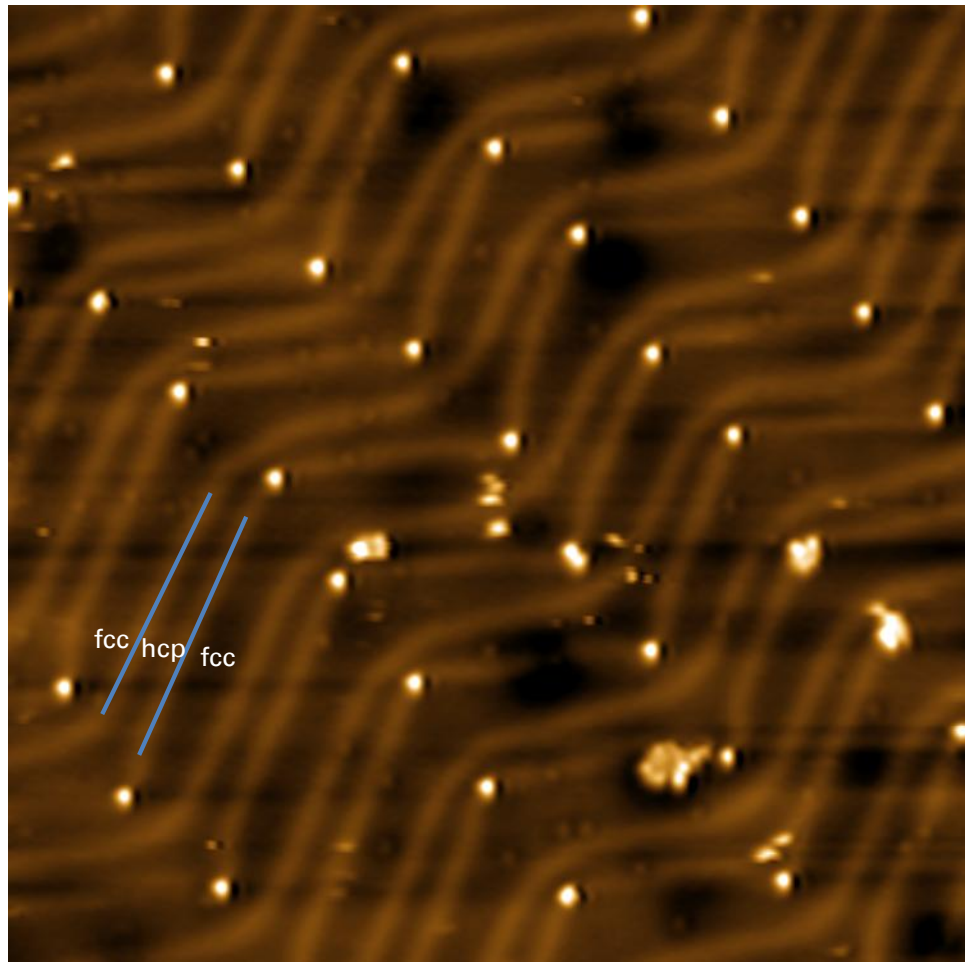
Figure 4.5 – STM image of the herringbone reconstruction of an Au(111) surface. Bright stripes indicated by blue lines correspond to transition areas between the fcc and hcp domains. In the kinks of the reconstruction adsorbates can often be observed depending on the cleanliness of the preparation. V_{sample} = -0.51 V, I = 292 pA, Image size = $56 \times 56\,\text{nm}^2$
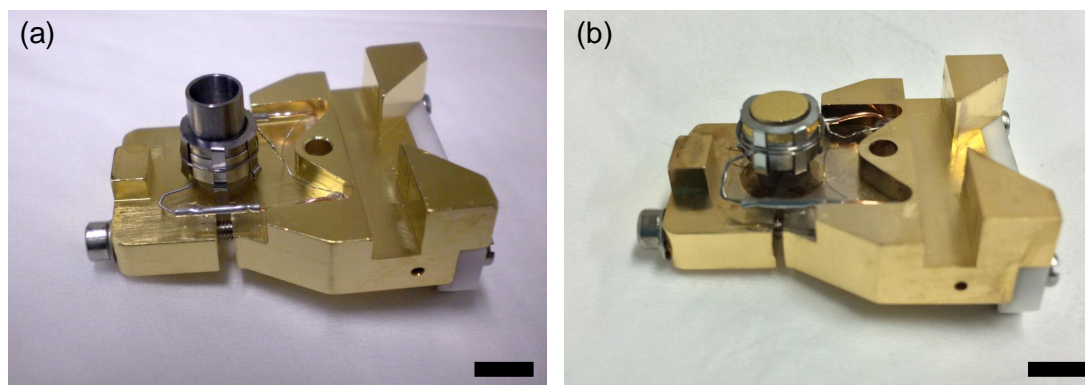
Figure 4.6 – (a) Evaporator for organic materials. Note the tiny crucible with a volume of 0.2 ml. (b) Au(111) sample holder for comparison. Scale bar equals 5 mm.

Au(111) sample   The standard preparation of an Au(111) single crystal involves subsequent cycles of sputtering and annealing [78]. For the sputtering, the sample is bombarded with Ne^+ ions to blast a single or a few monolayers of gold, and thus cleaning the surface. Afterwards the sample is annealed at about 720 K for about 15 minutes to smooth the surface of the crystal. After a few cycles of this procedure, the top surface layer should be flat with straight step edges. To avoid defects in the sub-surface layer, the sample is then flashed about three times to 790 K. A result of the preparation routine is shown in Figure 4.5. The stripes on the terrace are attributed to the so-called Au(111) herringbone reconstruction [78]. The reconstruction appears because of stress the fcc crystal undergoes during the transition from normal bulk stacking to the surface [79]. Thinner dark areas within the reconstruction can be attributed to the hcp phase (AB stacking), whereas broader dark areas belong to the fcc phase (ABC stacking). The bright stripes are transition areas of both phases. Due to a preferred surface-energy minimized state, adsorbates primary arrange at kinks of the reconstruction, as can also be seen in Figure 4.5.

Si(100) sample   The preparation of silicon samples consists of degassing the sample at temperatures below 1050 K, subsequent flashing to about 1300 K, and a slow cool down to room temperature in order to get a well-ordered surface reconstruction. A detailed description of the sample preparation protocol can be found in Chapter 6.

4.3 Molecular evaporator

In order to study single molecules on the predescribed surfaces, molecules have to be deposited in a controlled and reproducible way. The challenge of organic material lays in the low sublimation temperatures and the often small amount of material available. Therefore, most common UHV evaporators are not suitable for these materials. In the preparation routines for the here presented work, an evaporator consisting of a very small crucible mounted on an oven is used, to fit the purpose of the single molecule preparations (see

Figure 4.6). As the evaporator is constructed identically to the normal sample holder (see Figure 4.6(b) for reference), it fits all the electrical connections of the manipulator and sample storage.

The ceramic oven allows the precise control of temperatures slightly above room temperature, like 320 K used in this work. This controlled thermal input enables the evaporation of a very precise amount of material for single molecule experiments.

Typical evaporation temperatures for the molecules used in this work are about 320 K for ABP (see Chapter 5 and 7) and about 420 K for the molecular wheels (see Chapter 8).

5 ABP on Au(111)

Before the experiments for the molecular latch on silicon could begin, test experiments were performed with the promising candidate on Au(111).

Controlled displacement of single atoms or molecules using methods of scanning tunneling microscopy have been shown on different surfaces and were described in Chapter 3. On metals, lateral manipulation of atoms [49, 80], molecules of different complexity [50, 51, 81] as well as vertical manipulation [82, 83] are well established methods. Similar examples can be found on semiconductors [84, 85] and insulating layers [86]. All these experiments use a direct tip-particle interaction for the manipulation. Otherwise, manipulations using electric field [87] or inelastic tunneling electrons [88–90] have been studied. Only sporadically, manipulation of molecular clusters has been reported on metals [65, 91].

In this chapter, the controlled manipulation of a supramolecular structure composed of four ABP molecules induced by voltage pulses is shown. By applying voltage pulses on one selected molecule of the structure, the supramolecular assembly can be moved to any chosen position on the surface without destroying it.

Part of the results presented in this chapter have been published in *Moving Nanostructures: Pulse-Induced Positioning of Supramolecular Assemblies*, ACS Nano **7**, 191-197 (2013) by Anja Nickel, Robin Ohmann, Joerg Meyer, Maricarmen Grisolia, Christian Joachim, Francesca Moresco, and Gianaurelio Cuniberti.
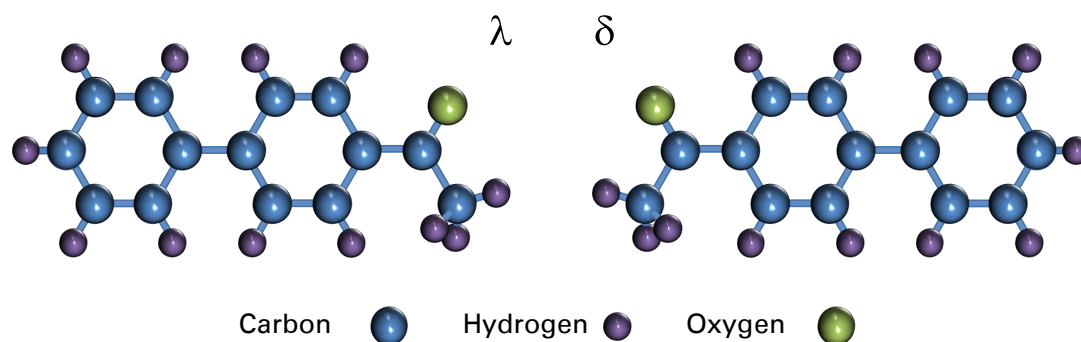
Figure 5.1 – Molecular structure of 4-acetylbiphenyl (ABP). Due to the prochiral nature of the molecule, two enantiomeric forms exist on the surface (λ and δ chirality).

5.1 Molecular self assembly

The ABP molecule used in this work is shown in Figure 5.1. It is composed of two phenyl rings and an acetyl group. Due to reduction of the degrees of freedom on the surface,
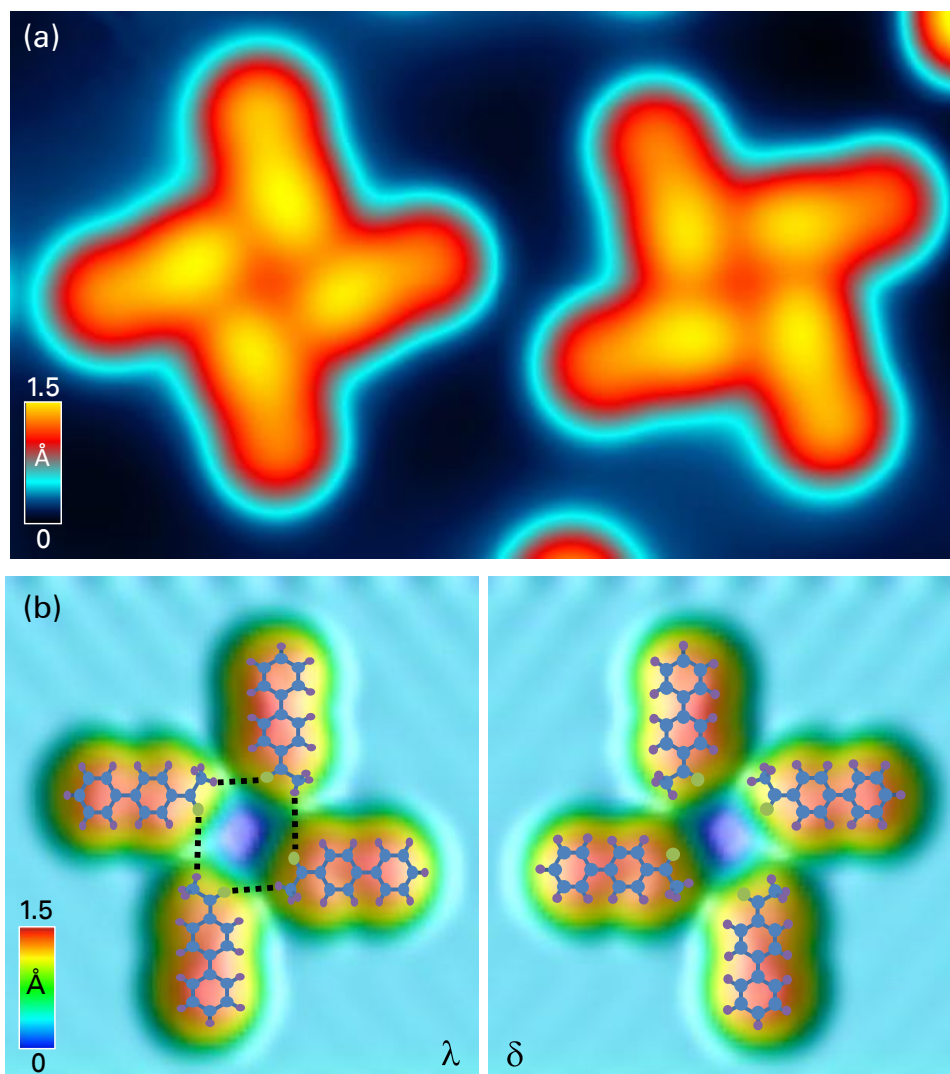
Figure 5.2 – (a) STM topography image of self-assembled tetramers of ABP on Au(111) (λ and δ chiral windmill motif). Image size = 3.84×6.93 nm^2, $V_{sample} = 1$ V, I = 2.9 nA. (b) Calculated STM image with the optimized geometry superimposed. The dashed lines symbolize the inter-molecular hydrogen bonds.

two enantiomeric forms of the molecule can be found, namely λ and δ. This is known as prochirality [92]. On Au(111), the ABP molecules self assemble into small weakly bonded supramolecular structures. Single molecules adsorb at defects and step edges and cannot be moved away by manipulation.

5.1.1 Tetramer assemblies (ABP$_4$)

In Figure 5.2(a), a STM topography image of a supramolecular ABP tetramer is presented. The ABP molecules are here organized in a windmill nanostructure. These windmills are present on the surface in two mirror symmetric forms as a consequence of the prochiral nature of the single molecules. Figure 5.2(b) shows a calculated constant-current image of the windmill, which was performed using the ESQC method in the group of C. Joachim at CNRS, Toulouse [70].

Carbon is not a conventional hydrogen-bond donor due to its relatively low electronegativity of 2.55 (Pauling scale), in contrast to nitrogen (3.04) or oxygen (3.44) [93, 94]. However, a tentative model of the tetramer structure suggests hydrogen bonding between aliphatic carbon groups and oxygen of the neighboring molecule. The calculated geometry confirms the hydrogen-bond like stabilization of the windmill nanostructure and shows a bond length of 3.1 Å [95, 96]. The hydrogen bonds are indicated by dashed lines in the image. The proposed structure agrees excellently with the distances in the windmill structure determined experimentally from the STM images.

The λ and δ chirality of the windmills, averaged over a large number of tetramers, are equally distributed as shown in Figure 5.3. Here, the green and blue bars highlight the enantiomeric supramolecular structures. On the small scale, there are domains of the two ABP_4 chiralities on Au(111), which are independent of the underlying surface reconstruction of fcc and hcp domains. In addition, the colored bars indicate the adsorption angle of the windmills individually for the two chiralities. Notice that the bars mark only the most vertical angle of the structure as the windmills exhibit fourfold symmetry. In Figure 5.3, the distribution of these angles is shown. Three energetically equivalent adsorption sites exist for the two chiralities within the $90°$ interval. This corresponds exactly to the surface symmetry of the Au(111) surface.

5.1.2 Trimer assemblies (ABP$_3$)

Besides the tetramers, supramolecular structures consisting of three ABP molecules can be found on the surface. The different configurations of the trimers are shown in Figure 5.5. All three configurations have mirror symmetric forms like the tetramers. Two of the trimer structures, rotor-like and triangular (Fig.5.5(a) and (c)), are enantiopure whereas the Y-like structure consists of a mix of the chiralities.

The occurrence of trimers and tetramers is dependent on the substrate temperature during molecule evaporation as well as coverage. Substrate temperatures below 333 K ensure trimers on the surface, independent on the coverage. At higher temperatures, tetramer structures can be observed at low coverage, whereas trimers and tetramers are built at high coverage. Obviously the assembly of the tetramer structures requires a higher diffusibility of the single molecules on the surface than that of the trimers.

The intermolecular binding of the trimer structures is different from the tetramer windmills. Figure 5.6 shows tentative models for the trimer rotor as well as the triangular structure. Both models suggest hydrogen bonds between the molecules, which are indicated in dashed lines. In case of the trimer rotor (Fig. 5.6(a)), the oxygen of one molecule interacts with the first phenyl ring of the neighboring molecule. Within the triangular structure (Fig. 5.6(b)), the interaction occurs between oxygen and second phenyl ring of neighboring molecules. Both models can only be realized if the acetyl group polarizes both phenyl rings inducing partial charges within the molecule. The effect of the polarization is dependent on the distance from the electronegative oxygen. Consequently, trimer windmills should be more stable than the triangular assemblies. This is proven by the much higher number of trimer windmills in comparison to triangles on the surface at low substrate temperatures during the preparation.
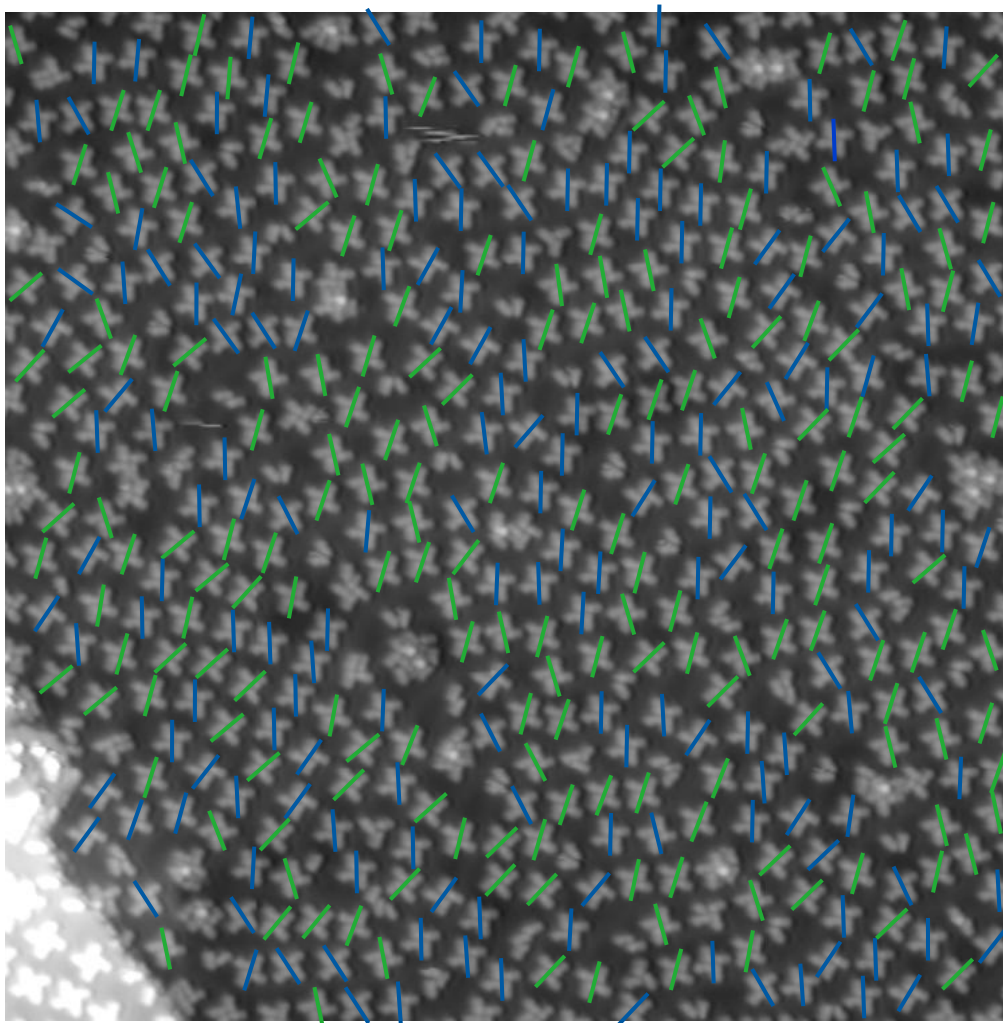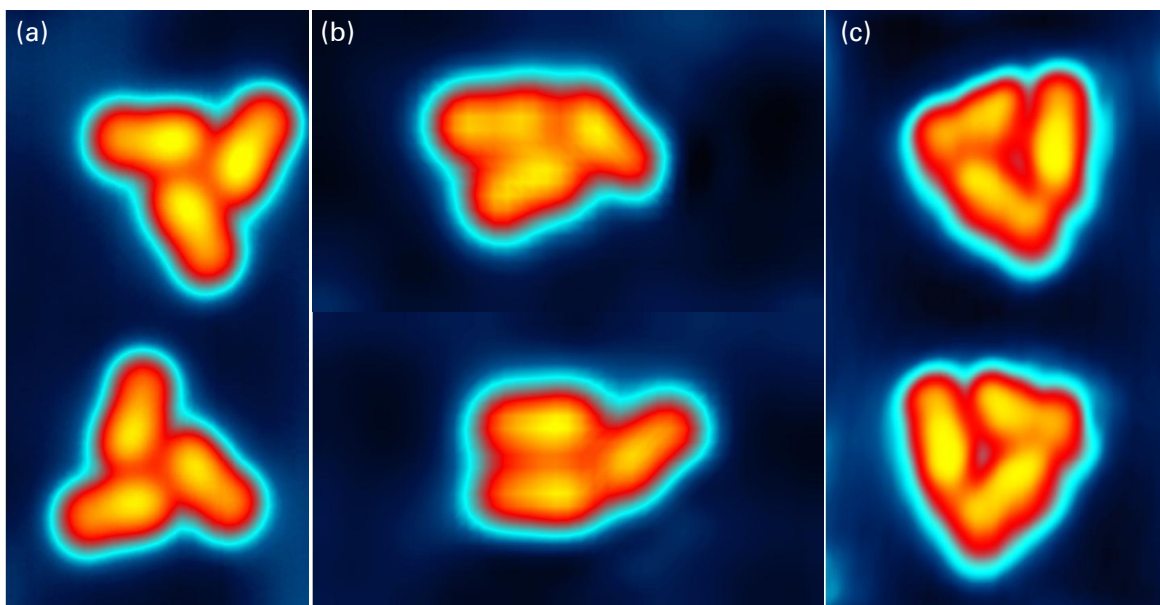
Figure 5.3 – STM image of an Au⟨111⟩ terrace covered with ABP tetramer structures. The colored bars indicate the angle of the structures for the λ and δ chiralities in green and blue, respectively. $V_{sample} = $ -0.46 V, I = 140 pA, Image size = 80×80 nm^2.

(a)

(b)
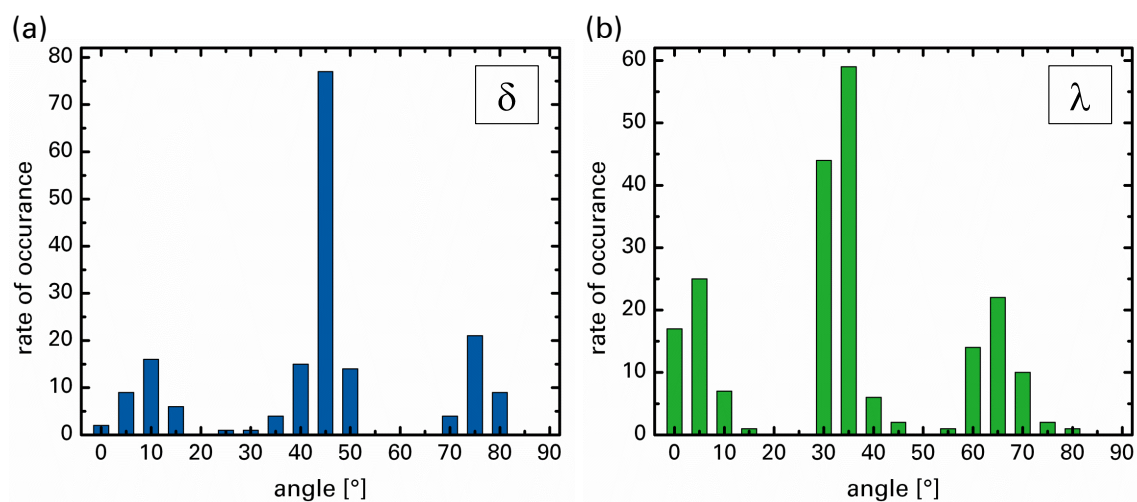
**Figure 5.4** – Adsorption angle distribution for λ and δ chiralities as indicated in Figure 5.3.

Figure 5.5 – Different configurations of ABP trimers. (a) rotor-like trimer. $V_{sample} = 0.03$ V, $I = 26$ pA, Image size $= 7.8 \times 3.9$ nm^2. (b) Y-like structure gives rise to a mixture of both molecular chiralities within one supramolecular structure. $V_{sample} = 0.03$ V, $I = 26$ pA, Image size $= 6.5 \times 7.6$ nm^2. (c) triangular structure. $V_{sample} = 0.1$ V, $I = 50$ pA, Image size $= 6.4 \times 3.9$ nm^2.

## 5.2 Directed manipulation of supramolecular structures

Attempts to move the supramolecular assemblies using the conventional lateral manipulation technique resulted in a destruction of the supramolecular nanostructures and the separation of its ABP components. In order to move the individual assemblies, voltage pulses were applied on top of or close to one of the ABP molecules of the nanostructure as it has been done so far on single molecules. These resulted in a controlled collective movement of all ABP molecules of the chosen assembly at the same time.

### 5.2.1 Manipulation of tetramers

In Figure 5.7, topography images taken before (top row) and after (bottom row) the voltage pulse are shown. By changing the applied voltage, different types of motions could be observed. For negative voltages (Figure 5.7 (a)), predominantly collective translational movement of all molecules of an ABP$_4$ windmill is found in the direction away from the position of the tip. For positive voltages, two possible movement types can be observed. Most frequently, translational movements are induced (Figure 5.7 (b)). Otherwise, a rotation of the supramolecular assemblies can be detected (Figure 5.7 (c)). For sufficiently high positive voltages, a total reorganization of the ABP$_4$ windmill nanostructure occurs (Figure 5.7 (d)). It is important to note that for positive voltages the direction of the translation is
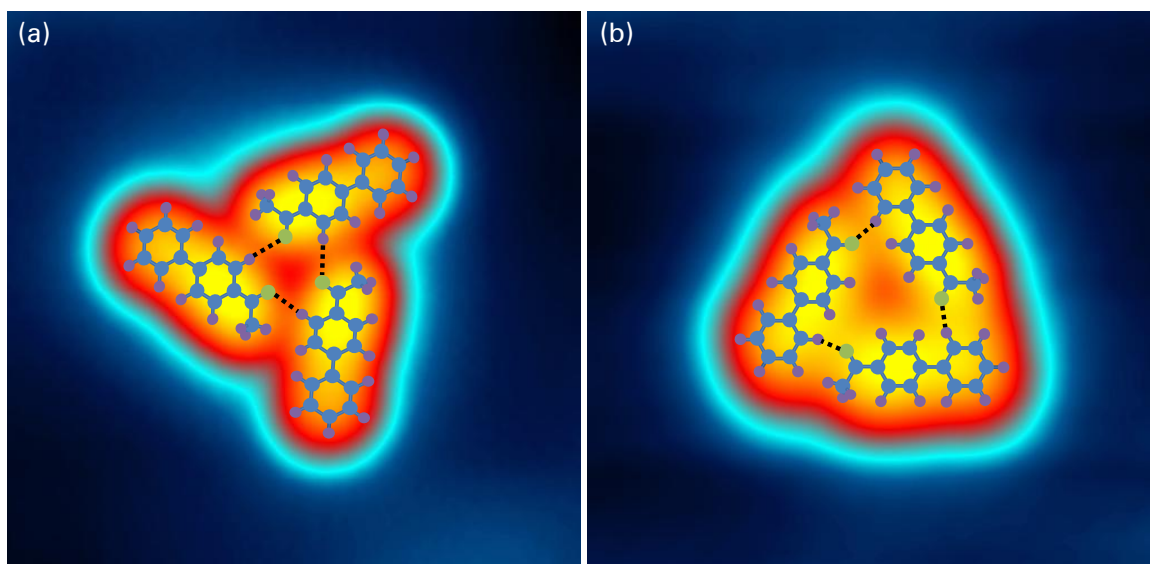
Figure 5.6 – Model structure of the ABP trimers. (a) rotor-like trimer. Hydrogen bonding between first phenyl ring and oxygen of the acetyl group. $V_{sample} = 0.02$ V, $I = 20$ pA, Image size $= 4.0 \times 3.9$ nm^2. (b) triangular structure. Hydrogen bond between second phenyl ring and oxygen. $V_{sample} = -0.1$ V, $I = 50$ pA, Image size $= 4.0 \times 3.9$ nm^2. Hydrogen bonds are indicated by dashed lines.
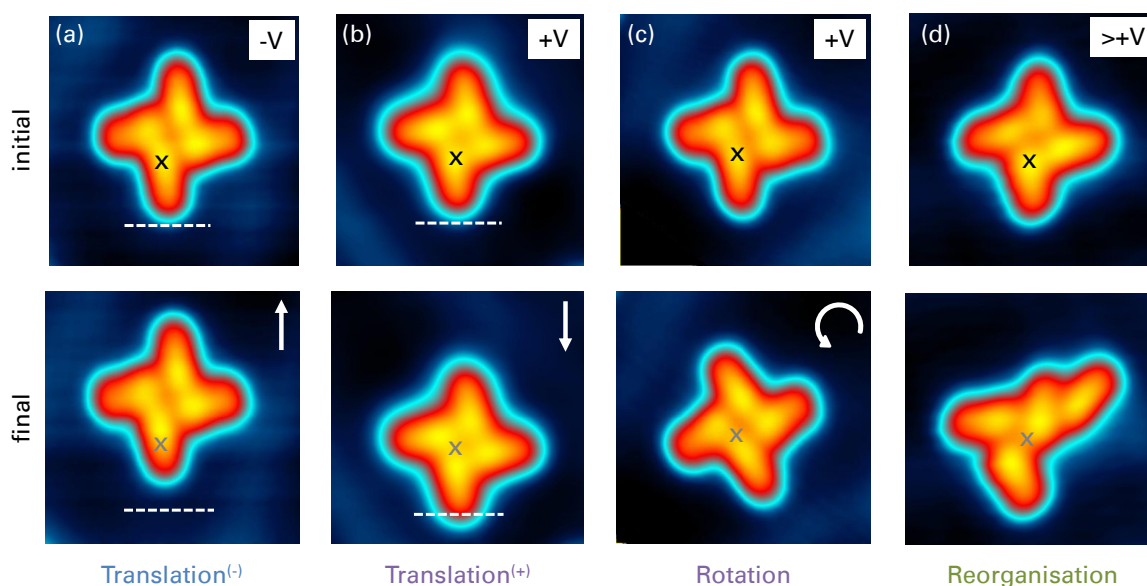
Figure 5.7 – STM topography images of self assembled ABP$_4$ on Au(111) taken before (top row) and after (bottom row) applying a voltage pulse at the position indicated by the black cross. In the majority of cases a negative voltage pulse leads to translation (a), whereas a positive voltage pulse leads either to translation (b) or rotation (c) or, for sufficiently high voltages, reorganization of the supramolecular structure (d). Note that the direction of translation is opposite for negative and positive voltages. The white dashed lines are a guide for the eyes, and the gray crosses indicate the position of the tip where the voltage pulse was applied. Image parameters: (a) $V_{sample} = -0.1$ V; (b-d) +0.1 V; $I = 50$ pA; Image size $= 5 \times 5$ nm^2. Manipulation parameters: (a) $V_{sample} = -2.3$ V, $I = 1.7$ nA, $t = 20$ s; (b) 2.1 V, 3 nA, 10 s; (c) 2.5 V, 0.5 nA, 10 s; (d) 2.7 V, 0.25 nA, 10 s.
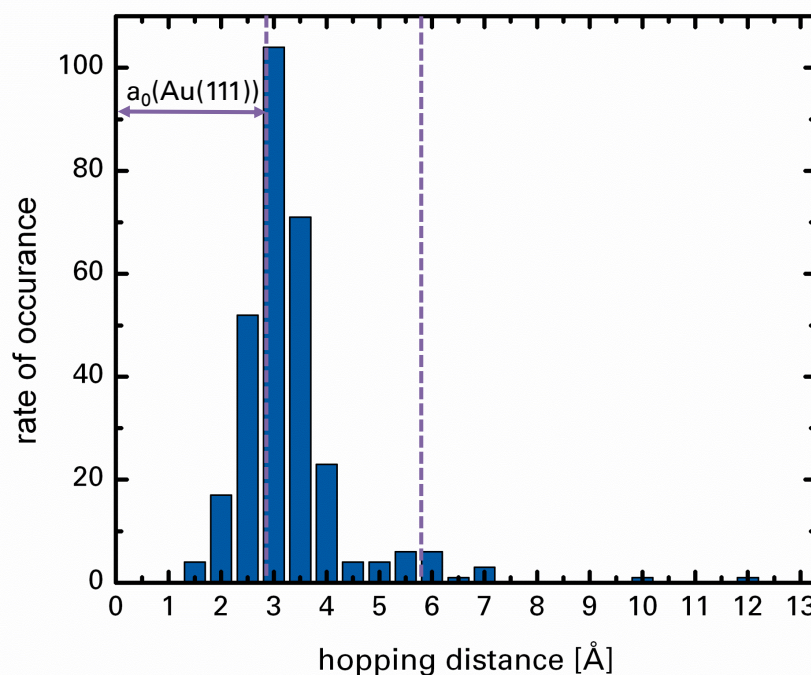
Figure 5.8 – Distribution of hopping distances of tetramer structures. The purple limits mark the surface lattice constant of Au(111), $a_0(Au(111))=2.9\,nm$.

opposite to that for negative voltages; that is, the center of the supramolecular structure moves toward the position of the tip.

For translational movements, the ABP_4 windmills can only be displaced discretely. The hopping distance is typically $3\,\text{Å}$ as can be seen in Figure 5.8. This corresponds to the surface lattice constant of Au(111). Rotational movements are mainly observed at positive voltage pulses (in more than 40% of the cases in contrast to less than 5% at negative voltages) with rotational angles of $15°(33\%)$ or $30°(66\%)$ in the clockwise or counterclockwise direction. Before manipulation, the windmills are adsorbed at energetically equivalent adsorption sites of the Au(111) surface as shown in Figures 5.3 and 5.4. The symmetry consideration explains the predominant $30°$ rotation. The rotation is possible on the open surface even without any geometrical constraints such as a surrounding cavity [97]. Considering that the windmill nanostructures are chiral, a possible rotational preference was investigated. However, out of the 200 measured rotational events, no significant preference for one or the other rotation direction was observed. If there is a preferential rotation direction due to the chirality of the molecules, as suggested by a recent work on a single chiral molecular rotor [98], it would be rather small. For the issued measurements, an upper limit for rotation directionality of about 5% can be given. This confirms that molecule-surface chirality is only a necessary condition for unidirectional rotation of an adsorbate.

The manipulation method using voltage pulses was explored as a tool to repeatedly move nanostructures over large distances. To do so, voltage pulses were applied consecutively to the windmill along a predetermined line on the surface. In Figure 5.9, such a manipulation procedure is shown. The left image shows the initial and the right image the final position of the windmill after applying a regular series of voltage pulses. The windmill follows the
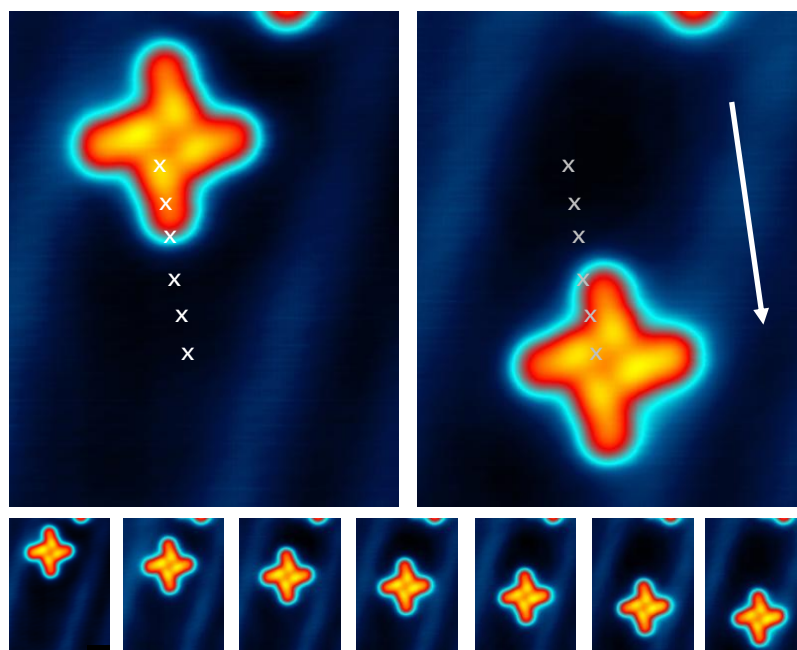
Figure 5.9 – Controlled lateral manipulation using consecutive voltage pulses. Total traveling length after six pulses is 3.6 nm. The brighter appearance of the right molecule of the windmill in the final position is due to the influence of the reconstruction lines of the Au(111) surface. At the bottom, the intermediate positions of the windmill after each pulse are shown. Manipulation parameters: 2.3 V, 1.7 nA, 10 s. Image size = 6.8×8.0 nm^2. The color scale is the same as in Figure 1b.

position of the tip stepwise along the predetermined line. At the bottom part of the figure, the intermediate positions after each pulse are presented. Importantly, by selecting the molecule within the nanostructure to which the voltage pulse is applied, the direction of the manipulation can be chosen. Intact windmills can be controllably moved to defined positions on the surface. This can be seen in Figure 5.10. By moving two windmills to a desired position, a new nanostructure is built. Moreover, this example shows that the Au(111) surface reconstruction does not affect the windmill motion. Notice that such highly controlled surface positioning does not require the complex intramolecular mechanical mechanisms described for single-molecule machines [99].
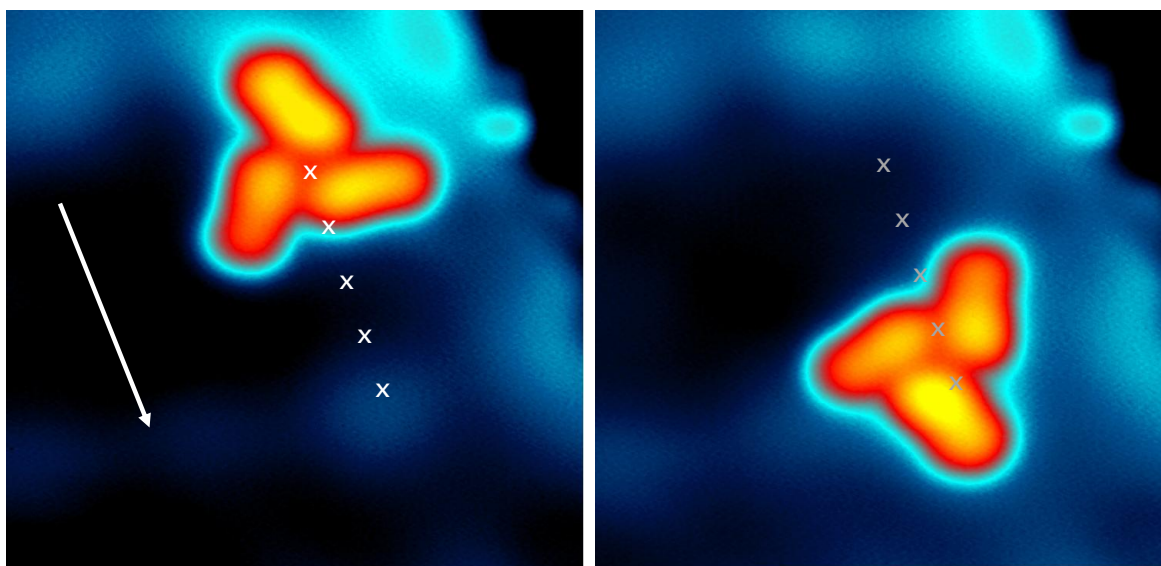
5.2.2 Manipulation of trimer structures

The above described method of consecutive voltage pulses to position ABP$_4$ nanostructures on the Au(111) surface was also adopted to move trimer structures. It turned out that two ABP$_3$ assemblies, rotor and Y-like structure, can be moved as reproducibly as the tetramer structures. This applies particularly for the direction of the movement during voltage pulses with different polarities. For positive bias, the supramolecular trimers follow the position of the tip, whereas for negative voltages the ABP$_3$ structures will move away from the tip apex. An example of a long distance manipulation of a trimer windmill is shown in Figure 5.11. Unlike the tetramer manipulation, the trimer nanostructures tend to rotate during the lateral manipulation as can also be seen in the figure. This means, the positioning is not as precise
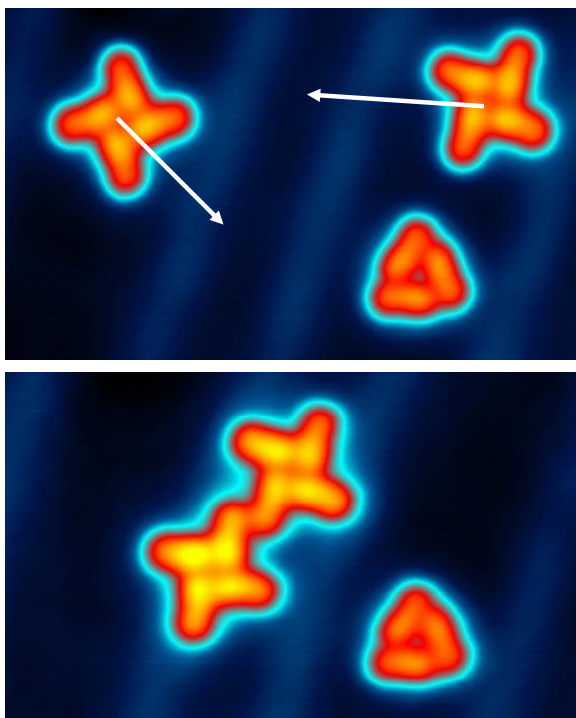
Figure 5.10 – Construction of a novel nanostructure by bringing two windmills together. The molecular aggregate on the bottom serves as reference for the movement of the two windmills. The herringbone reconstruction of the Au(111) surface does not limit the motion. Manipulation parameters: 2.3 V, 1.7 nA, 10 s. Image size = 12.5×7.3 nm^2. The color scale is the same as in Figure 1b.

Figure 5.11 – Lateral manipulation of a trimer nanostructure using consecutive voltage pulses. The position of the tip during each pulse is highlighted with a cross. Note, the apparent height difference of the molecules within the supramolecular structure is only due to the underlying surface reconstruction. $V_{sample} = 0.017$ V, $I = 20$ pA, Image size = 6.9×6.7 nm^2. Manipulation parameters: 2.5 V, 25 pA.

(a)

(b)
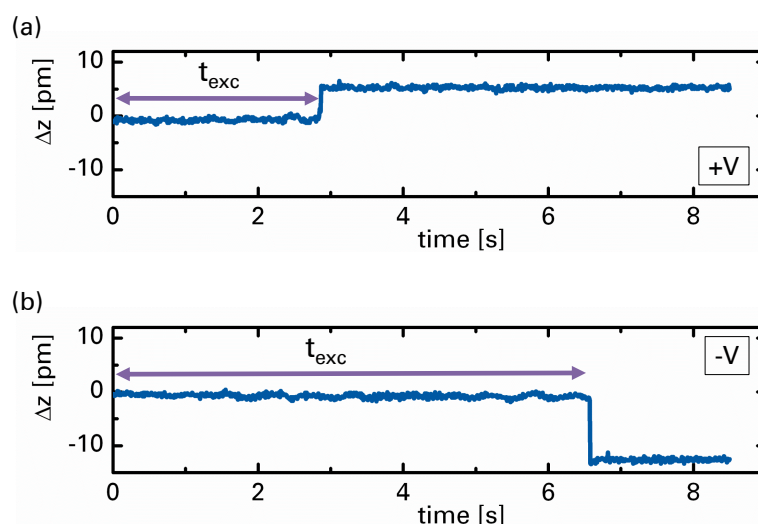
Figure 5.12 – Tip height traced during voltage pulses over 8.5 s time interval. (a) Tip height increases when a positive voltage is applied. $V_{sample} = 2.3\,V$, $I = 1.3\,nA$. (b) Decrease of the tip height during a negative voltage pulse. $V_{sample} = -1.9\,V$, $I = 1.7\,nA$. t_{exc} is the time interval necessary to excite a movement of the supramolecular structure.

as in case of the ABP_4 windmill structures. The hopping distance of the trimer structures is in agreement with the hopping distance of the tetramer structure about 3 Å. The manipulation is also not restrained by the herringbone surface reconstruction.

Attempts to manipulate the triangular structure were not successful. Both conventional lateral manipulation and the voltage-pulse technique were used to position the triangles. Conventional lateral manipulation caused ultimately the destruction of the supramolecular structures, whereas no parameters for the voltage-pulse manipulation could be found that caused movement.

5.3 Control of the positioning

5.3.1 Statistical analysis

In order to understand the manipulation of the supramolecular structures, the tip-height traces taken during the voltage pulses of the manipulation of the tetramers were analyzed systematically. As the pulses were applied in constant-current mode, a change in the tip height should indicate the movement of the supramolecular assemblies. Two representative examples of such traces, one for the positive voltage and one for the negative voltage, are shown in Figure 5.12. A jump in the height trace indicates a sudden change in the conductance at the position of the tip. For positive voltages, usually an increase in tip height can be observed (see Figure 5.12(a)) which corresponds to an increase in the local conductance. On the contrary, for negative voltages the tip height usually decreases during the first jump corresponding to a decrease in the local conductance (see Figure 5.12(b)). This agrees with the observation that for positive voltages the structures move toward the tip, whereas for negative voltages, the center of the supramolecular structures moves away from
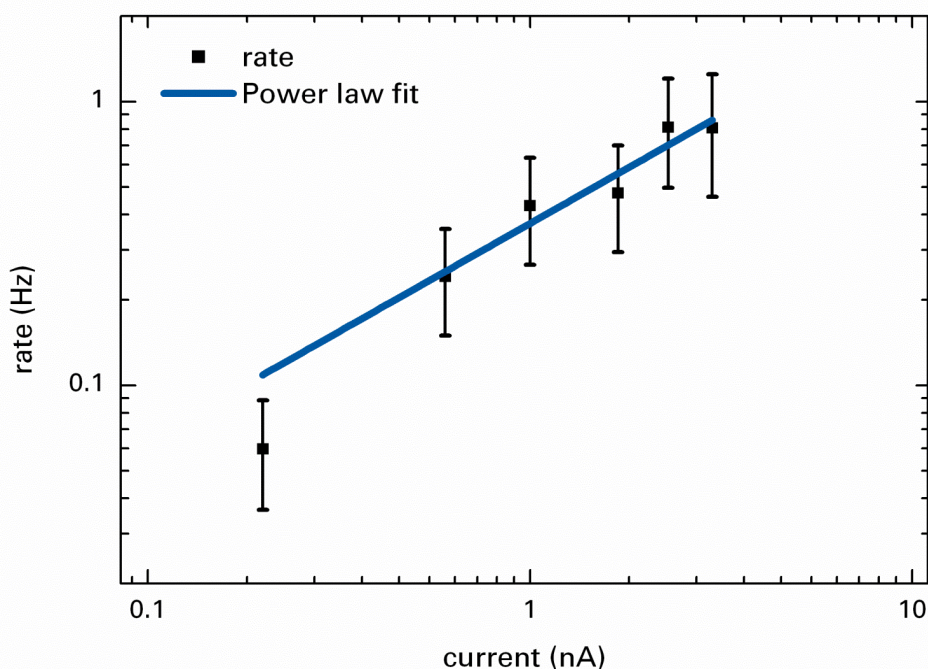
Figure 5.13 – Inverse of the excitation times (*i.e.*, rate) as a function of current plotted in log-log scale. Bias voltage: -1.8 V. The fit (blue line) shows that the rate depends linearly on the current indicating a one-electron process. Measurements at other voltages show the same dependence.

the tip.

After the first jump, more jumps can occur. For the manipulation with negative voltages the structures will move further away from the tip. For positive voltages, the nanostructures are trapped under the tip apex and no further lateral movement will be observed. A jump in this case will show the rotation of the supramolecular assembly.

The rate as well as the quantum yield of the event were deduced from the time it takes for the first jump to occur, t_{exc}. In Figure 5.13 the rate of the manipulation at -1.8 V is plotted as a function of the current in double-logarithmic scale. The rate describes the inverse of the average excitation times, $\tau = \overline{t_{exc}}$, at a given current. Fitting the data to a power function reveals an exponent of $N = 0.76 \pm 0.13$. In terms of measurement accuracy, this indicates an inelastic one-electron process, as the other voltages show the same linearity [100].

The quantum yield describes the probability per electron that a movement is triggered. The yield for a given voltage is calculated via $e/(\tau I)$, where e is the elementary charge, I the current, and τ the before mentioned average of excitation times. In Figure 5.14(a) the yield as a function of the applied bias voltage is shown. It is evident that the behavior for positive and negative voltages differs. The threshold voltage, which is the voltage above or beyond no movement could be achieved, to excite an event is much lower for negative than for positive voltages, where values above 2 V need to be applied to trigger an event. For positive voltage pulses, the quantum yield shows a maximum value at about 2.5 V, whereas for larger voltages, a reorganization of the assemblies takes place (Figure 5.7(d)).

(a)

(b)
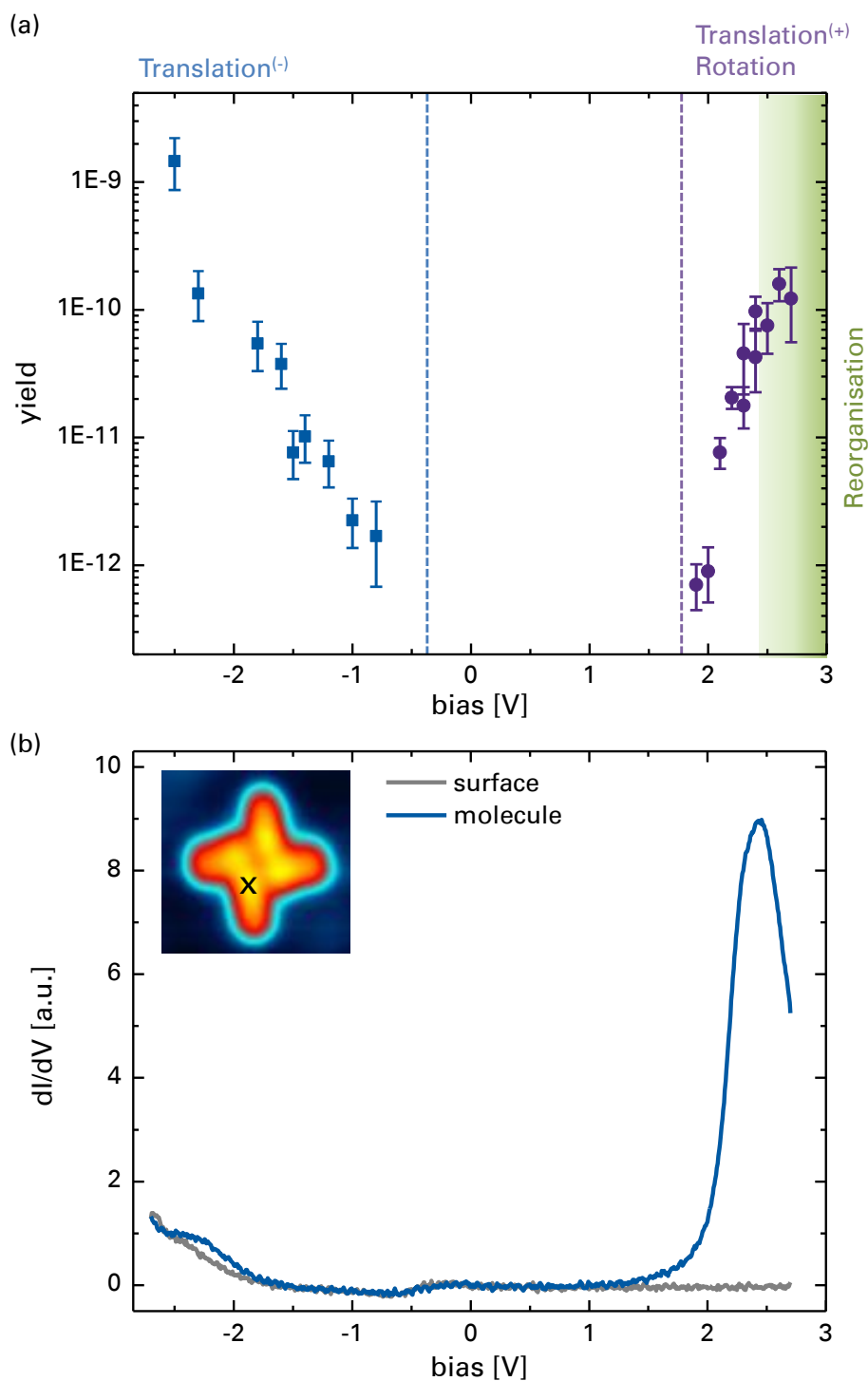
Figure 5.14 – (a) Quantum yield plotted as a function of bias voltage on a semi-logarithmic scale. (b) dI/dV spectra taken on top of the supramolecular structure (blue) and an off spectrum taken on the bare Au(111) surface (gray). The inset shows STM images taken at 0.1 V (the black cross indicates the position of the tip during the spectrum).
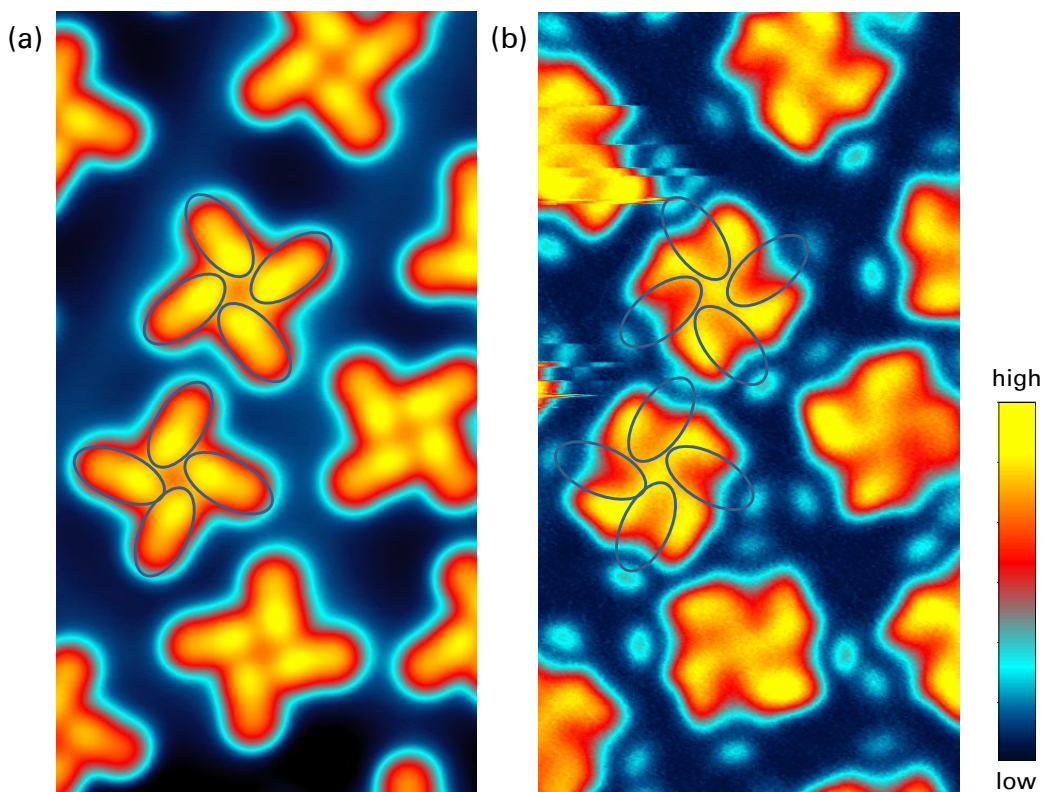
Figure 5.15 – Electronic structure of the tetramer structures. (a) Topographic image. $V_{sample} = -1\,V$, $I = 190\,pA$. (b) dI/dV map at $2.15\,V$, $I = 25\,pA$, LockIn frequency $833\,Hz$, $RC = 0.16\,Hz$. For better visualization the molecular shape is highlighted with ellipses. Image size $= 6.8 \times 12.7\,nm^2$.

5.3.2 Electronic structure

To obtain the electronic structure of the supramolecular structures, the derivative of the STM tunnel current was recorded. The dI/dV spectrum was taken at the same position as a voltage pulse would be applied for manipulation. In Figure 5.14(b) the spectrum is shown. For positive voltages, a well-resolved resonance at about $2.5\,V$ is observed which can be assigned to the lowest electronic excited state of the ABP adsorbate [101]. For negative voltages, the spectrum appears relatively flat. Nevertheless, a broad and weak resonance at about $-2.2\,V$ can be distinguished in the spectrum.

For positive voltages, the energy onset position of the observed resonance exactly corresponds to the measured quantum yield (see Figure 5.14), indicating the presence of an inelastic input channel on the assemblies. For negative voltages, the energy onset begins already at $-0.8\,V$, and because of the broadness of the resonance, also in this case, the increase of the quantum yield can be explained by the electronic resonance. Such localized inelastic excitations on just one ABP molecule of the supramolecular structure are enough for the complete nanostructure to translate or to rotate without any internal apparent structural change.

Once a threshold voltage, where tunneling in molecular resonances is possible, has been reached, the supramolecular structure can be moved. For voltages exceeding $2.5\,V$, the nanostructure is destroyed. In this case, some hydrogen bonds are broken and a new
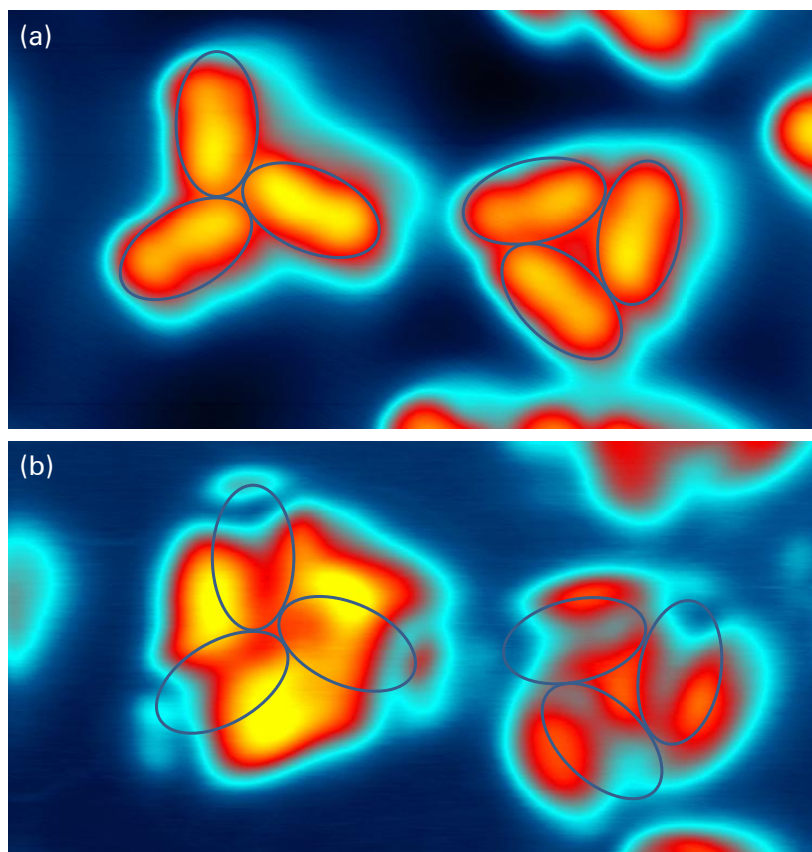
Figure 5.16 – dI/dV map of the two enantiopure trimer configurations. The position of the molecules is highlighted with ellipses for better visualization. (a) Topographic image $V_{sample} = 0.1\,V$, $I = 41\,pA$. (b) Differential conductance map $V_{sample} = 2.15\,V$, $I = 41\,pA$, LockIn frequency= 833 Hz, RC= 0.16 Hz, Image size $= 7.6 \times 4.1\,nm^2$.

non-covalently bonded network is formed (see 5.7 (d)), which differs significantly from the self-assembled arrangement. Occasionally, a reversal of this reorganization can be observed by additional voltage pulses, recovering the original windmill configuration. Notably, the structural chiral fingerprint remains in the new structures. For voltages between 2.5 V and the lowest measured negative value of -3.0 V, the strength of the hydrogen bonds between the ABP molecules in a windmill is large enough to keep the nanostructure intact during its excitation and its concerted motion (translation, rotation). From the statistical analysis of the time series of the voltage pulses, it can be deduced that the process is driven by the inelastic tunneling of a single electron. The quantum yield is in good agreement with the dI/dV spectrum, confirming an inelastic input channel.

As shown in Figure 5.7, the tip was placed on one of the molecules close to the center of the structure during the voltage pulses. To exploit the distribution of the inelastic input channel over the assemblies dI/dV maps were recorded. In Figure 5.15 the conductance map at 2.15 V as well as a topographic image of the tetramer structures is shown. For better visualization, the molecular positions of both chiralities are highlighted in each image. The input channel is obviously not uniformly distributed over the molecular assembly. The mapped state has a maximum in the middle of the tetramer as well as on the outer part of each molecule, where the functional group is situated. This maximum remains until the first
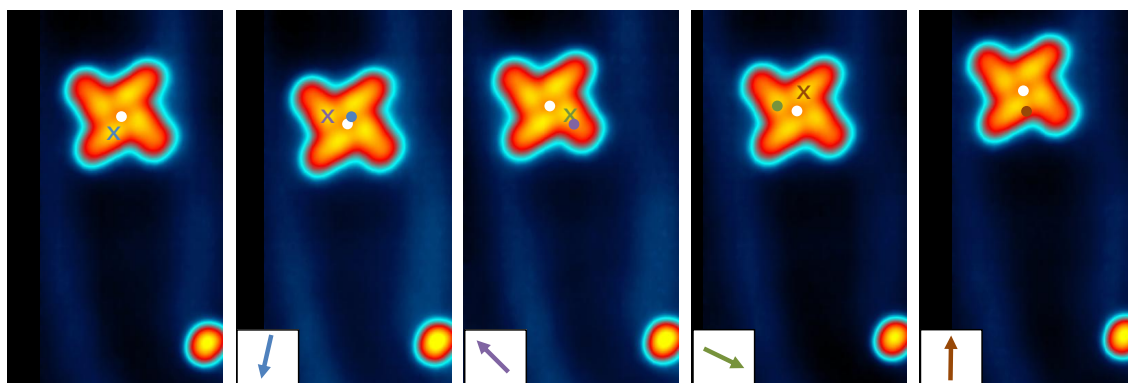
Figure 5.17 – Choosing the direction of motion by positioning the tip at a specific molecule of the supramolecular structure. The position of the tip during the voltage pulse is indicated by the colored crosses. The different directions are visualized by the corresponding colored arrows. To follow the motion of the structure, its center is represented by a white circle. The colored circles denote the previous position of the structure in this sequence of images. Manipulation parameters: 2.6 V, 0.25 nA, 10 s. Image size $= 9.8 \times 5.6$ nm^2.

phenyl ring ends (compare to Figure 5.2), and a sharp minimum appears. On the end of each molecule a distinct maximum emerges. This agrees well with the observation that the manipulation is more controlled when the voltage pulses are placed on the first phenyl ring. Figure 5.16 shows the conductance map at 2.15 V as well as a topographic image of the two enantiopure trimer structures. Here, the maximum of the mapped state is also located on the outer side of the assemblies with a clear minimum at the position of the second phenyl ring and a maximum on the end, see Figure 5.6 for comparison. Also a difference is apparent: In case of the rotor-like trimer the input channel shows a minimum in the center of the assembly. This could explain why the positioning of the rotor-like trimer is less stable than the positioning of the tetramer windmill which has a maximum in the center.

The triangular structure has also a maximum in the center of the assembly, but maxima at the end of each molecule are much less pronounced. This gives rise to the fact that the second phenyl ring serves as a binding partner for the oxygen of the neighboring acetyl group. The minima along the molecules of the assembly gives an explanation for the fact that the triangular structures cannot be moved via voltage pulses, as there is no input channel for the inelastic tunneling in this particular structure.

5.3.3 Directionality

As already discussed, the positioning of the supramolecular assemblies depends on the polarity of the voltage pulses as well as the location of the tip apex on the structure. The polarity depicts the first parameter for the direction of the movement. If the voltage pulse is positive, the center of the nanostructure will move under the tip while the center of the supramolecular structure will move away from the tip at negative voltage pulses. This attractive or repulsive interaction is used to move the whole structure in a chosen direction by carefully selecting the position of the tip on the structure (see Figure 5.17).

For simplicity, the case of a positive voltage pulse on a tetramer windmill is chosen. If the

tip is placed over the center of the structure and a voltage pulse is applied, no translational movement occurs. If the same voltage pulse is applied by positioning the tip above one molecule in an off-center position, this results in an asymmetric geometry. The center of the assembly will be attracted by the tip and will move parallel to the chosen molecule in the direction of the tip. By choosing the molecule of the structure on which the pulse is applied, the direction of the movement of the whole structure can be directly selected.

An example of directed manipulation is presented in Figure 5.17. The directions of motion are selected by positioning the tip above distinct molecules of the supramolecular structure. The observed dependence of the movement on the polarity cannot be explained straight-forwardly. Recent studies on single molecules suggest an electrostatic effect between tip and molecule, which acts additionally to the hopping excitation [102]. When comparing to the work of Ohara *et al.* [102] and Swart *et al.* [89], it is, however, evident that for positive voltages single molecules can hop either away or toward the tip. The latter was observed on an ultrathin insulating layer and agrees with the measured polarity dependence presented in this thesis. For a complete rationale, many factors may need to be considered, such as the type of surface, quantum mechanical effects, or the local charge distribution.

In general, the collective movement of ABP molecules on a metal surface purely electronically with voltage pulses is possible due to a weak molecule-substrate coupling.

5.4 Conclusion

The experiments presented in this chapter demonstrate a method to controllably move supramolecular structures on a metal surface with a scanning tunneling microscope. As a model system, ABP molecules were used, which self-assemble on the gold (111) surface into different supramolecular structures composed of three or four non-covalently bonded molecules. By applying voltage pulses on top of one molecule, the whole structure can be manipulated in a controlled manner, preserving its native structure. This provides a novel procedure to gently and purely electronically manipulate individual nanostructures to desired positions on surfaces without the need for complex intramolecular mechanical mechanisms, opening a new route for the construction of artificial molecular devices.

6 Silicon (100) surface preparation

The huge impact of the invention of the STM was not only due to the first observation of atoms on surfaces, but by solving one of the most prominent problems in the field of surface science: The structure of the (7×7) reconstruction of the Si(111) surface [47]. From its discovery in 1959, the reconstruction of Si(111) was mainly investigated using diffraction methods like LEED [103]. But LEED, as any other diffraction method, is not without ambiguity and needs elaborated model-dependent calculations due to multiple scattering. Another problem is the high computational effort due to the large number of atoms within the unit cell. In case of Si(111), 98 atoms need to be included in the calculations just for the two top layers. After the new insight from STM imaging, a detailed model could be established called the dimer adatom stacking fault model (DAS) (see Figure 6.1) [104].

After this scientific breakthrough, research moved towards the Si(100) surface [105] promising innovations such as quantum logic gates [106] and molecule based electronics as future applications [10, 107]. Because of the state-of-the-art context of the Si(100) surface, in this thesis the latter was explicitly used for investigating the switching of a molecular latch (see Chapter 7).

Therefore, this chapter discusses the Si(100) preparation used to investigate the switching of ABP carried out in this work. For this purpose, superior surface quality regarding cleanliness and roughness is crucial. In the following, a preparation routine providing the needed surface quality is presented.
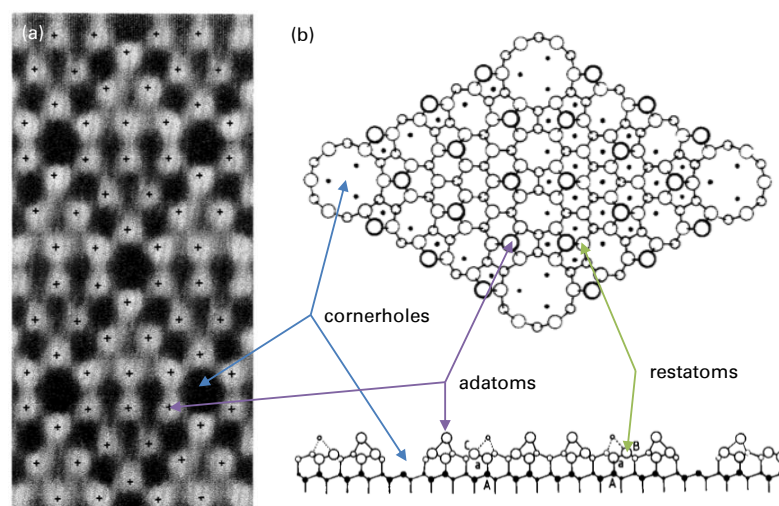
Figure 6.1 – (a) STM image of the Si(111)(7×7) reconstruction [47]. The cornerholes as well as the 12 adatoms per unit cell can be clearly distinguished in the image. (b) top and side view of the DAS model after Takayanagi [104]. The position of the restatoms and the underlying layers could be concluded from further TEM investigations.
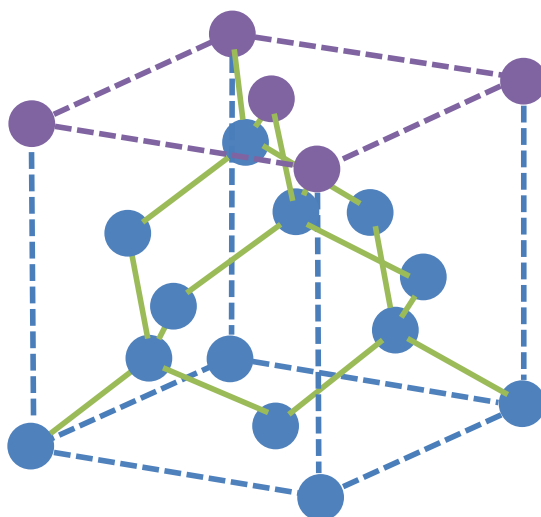
Figure 6.2 – Unit cell of the silicon crystal. One (100) facet of the diamond structure lattice is indicated in purple. The binding sites of the atoms within the unit cell are colored in green.

6.1 Si(100)(2×1) reconstruction

As each silicon atom has four bonding sites, it crystallizes in a diamond crystal lattice [77]. In Figure 6.2 the unit cell of the silicon crystal is shown. Atoms of one (100) facet are indicated in purple. If the periodicity of the crystal is broken by cutting the lattice along the (100) plane, two binding sites of each surface atom will be free and so-called dangling bonds will protrude out of the surface (see Figure 6.3 left). As unpaired electrons are energetically unfavorable, the surface atoms will bend to each other forming dimer rows and building a (2×1) reconstruction [108]. One dangling bond per surface atom will remain within the reconstruction. This is also illustrated in Figure 6.3. The surface atoms will relax further due to steric hindrance between the dangling bonds forming a (4×2) reconstruction.

The (4×2) surface reconstruction strongly depends on the temperature and the bias voltage during imaging with STM as the dimers flip with high frequency [109]. At room temperature and high bias voltages the dimer rows appear symmetric and a (2×1) reconstruction is observed [110]. At temperatures below 65 K and bias voltages near the gap a c(4×2) or p(2×2) reconstruction can be distinguished due to quenching of the dimer flipping [111].

6.2 Surface preparation and characterization

For the preparation of an atomically clean Si(100) surface, many different experimental techniques are available. The techniques vary from simple cleaving of silicon crystals and molecular beam epitaxy, to electron-bombardment heating and resistive heating of silicon wafers [112]. All techniques need to bear in mind the interlattice diffusion within the silicon crystal as well as the high reactivity at elevated temperatures. Therefore, the preparation of silicon is carried out in ultra-high vacuum. For the first aspect, the sample should be protected from transition metals like nickel or chrome as well as alkali metals like sodium. This means
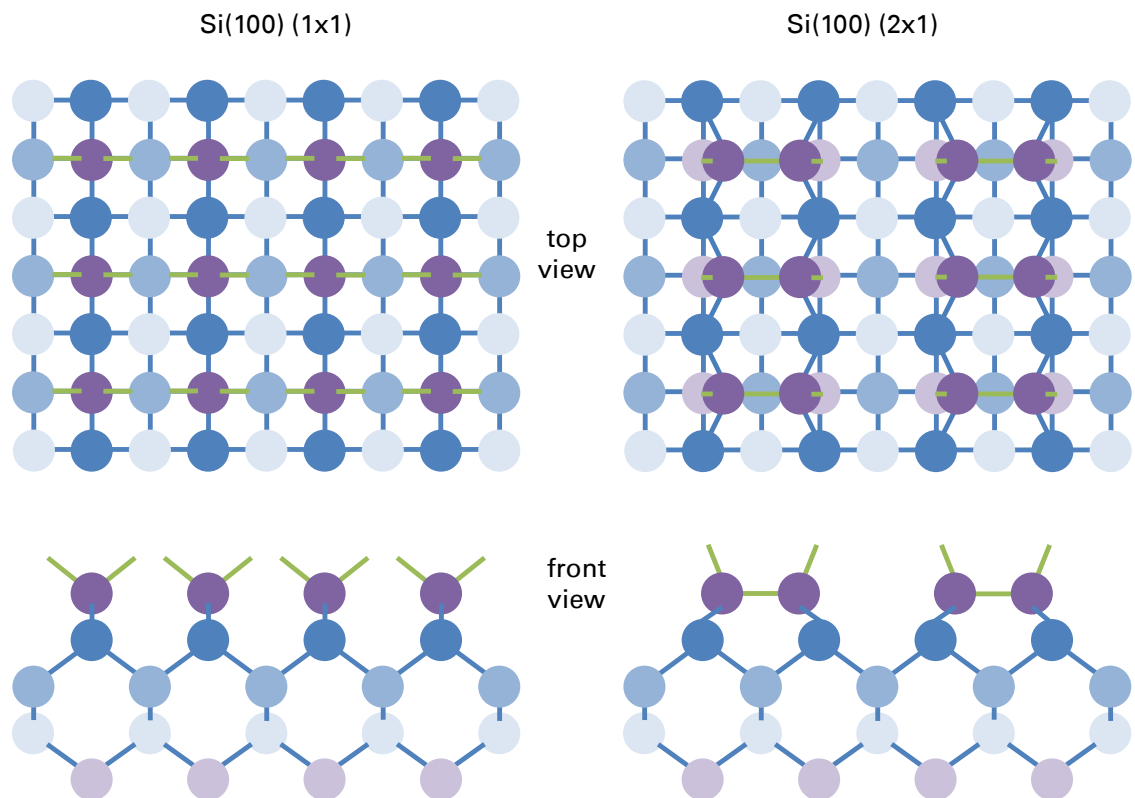
Figure 6.3 – Bulk terminated and reconstructed silicon (100) surface. The top-most surface atoms are indicated in purple (see also Figure 6.2), whereas the dangling bonds are hinted in green. Note the bending of the surface atoms.

Figure 6.4 – Silicon sample holder with mounted Si(100) sample.

a careful material selection of the sample holder as cabling and metal bodies tend to contain transition metals. Molybdenum has been proven to be the material of choice. Moreover, the instruments for mounting the sample should be coated with Polytetrafluoroethylene (PTFE). As most of the sodium within a laboratory is originated from perspiration and respiration, the sample should be particularly handled with care outside of the vacuum system. To avoid contamination of the sample due to the high-temperature reactivity, the base pressure of the vacuum system is conveniently kept under $1 \cdot 10^{-9}$ mbar.

The silicon sample preparation within this thesis was carried out in the already described ultra-high vacuum system (see Chapter 4) by means of resistive heating up to 1320 K. This represents a huge experimental challenge for the setup. To avoid the contamination of the surface during the preparation procedure, the base pressure of the system is about $7 \cdot 10^{-11}$ mbar and the pressure during the preparation was kept below $2 \cdot 10^{-9}$ mbar.

The sample holder for the silicon wafer is presented in Figure 6.4. Based on the sample holder principle described in Chapter 4, this high-temperature version makes use of molybdenum blocks and sheets for mounting the sample. As the cabling and electrical contact to the manipulator is realized by soldered copper wires, the sample holder has to be cooled with liquid nitrogen during high-temperature treatment to prohibit melting of the soldering points and the wires. For contact-free temperature measurements, an IS-12 pyrometer of LumaSense for semiconducting materials is used.

The silicon wafer for the samples was purchased from the Institute of Electronic Materials Technology in Warsaw [113]. The polished (100) wafers are n-type antimony doped with a specific resistivity up to 25 mΩcm. As the current feedthrough of the manipulator only allows currents up to 6 A, the thickness of the used wafers was chosen to be 380 μm to ensure high-temperature treatment.

The silicon preparation procedure is carried out as follows:

- **Mounting the precutted sample to the sample holder**. The molybdenum sheets should be pressed as hard as possible to the sample to ensure a proper contact for the resistive heating. The resistance between the heating contacts should be below 50 Ω. After the assembly the sample holder is cleaned in ultrasonic bath with first isopropanol and then distilled deionized water. Subsequently, the sample is transferred into the vacuum system.
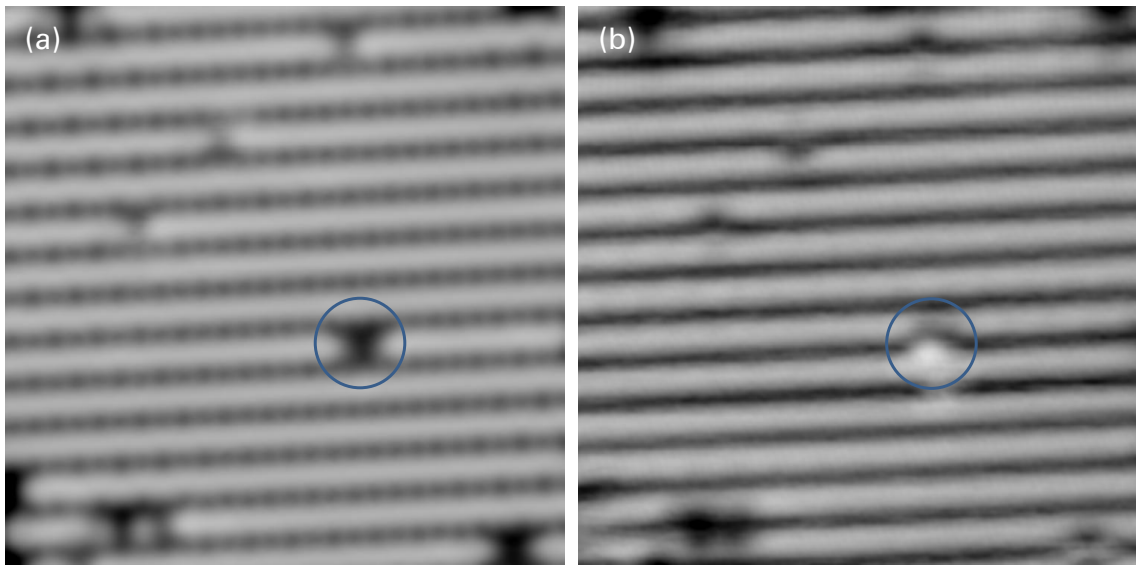
Figure 6.5 – Occupied (a) and unoccupied (b) states of a clean prepared Si(100) surface with (2×1) reconstruction. Note the differing appearance of the highlighted feature. Image parameters: (a) $V_{sample} = $ -2.1 V, I = 51 pA, $V_{sample} = $ 3.6 V, I = 40 pA, Image size = 10×10 nm^2

- **Degassing the sample**. To clean the sample and the sample holder from carbon contamination, the sample is annealed at about 1050 K until the pressure in the vacuum system returns to initial pressure. The sample holder has to be cooled during the whole preparation to avoid melting of the solder joints or the cabling.

- **Flashing the sample**. The sample is flashed up to 1320 K to remove the native oxide layer of the silicon crystal and to ensure a proper reconstruction. The formation of the reconstruction is also strongly dependent on the cool down rate. It should be about 2 K/s [114].

After preparation, the sample is transferred to the STM and cooled down to operating temperature.

For the characterization a metallic tip is used. A silicon coated tip leads to a broadening of the gap and a degradation of the resolution. More often imaging at one polarity of the bias voltage will not be possible. Changing the tip after sample contacts as well as regularly with each new sample is strongly recommended.

In Figure 6.5 images of the occupied and unoccupied states of a Si(100) sample prepared with the method described above are shown. Characteristic dangling bond rows of the (2×1) reconstruction can be observed. By comparison of the two images, the ability of STM to probe the local density of states becomes apparent. When imaging metals, areas of lower density of states (darker regions in the color code) correspond mostly to areas of lower topographic feature, like on a step edge. In case of semiconductors, features can appear lower (dark) because at the set bias voltage no tunneling is possible, whereas at a different bias the feature will appear high. In Figure 6.5(a) the highlighted attribute appears lower than
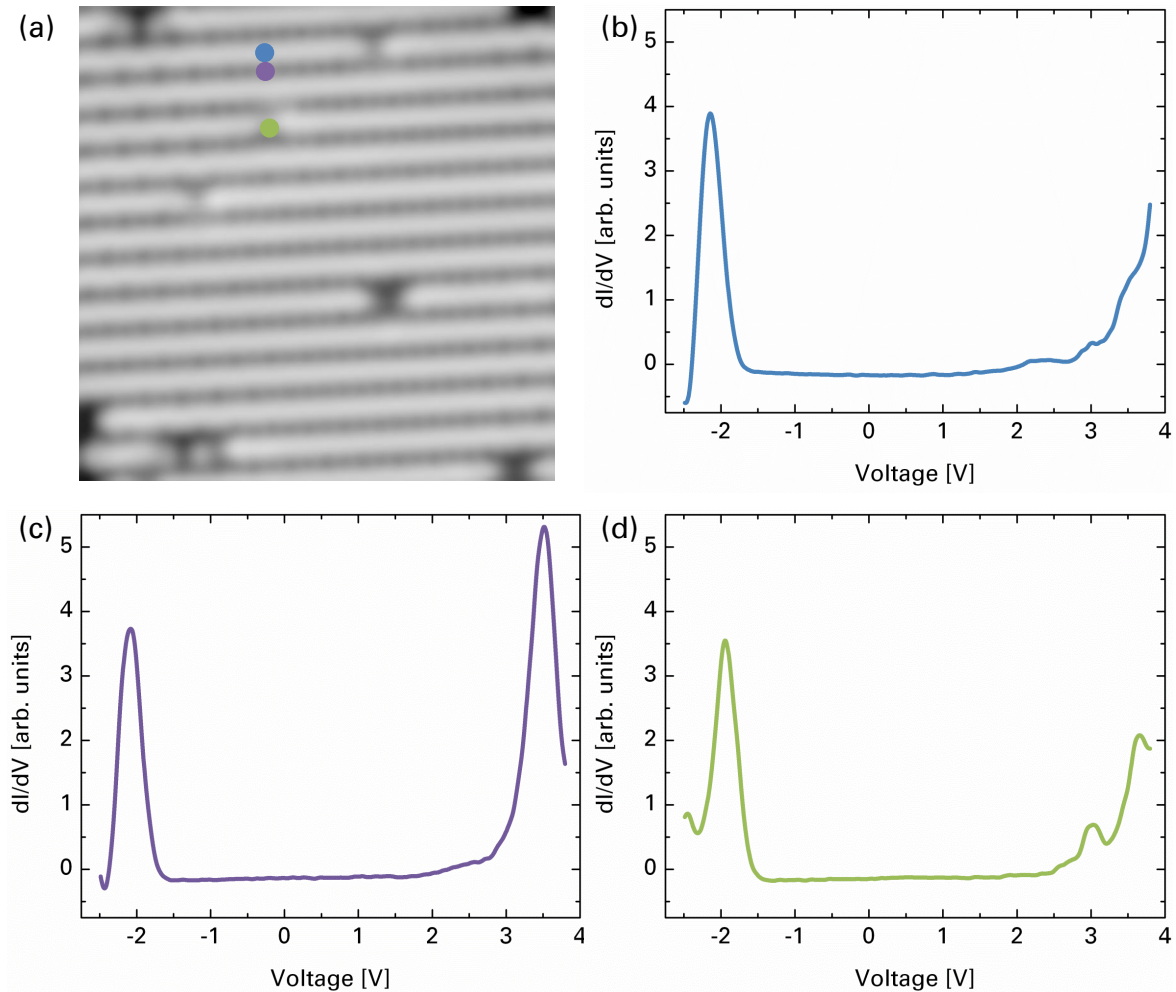
Figure 6.6 – Spectroscopic analysis of a cleanly prepared Si(100) surface with (2×1) reconstruction. Dots mark the position of the tip during the spectra according to the color code. (a) Image parameters: V_{sample} = -2.1 V, I = 51 pA, Image size = 10×10 nm^2, (b) Spectra taken on the dangling bond row (blue dot), (c) Spectra taken between dangling bond rows (purple spot), (d) Spectra taken on defect (green dot)

the surrounding silicon surface while in Figure 6.5(b) the feature protrudes from the surface. By further comparison, there seems to be a slight shift between the two images. As the images are taken within five minutes at a temperature below 6 K thermal drift can be ruled out. As mentioned before, below 65 K the surface is assumed to show a (4×2) reconstruction. As the images are taken at relatively high bias voltages, the dangling bond rows appear symmetric. Buckling can only be observed in the top left corner of Figure 6.5(a). Through imaging the occupied and unoccupied states of the silicon surface, the higher and lower part of the buckled dimer within the (4×2) reconstruction can be observed individually in the whole image [115].

Furthermore, the pristine (100) surface was characterized by means of scanning tunneling spectroscopy. The results can be found in Figure 6.6. Spectra were taken on and between the dangling bond rows as well as at a defect. The position and shape of the peak at about -2.1 V is similar for all three sites. Although the measured gap is about 3 V in each case, the shape of the peak on the positive voltage regime is differing. On the dangling bond row ((b),
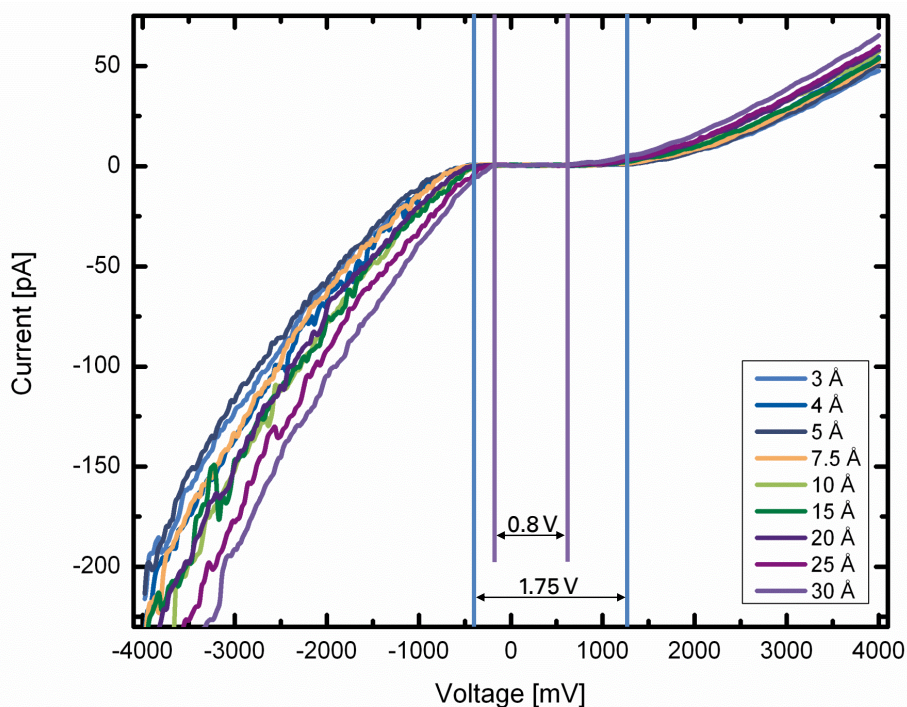
Figure 6.7 – Current-voltage characteristics as a function of tip-sample separation. The larger the tip displacement, the lower is the band gap. Band gap(30 Å)= 800 mV, band gap(3 Å)= 1750 mV

blue dot) the peak is very broad, whereas between the dangling bond rows ((c), purple dot) the peak is narrow and shifted to lower voltage values. In case of the defect ((d), green dot), the spectra shows two peaks. For (b) and (c) the shift of the peak can be explained by the energy split up of the buckled dangling bonds [115]. At surface defects the position of the peak shifts because of missing dimers. In the present case, this is a single dimer vacancy defect which means that two adjacent silicon atoms lying perpendicular to the dangling bond row are absent [116].

The size of the gap in the shown spectra is larger than the value given in literature of about 1.1 eV [77]. Although the band gap is dependent on doping level and temperature, the discrepancy is large. The large gap can be explained by a possible coating of the metallic STM tip with silicon. To prove this, a series of current-voltage characteristics of the silicon sample was taken for different tip-sample separations. The I-V curves are plotted in Figure 6.7. Here, the strong dependence of the measured band gap on the distance of the STM tip to the sample is evident [117]. For a small separation, this means a big offset of 30 Å, the gap is about 0.8 V. If the distance is increased by a factor of ten, the band gap can be measured to be 1.75 V. As most of the experiments were performed with a large tip-sample separation to prevent the tip from crashing the gap appears larger. This has to be taken into account especially when adsorbates should be analyzed. States could be present in the large gap and the particles could appear much smaller at the scanning bias voltage. Moreover, in case of the molecular latch it is possible that, even if the switching is successful, one conformation cannot be imaged at all, because the molecular states are present in the silicon gap.

7 ABP on Si(100)

One basic problem for the realization of an atomic circuit on silicon using dangling bonds is the finding of a suitable molecular latch (see Chapter 2). The function of the latch is to passivate and de-passivate a single dangling bond in order to open and close the circuit. The ideal candidate will consist of one part that binds strongly to the surface, the anchor group, and a second part that weak binds to the dangling bonds. Moreover, the weak bond needs to be broken and rebuild non-thermally to open and close the possible circuit. The switching of the optimal molecule has to be externally controlled and reproducible.

One promising archetype, acetophenone, consists of an acetyl group as an anchor group that binds covalently to the silicon surface, and one phenyl ring as a weak bond to the surface. This molecule has been thoroughly studied on Si(100) by STM [118–120]. However, considering possible surface leakage currents, the acetophenone molecule can be too small for a reliable latch. Moreover, preliminary experiments show that acetophenone cannot be controllably deposited on a surface in UHV conditions.

Another candidate is represented by ABP. The molecular structure is shown in Figure 5.1. Also in this case, the acetyl should work as an anchor group. One or both of the two phenyl rings should make the breakable surface bond. The interaction of this molecule with the Si(100) surface as well as its switching properties are described within this chapter.

7.1 Basic topography

An overview image of ABP on the Si(100) surface is shown in Figure 7.1. In addition to the target molecule and typical for a Si(100) surface, a variety of adsorbates with differing shape and size can be found. Moreover, the surface exhibits various depressions perpendicular to the (2×1) surface reconstruction. These are caused due to contamination of the substrate by transition metals like nickel [121].

Nonetheless, a sufficient number of ABP molecules are well deposited and can be imaged on the surface. Examples are highlighted using blue circles in Figure 7.1. The molecules always align along the (2×1) surface reconstruction rows in $\langle 110 \rangle$ direction revealing two distinct maxima.

To investigate the switching of the molecule for the latching effect, voltage pulses were applied. Figure 7.2 shows a cycle of reproducible switching events between two stable configurations of the ABP molecule on Si(100). The crosses within the images mark the position of the tip during the voltage pulse. The second stable configuration exhibits only one maximum, approximately at the position of the higher maximum of the first configuration. The second maximum appears as a shoulder in the linescan as shown in Figure 7.3. For
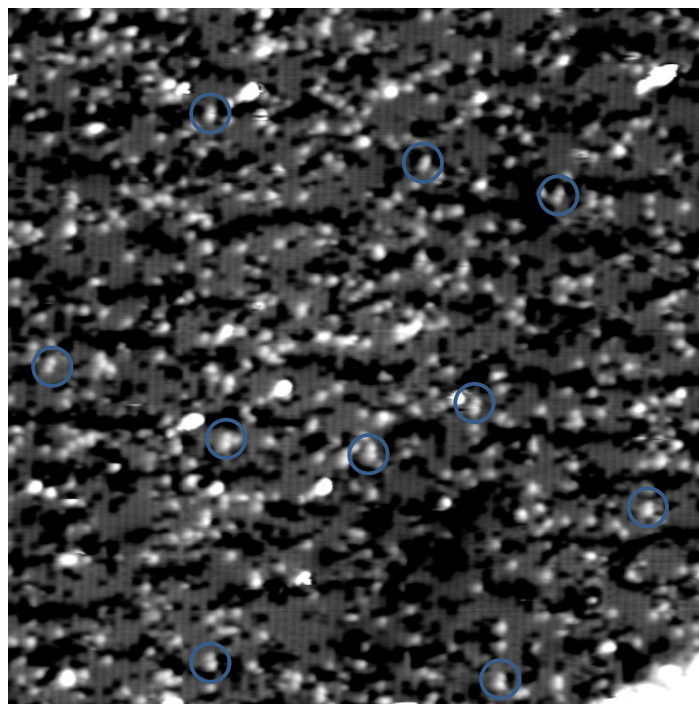
Figure 7.1 – Overview image of the silicon surface after the evaporation of ABP. Examples of molecules are highlighted by blue circles. Note that the molecules always adsorb along the (2×1) reconstruction. V_{sample} = -2.6 V, I = 33 pA, Image size = 80×80 nm^2.

simplicity, the conformation with one maxima is called "1" and the conformation showing two maxima "2".

After artificially producing conformation 1, voltage pulses were also applied to native features with only one maximum in the overview image (Figure 7.1). No switching could be achieved. This confirms the assumption that the molecules adsorb intrinsically in conformation 2. It can, however, not be excluded that few molecules in conformation 1 are also present on the silicon surface.

## 7.2 Calculations on conformation and energy barrier

To verify the ability of the ABP molecule to act as a molecular latch by passivating dangling bonds on the Si(100) reconstruction, density functional theory (DFT) calculations were performed by the theory group within the chair of materials science and nanotechnology [122, 123]. The results for the theoretical adsorption positions are shown in Figure 7.4. In both conformations the ABP molecule is bonded covalently to the silicon surface via the acetyl group as well as the first phenyl ring. These bonds represent the required anchor of the molecule to the surface. Conformation 1 corresponds to the depassivated position of the latch as only the anchor group is bonded. On the other hand, in conformation 2 also the second phenyl ring bonds covalently to the surface and blocks dangling bonds of the surface reconstruction. This conformation corresponds, consequently, to the passivated position of the latch. In this way, the reversible switching of the ABP has been demonstrated showing that the molecule works as a latch on Si(100).
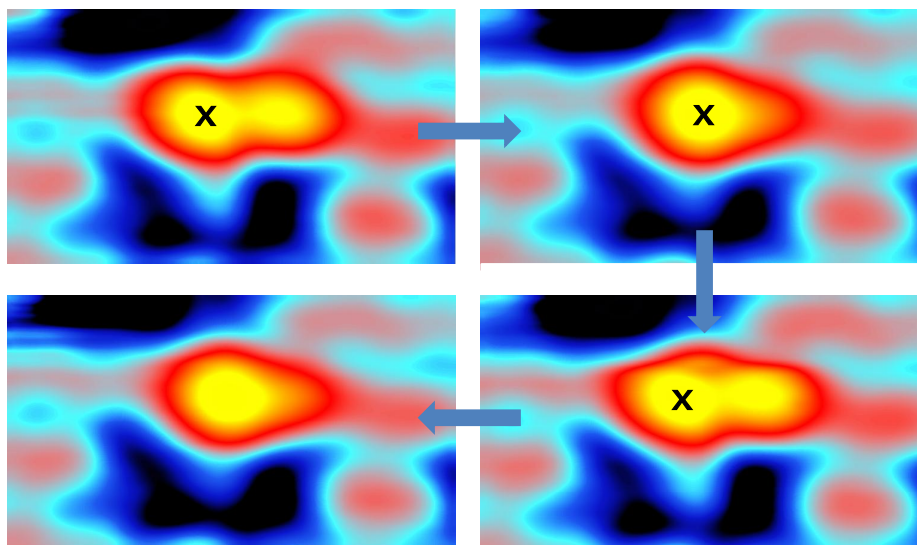
Figure 7.2 – STM images of the switching between two recurring conformations. The crosses mark the position of the tip during the voltage pulses.
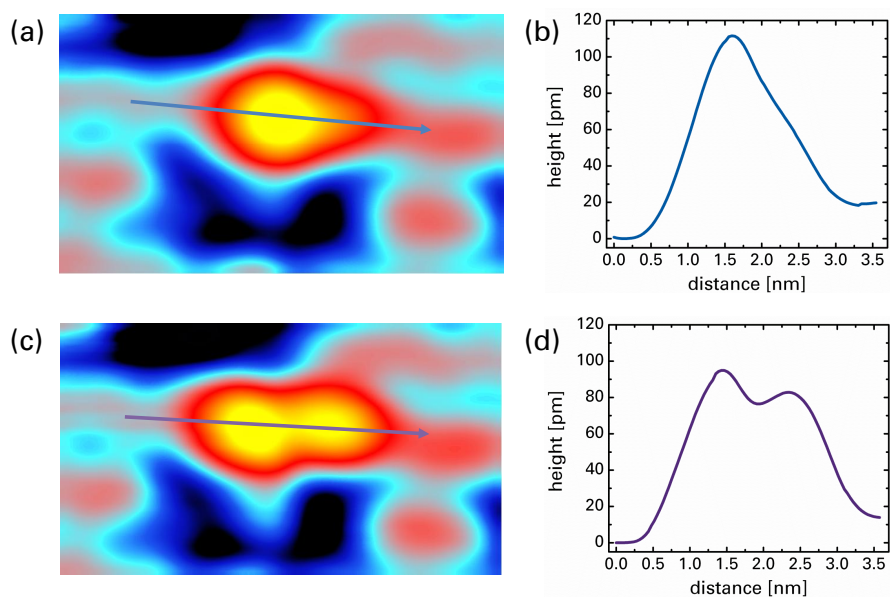
Figure 7.3 – STM images of the two conformations, (a) and (b), and the corresponding linescans, (c) and (d), respectively. The conformations are named after the number of maxima visible, 1 and 2, respectively.

Conformation 2   Conformation 1

side
view

top
view
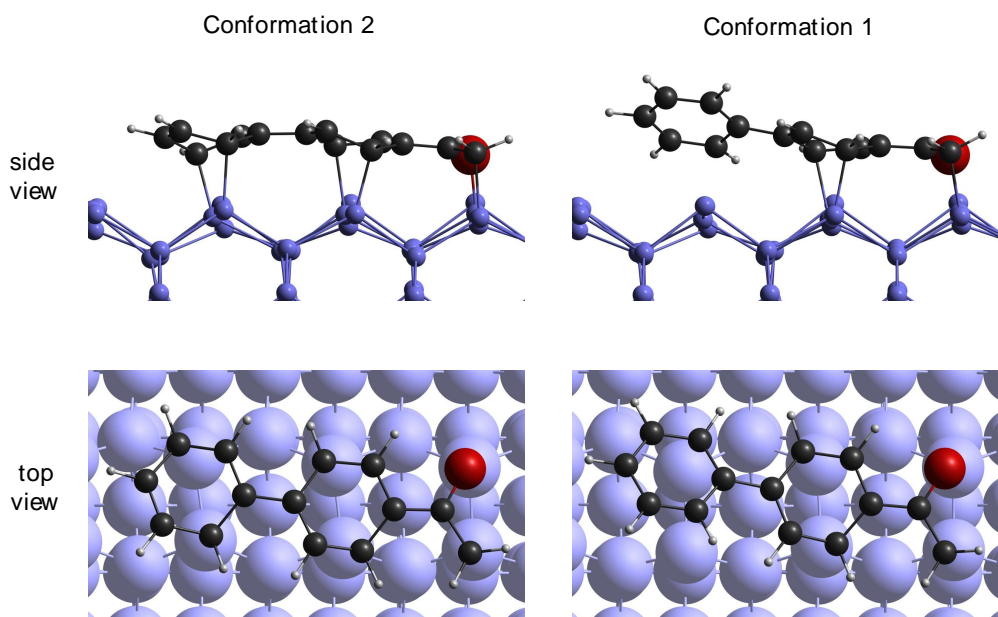
Figure 7.4 – DFT-calculated conformations of the molecular switch. In conformation 2 the anchor group as well as both phenyl rings bind to the surface. In the conformation 1 the bond of the second phenyl ring to the surface is broken and two surface atoms are depassivated.

As DFT is a ground state theory, DFT could not prove the switching path of the molecule from conformation 1 to conformation 2 and back. The switching is, as the following section will show, a result of excited electronic states.

However, the switching of ABP is possible because, as is supported by the findings of Patitsas *et al.* [124], a tunneling current can break the Si-C bond of adsorbates containing π bonds, whereas adsorbates consisting exclusively of saturated C-C bonds are entirely stable. The π bonds adsorb energy from scattered tunneling electrons, which can be selectively channeled into Si-C bond breaking. Specifically, the experiments of Schofield *et al.* [119] show the switching from a flat confirmation to an upstanding one using the example of acetophenone. Figure 7.5 shows the energy path for the switching of the ABP molecule estimated by nudged elastic band method [125], calculated by D. A. Ryndyk. The energy is related to the adsorption energy of the molecule to the surface and "n" counts the number of possible geometries of the molecule. The potential barrier between conformation 2, the passivating configuration, and conformation 1, the depassivating configuration, is about 0.6 eV. Moreover, conformation 2 is obviously the global minimum of the energy path and represents the naturally most favorable configuration as confirmed in the experiments. The switching of the molecule shows that the energy barrier is sufficiently small to be overcome by STM induced voltage pulses.
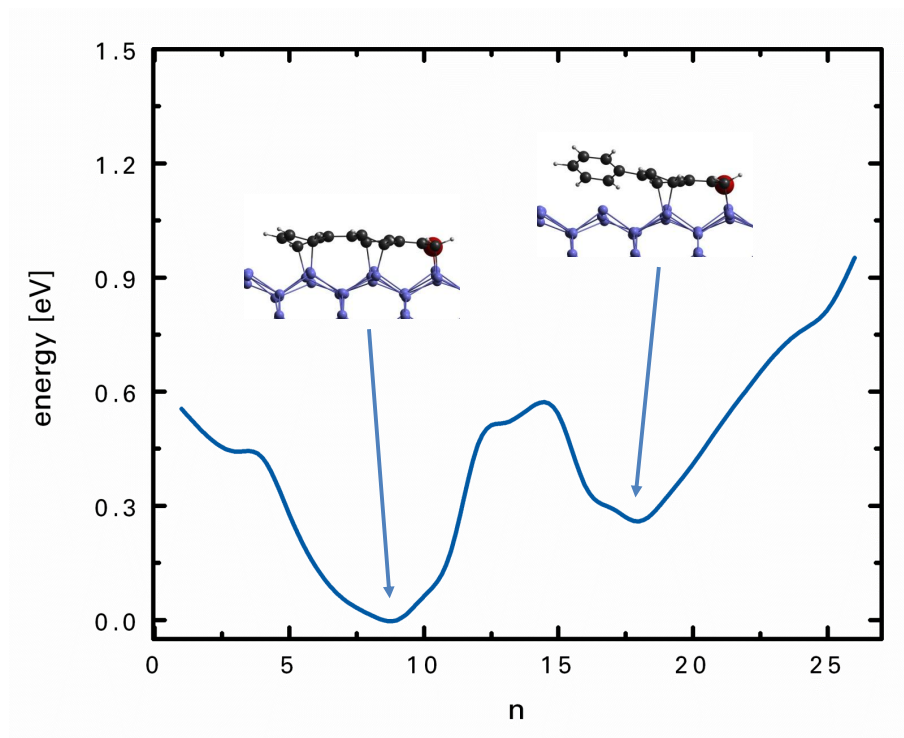
Figure 7.5 – Adsorption energies for 27 different adsorption configurations of ABP on Si(100). The potential barrier of 0.6 eV between configuration 1 and 2 can be overcome by STM experiments.
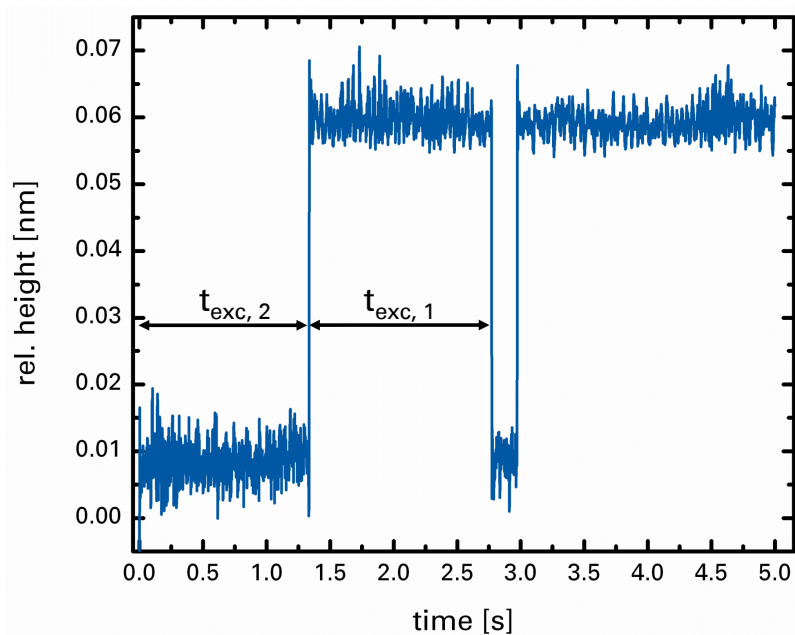
Figure 7.6 – Example of a tip-height trace during a voltage pulse on ABP on Si(100). The tip height switches between two distinct heights associated to the two conformations of the molecule. $t_{exc,n}$ are the time lengths the molecule spent in conformation 1 or 2, respectively, until it switched to the other conformation.

7.3 Switching

Controlling the switching of the molecular latch is one of the main goals of this thesis. To optimize the switching parameters, experiments were performed at different voltages and currents. During the voltage pulses, the current was kept constant and the tip height was recorded. A typical tip-height trace of such an experiment is shown in Figure 7.6. Through one voltage pulse of a typical time scale of 5 s multiple switching events can occur. A sudden jump in the tip height indicates a change of the conformation of the ABP molecule. As shown in the linescans of Figure 7.3, the apparent height of the molecule in conformation 1 is larger than in conformation 2. Therefore, the lower tip-height distance can be assigned to conformation 2, whereas the relatively higher distance attributes to conformation 1. The aspect ratio between both heights is about 1:10.

From the tip-height traces, the excitation times for both conformations were determined. The excitation time indicates the time interval until the molecule changes its conformation (see also Figure 7.6). For different bias voltage-tunneling current pairs, more than 5000 switching events were recorded and excitation times for each conformation measured. To obtain the average excitation time τ of one conformation at a given voltage and current the excitation times $t_{exc,n}$ were binned. The time bins are plotted against the particular number of events within the time bins. One example of a typical distribution of excitation times is shown in Figure 7.7. Here, a bias of -3.4 V and a current of 35 pA was applied and the time lengths were analyzed in which the molecule stayed in conformation 1. Well over 300 switching events contributed to this particular statistical analysis. As the molecule has no memory of the time spent in any particular conformation, the distribution is fitted to an exponential function

$$y(t) = const. \cdot e^{-\frac{t}{\tau}}$$

to acquire the average excitation time τ.

The inverse of the exponential time constant gives the switching rate, R, for the particular bias voltage and tunneling current. In Figure 7.8 the switching rate is plotted as a function of tunneling current at a voltage of -3.4 V. The blue line represents a least-square fit of the data and corresponds to the power function

$$R = const. \cdot I^{2.3 \pm 0.3} \ .$$

The exponent in this function is known to acknowledge the number of electrons that participate in the process [100]. Here, two electrons are necessary to excite the conformational change. This means that one electron excites the molecule during the voltage pulse, but the energy transfer in not enough to overcome the reaction barrier. During the lifetime of this first excitation, a second electron is needed to deposit enough energy to promote the molecule to a higher quantum state and to ensure the switching. This effect is known as vibrationally assisted ladder climbing [75].

From the average excitation time the switching yield Y, which is the probability of switching
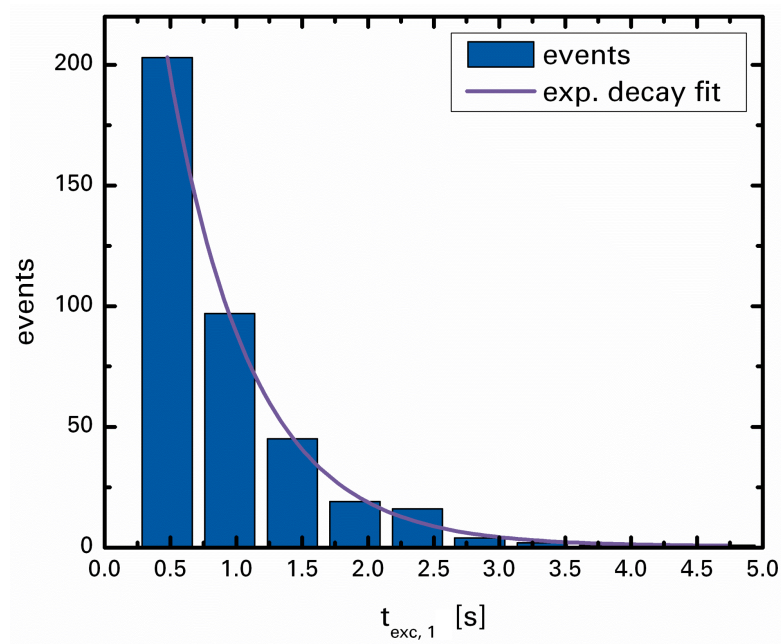
Figure 7.7 – Example of a distribution of t_{exc} during a voltage pulse of -3.4 V of the switch from state 1 to state 2. The number of events is summed up within time bins of about 0.5 s and fitted by an exponential decay function to obtain the average excitation time τ.
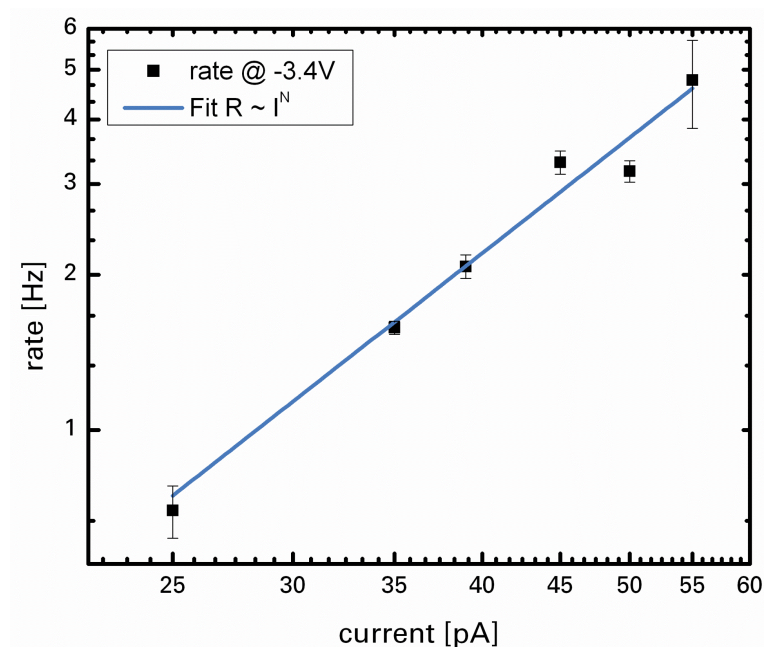
Figure 7.8 – Switching rate, R, as a function of tunneling current, I, for a bias voltage of -3.4 V. The blue line is a least-square fit of the data and corresponds to the power law $R \sim I^N$.

(a)

(b)
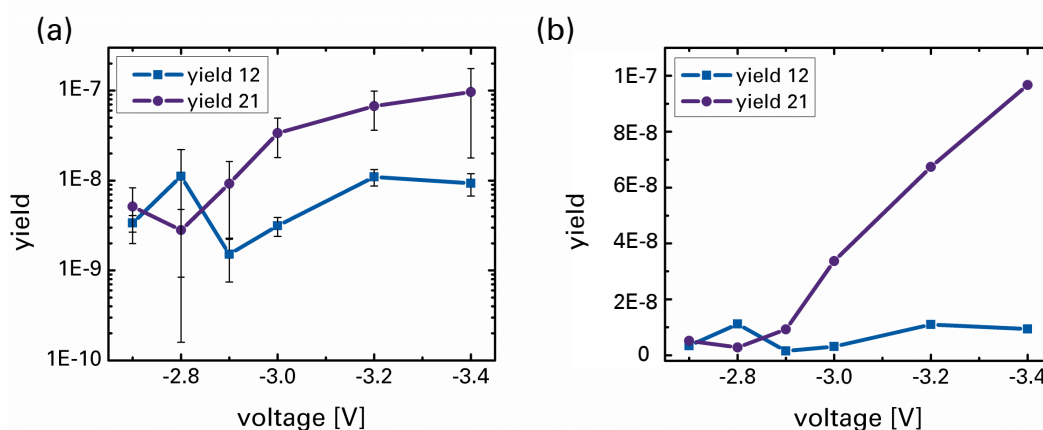
Figure 7.9 – Switching yield, Y, as a function of bias voltage. The blue data points belong to the switching from state 1 to state 2, whereas the purple data belongs to the switching from state 2 to state 1. (a) semilogarithmic scale, (b) linear scale.

per electron, can be obtained using the equation

$$Y = \frac{I\tau}{e} \; ,$$

where I is the tunneling current and e the elementary charge. The yield for both conformations is shown in Figure 7.9. The yield of the switching from state 1 to state 2, Y_{12}, is nearly independent from the bias voltage, whereas the yield for the reversed switch, Y_{21}, is increasing with the bias voltage. This different behavior can be understood as the following. To switch 4-acetylbiphenyl on Si(100) from conformation 2 to conformation 1, the bond between the second phenyl ring and the surface is cleaved allowing this ring to line up. Bond cleavage using STM has been shown for different systems with the common feature that the electrons have to tunnel resonantly in the molecule to overcome the dissociation energy [74, 126, 127]. Once the electron energy coincides with the energy level of the resonance, the probability for a switching event, Y_{21}, grows strongly (compare to Figure 5.14).The voltage for the yield onset of the switch agrees well with the bias value of Patitsas *et al.* [124], V_{Sample}=-2.7 V, if the temperature difference is taken into account.

For the reversed case of the switching from state 1 to state 2, the molecule has not only be flattened to the surface, but the reactive phenyl ring has to be aligned to the directional dangling bond of the corresponding surface atom for bond formation. For the bond formation, or association, using STM on metals the reported bias voltages are small (V_{bias}<1 V) [128, 129]. On Si(100) higher bias voltages (V_{bias}>2 V) have been reported for the flipping of acetophenone from one flat configuration to mirror symmetric one [119]. Although the flipping includes also bond breaking, this energy gives an upper limit and is therefore in agreement with the presented experiment.

7.4 Conclusion

In this chapter the switching of ABP on Si(100) is shown. Experimentally, the molecule can be transferred from the native, two-maximum conformation to a one-maximum conformation,

and back, by applying voltage pulses on top of the molecule. Density functional theory calculations confirm two adsorption geometries for the ABP molecule. NEB provides insight into the reaction barrier, which is sufficient small for a tip-induced switching. The statistical analysis of different molecules and tips indicates a two-electron process underlies the switching.

In this investigation, a molecular bidirectional switch on the ubiquitous silicon surface was observed for the first time. It is especially important that the molecule adsorbs along the dimer row of the Si(100)(2×1) reconstruction, so it passivates and de-passivates a dimer of a possible atomic wire perpendicular to the reconstruction on a hydrogen-passivated surface. This can lead to an inverter or a follower (see Chapter 2, Figure 2.1) and ultimately to logic gates on the atomic scale.

8 Further manipulation experiments: Lateral manipulation of a double-wheel molecule

In this chapter, the mechanics of a boron-subphthalocyanine double-wheel molecule adsorbed on Au(111) is described. The molecule is composed of two subphthalocyanine wheels connected by a carbon axis. Each wheel integrates an electronic tag (a nitrogen atom) which was designed to monitor the intramolecular rolling of the molecule. It will show that the molecule can be manipulated laterally with the STM tip in pushing and pulling mode (see chapter 3). Moreover, a different manipulation regime can be observed which is related to a rolling motion. The described results have been published in Anja Nickel, Joerg Meyer, Robin Ohmann, Henri-Pierre Jacquot de Rouville, Gwenael Rapenne, Francisco Ample, Christian Joachim, Gianaurelio Cuniberti, and Francesca Moresco, *STM manipulation of a subphtalocyanine double-wheel molecule on Au(111)*, J. Phys: Condens. Matter **24** (2012) 404001.

8.1 Introduction

Understanding the motion and the intramolecular mechanics of a single molecule on a surface is of great importance for the development of mechanical molecular machines [130]. In the last few years, several examples of molecular mechanical machines have been demonstrated including molecular gears [54, 55, 131], motors [56, 57, 132, 133], wheels [134], and different kinds of nanovehicles [58, 59, 135, 136]. Moreover, the manipulation of a molecule with the tip apex of a scanning tunneling microscope has become a well established technique to study the mechanics of a single molecule on a surface [51]. The basic principles for manipulation of single atoms or molecules can be found in section 3.4.1. In addition, detailed information on the manipulation process can be found in the tip height traces recorded during the manipulation.

The STM manipulation signal for molecules is normally more complex than for single atoms or small molecules like CO, especially when the mechanical internal degrees of freedom of the manipulated molecule play a role. For example, and in addition to a rigid like lateral-type motion on the surface, intramolecular conformation changes can be induced during the manipulation [137]. Normally, manipulation signals for complex molecules do not show the regular periodic modes over long periods observed for single atoms and small molecules. Changes from one mode to another during manipulation are often observed. In some cases, manipulation signals do not present any periodicity and the peaks are irregular in intensity,
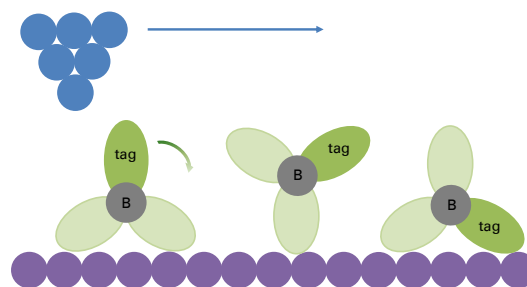
Figure 8.1 – Schematic idea of the experiment. By rolling the molecule, the position of the tag changes, influencing the apparent height of the molecule wheels in the STM images.

length and shape [138]. Molecular flexure and reorientation of the internal conformations play a major role, as well as the reorientation of the molecule relative to the surface [51,138]. The large interest in the development of nanovehicles which can be driven by molecular manipulation has recently stimulated the design and synthesis of molecules that mimic macroscopic machines, transposing mechanical functions at the scale of a single molecule [139]. The control of complex functions at the molecular scale and the design of appropriate molecules are, however, still very challenging.

The basic movement of vehicles is the rolling on a surface. In recent years, a rolling of a double-wheel molecule which was composed of two triptycene wheels connected by a carbon axle was shown [134]. By careful analysis of the manipulation signal, the rolling of the wheel was concluded. As the interpretation of the tip height traces is very challenging it would be more convenient to conclude the basic operation not only from the manipulation signal, but also by comparing the initial and final STM topographic images. Therefore, a double-wheel molecule was synthesized to control a complete rolling motion at the atomic scale. To allow the detection of the rolling electronic tags (nitrogen atoms) were added to the molecular wheels.

The idea of the experiment is schematically shown in figure 8.1. In the topographic STM images, the position of the tag can be determined by measuring the apparent height of the corresponding wheel. By lateral manipulations, the double-wheel molecule can be moved along the surface, mostly showing STM feedback loop manipulation curves which are similar to the curves observed for rigid molecules and single atoms. In a few cases, a different STM feedback loop manipulation signature is observed and the rolling of a wheel confirmed by a change in the position of the tag.

8.2 Experimental details

The double-wheel molecules (Figure 8.2) were evaporated from the molecular evaporator for 2 min at a temperature of about 420 K onto the clean Au(111) surface kept at room temperature. As the molecules are expected to be relatively unstable against heat and light intensity, the evaporation temperature was kept as low as possible. After evaporation, the sample was transferred immediately into the STM to minimize thermal and light induced
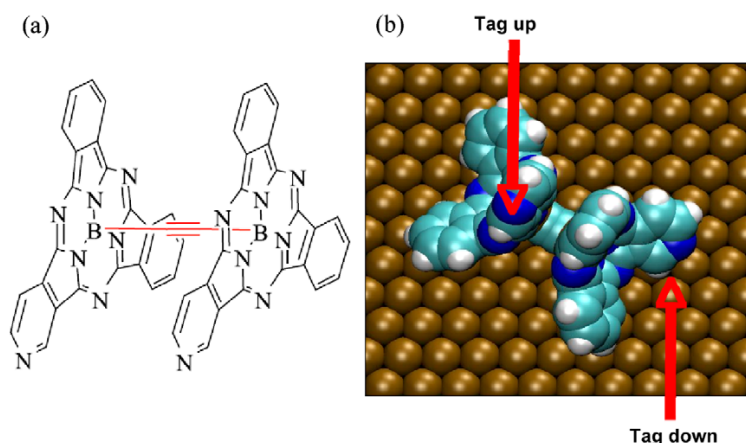
Figure 8.2 – (a) Chemical structure of the double-wheel molecules. (b) Optimized conformation of the double-wheel molecules adsorbed on an Au(111) surface using the semi-empirical ASED+ calculations [140] indicating one among many possible positions of the nitrogen tags.

dissociation. Because the molecules are very mobile on the surface, low tunneling currents (I=20-50 pA) and bias voltages (V_{sample} = 0.1-0.5 V) were used to image the molecules. Lateral manipulations were performed in constant current. A STM tunneling resistance of some MΩ corresponding to a tip height of a few Å above the surface was sufficient to move the molecule in a controlled way. The double-wheel molecules consist of two subphthalocyanine molecules connected by a linear 2-carbon (acetylenic) axis. The molecules were synthesized in the group of G. Rapenne at CNRS, Toulouse (France). The details of the synthesis process are described elsewhere [141].

The chemical structure is presented in figure 8.2 together with the optimized conformation of a double-wheel molecule adsorbed on an Au(111) surface using the semi-empirical ASED+ calculations performed in the group of C. Joachim at CNRS, Toulouse (France) [140]. The additional nitrogen on one of the three subunits of a subphthalocyanine wheel can be considered as a tag because it brings $\pi*$ orbitals per wheel in the electronic gap between the highest occupied molecular orbital (HOMO) and the lowest unoccupied molecular orbital (LUMO) of the molecule. This state can be imaged differently depending on whether the nitrogen is close or far away from the surface. It was designed to monitor the rolling motion in the STM topographic images.

8.3 Imaging the molecular tag

Despite all caution, the molecules do not stay intact through prolonged storage. However, the imaging of the decomposed molecular wheels shows the successful synthesis of the nitrogen-tagged subphthalocyanine molecules. In figure 8.3 a topographic STM image of the mono wheels is shown. The imaging proves to be very difficult as half of the fragments remain very reactive after the breaking. However, the asymmetric triangular shape of the wheels is visible. One of the angles of each wheel appears higher than the other two subunits indicating the position of the nitrogen tag (vs. [142]).

The adsorption of the well-stored and fresh double-wheel molecules on Au(111) with the in section 8.2 reported conditions leads to a submonolayer coverage, where single molecules are uniformly distributed on both fcc and hcp domains, while defects and molecular fragments occupy the elbows of the herringbone reconstruction (figure 8.4). No preferential orientation
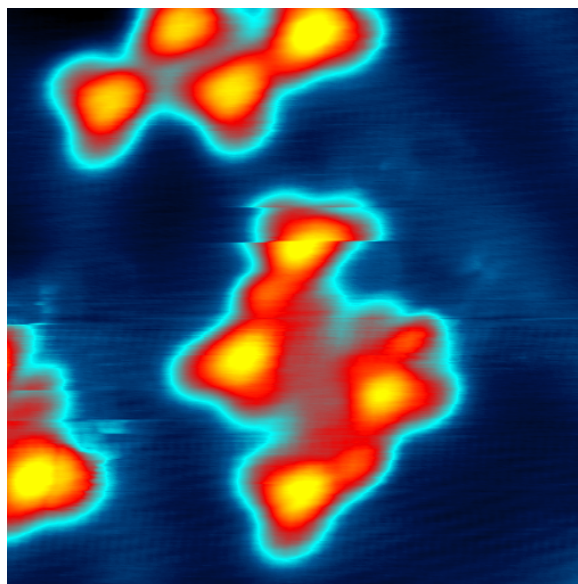
Figure 8.3 – STM image of the decomposed molecular double wheels. Note the asymmetric triangular shape of each wheel. Tunneling parameters: $V_{sample} = 0.054$ V, I = 50 pA. Image size = 8.3×8.3 nm^2.
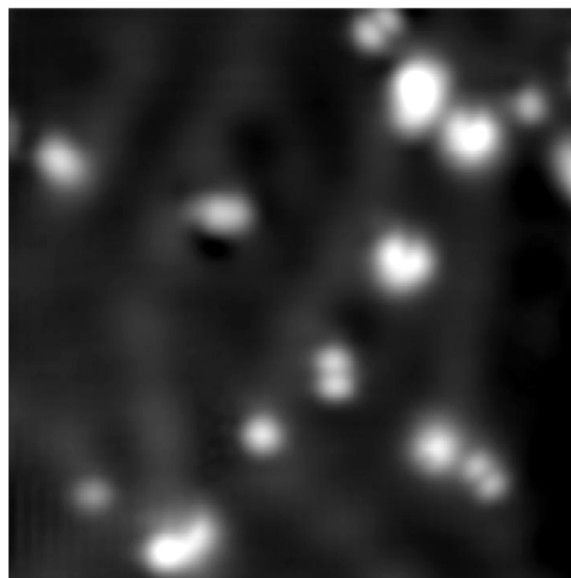

Figure 8.4 – Overview STM image showing several adsorbed double-wheel molecules with different orientations. Defects and molecular fragments are also visible on the surface. Tunneling parameters: $V_{sample} = 0.12$ V, I = 20 pA, Image size = 13.4×13.4 nm^2.

of the molecule was observed in the STM images. In Figure 8.5, STM images of the single molecules and the corresponding linescans along the wheel axis are presented. The double-wheel molecules typically show two lobes corresponding to the two subphthalocyanine molecule wheels. As one can see, the complete molecule has a total apparent length of about 15 Å. Two slightly different conformations, present in almost equal amounts on the surface, are observed. In the first one (Figures 8.5 (a) and (b)) the wheels appear parallel and have an apparent height between 0.7 Å and 0.9 Å. In the second case (Figures 8.5 (c) and (d)), the double-wheel molecule is slightly asymmetric and shows an apparent height between 0.9 and 1.15 Å. For both conformations, we ascribe the different apparent height of the lobes to the different position of the tag, where the highest wheel corresponds to the tag near to the upper position and the lowest one to a tag close to the surface. To confirm this interpretation, a representative constant current STM image had been calculated using one among many of the minimum energy conformations of the double-wheel molecule adsorbed on the Au(111) surface. In this specific case, a molecule with a tag up and a tag down
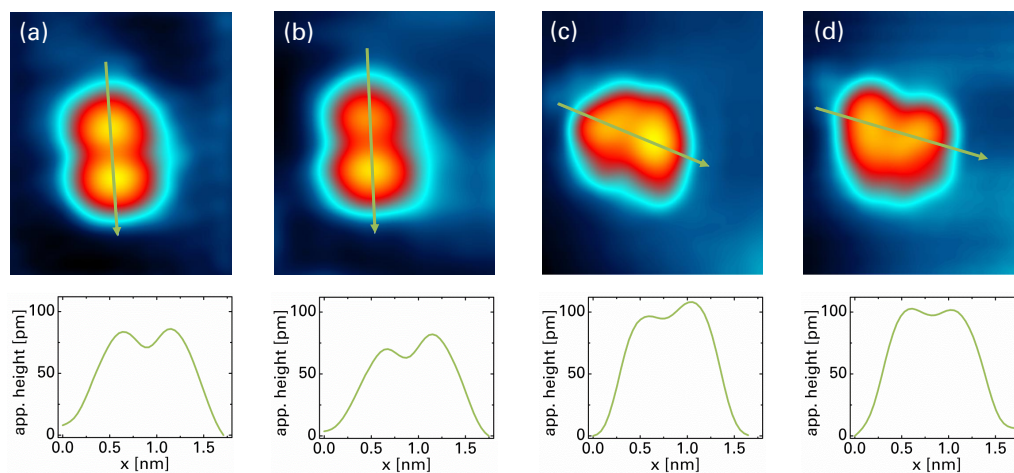
Figure 8.5 – STM images and corresponding linescans of a given double-wheel molecule on the Au(111) surface. The molecules show two lobes, each lobe corresponding to a single wheel. Tunneling parameters: (a) and (b) $V_{sample} = 0.08$ V, I = 35 pA; (c) and (d) $V_{sample} = 0.01$ V, I = 50 pA. Image size = 2.3×2.7 nm^2
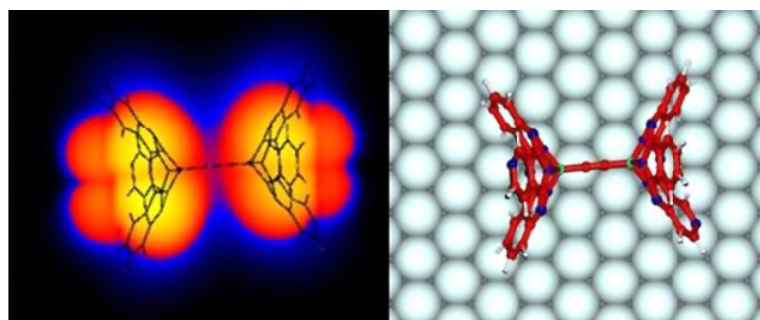
Figure 8.6 – ESQC calculated STM image of the double-wheel molecule adsorbed on an Au(111) surface with one tag up and one tag down. The selected molecular conformation, optimized by ASED+, is also presented. Image size: 2 nm $\times$ 2.5 nm, voltage bias 0.12 V and feedback loop set up current 20 pA. Notice the tip facet effect indicated by the two small bumps before and after the molecular skeleton. The wheels are quite high on the surface and are creating a lateral interaction between the facet of the tip and the molecule introducing a tunnel current far before the end atom of the tip apex reaches a wheel.
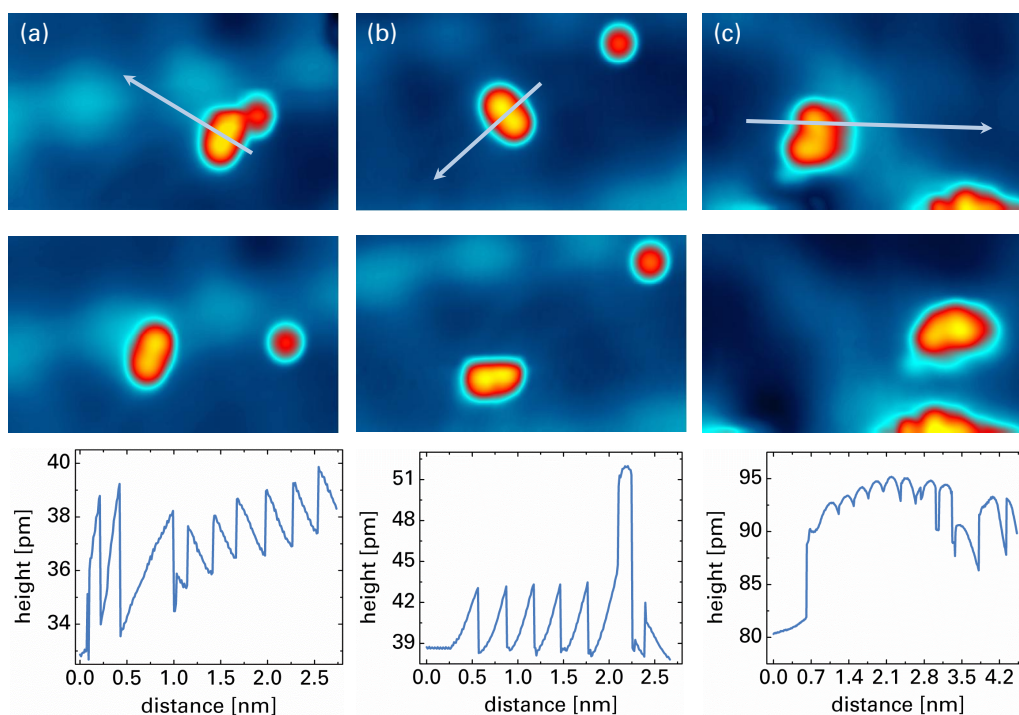
Figure 8.7 – Examples of lateral manipulation of a double-wheel molecule. Upper panel: STM images before the manipulation; central panel: STM images after the manipulation; lower panel: manipulation curves as described in the text. The arrows indicate the manipulation path. Different manipulation modes could be observed: (a) pulling mode, (b) pushing mode, and (c) sliding mode. The small fragments on the surface can be used as reference for the movement of the molecule. The bright structures in the background are due to the herringbone reconstruction of the Au(111) surface. Tunneling parameters: (a) and (b) $V_{sample} = 0.08$ V, I = 35 pA; (c) $V_{sample} = 0.01$ V, I = 50 pA. Tunneling resistance for lateral manipulation R = 6 MΩ. Image size = 6.0×3.6 nm^2

was considered. This conformation is shown in figure 8.6 together with the corresponding calculated STM image. Since the tip apex used in those ESQC calculations are perfect (111)-like facets with a single end gold atom, the calculated image shows a stronger internal contrast as compared with the experimental ones. The effect of the nitrogen tag is clearly visible in the calculated image. As already observed in [55], the electronic effect of the nitrogen tag is not exactly localized at the position of the nitrogen atom in the molecular structure. The tunneling current captures the tunneling channels introduced by the molecular electronic states. Those states do not necessary have their maximum weight at the exact position of the nitrogen atom.

8.4 Manipulation and rolling

A chosen double-wheel molecule was manipulated with the STM tip in constant current mode by pushing it with the tip along one wheel (8.1). Because of the high mobility of these molecules on the Au(111) surface, a tunneling resistance of about 4 MΩ was sufficient to move a double-wheel molecule along the surface.

As shown in the examples of Figure 8.7, the molecule can be rigidly manipulated from one
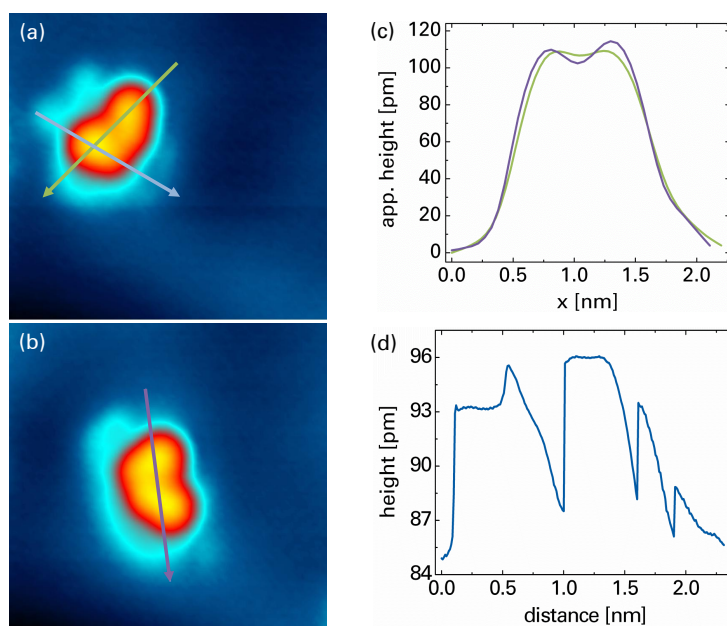
Figure 8.8 – Example of lateral manipulation with rolling of a double-wheel molecule. (a) STM image before the manipulation (the black arrow indicates the manipulation path); (b) STM image after the manipulation; (c) linescans over the line indicated by green and blue arrows in (a) and (b) showing the change in apparent height of a wheel after the manipulation; (d) corresponding manipulation curve. Tunneling parameters: $V_{sample} = 0.01$ V, I = 50 pA. Tunneling resistance by lateral manipulation: R = 4 M. Image size $= 3.7 \times 3.5$ nm^2

adsorption site to the next one without any apparent changes in the position of the tag. Depending on the manipulation parameters and on the tip apex shape, feedback loop STM manipulation curves have been recorded, which are typical for a partial pulling (Figure 8.7(a)), pushing (Figure 8.7(b)), or sliding mode (Figure 8.7(c)) of the double-wheel molecule [50]. In all cases, those manipulation signals show a periodic part with a periodicity of about 3 Å. This corresponds to the average atomic distance on the Au(111) surface [78] and indicates the rigid jumping of the molecule from one adsorption site to the next. Before or after the periodic signal indicating a simple translation, a non-periodic trace in the manipulation curve can be observed. This indicates a change in the adsorption orientation of the molecule on the surface after the manipulation experiment, as confirmed by the changed orientation of the molecule in the STM image after manipulation. The same manipulation signal is often not maintained through the whole path and many combinations of pushing, pulling, sliding, and planar reorientations have been observed. In particular, as shown in the example of Figure 8.7(a), after a short pushing manipulation sequence, the molecule is pulled by the tip. On the other hand, in the second example (Figure 8.7(b)), the pushing mode ends with a reorientation of the molecule on the surface followed by a short pulling. In Figure 8.7(c) and after a sliding-like manipulation sequence, the double-wheel molecule rotates laterally and is afterwards pulled by the tip. In all described cases, the apparent height of the lobes remains unchanged during a manipulation sequence, as can be quantitatively confirmed by comparing the line scans over the molecule. Those manipulation signals indicate that no

rolling of the wheels takes place here, as the Au(111) surface is generally too flat to facilitate the intramolecular rolling of a double-wheel molecule.

In a few cases, however, the successful rolling of a double-wheel molecule on the Au(111) surface over a short path was achieved. In those cases, as shown in the example of Figure 8.8, the manipulation curves present wider non-regular peaks and the apparent height of one lobe is changed after the manipulation. As can be clearly seen in the line scans recorded over the wheels before and after a manipulation (Figure 8.8(b)), the two lobes of the molecule have the same apparent height before the manipulation, while one of the lobes appears about 6 pm higher than the other after the manipulation. This change in the apparent height of the molecule in the STM image represents the signature of an intramolecular rolling of one of the wheels, with the consequent change in the position of the tag to the upper position. However, less information can be extracted from the manipulation curve in this case (Figure 8.8(d)), because a planar rotation of the molecule on the surface accompanies the rolling of the molecule, making a straightforward interpretation of the STM feedback loop signal difficult. In the example of Figure 8.8, after a rolling and then a possible reorientation on the surface, the molecule is finally pulled by the tip, jumping over a further two adsorption sites, as shown in the last part of the manipulation curve (Figure 8.8(d)).

8.5 Conclusion

In this chapter the lateral manipulation of a double-wheel molecule was shown. The wheel was equipped with nitrogen tags to distinguish between conventional manipulation and rolling motion not only from the manipulation sequence but from the change in the topographic images. The presence of the tags could be shown in the asymmetric fragmented molecules as well as in the linescans of intact double wheels.

In most cases, the molecules were moved rigidly over the surface, resulting in pushing pulling and sliding of the wheel. In few cases, rolling could be achieved, monitored in a different tip height trace during the manipulation and a change in the apparent height of the molecules.

9 Conclusion and outlook

The aim of this thesis was the fundamental investigation of a promising molecular candidate, 4-acetylbiphenyl (ABP), as a potential candidate for a molecular latch on a passivated silicon surface.

The idea of atomic-wire circuits on hydrogen-passivated silicon and the need for a molecular latch is explained in Chapter 2. Here, it is described in detail how atomic wires can be built on passivated semiconductors with emphasis on the Si(100) surface. The wires are fabricated by extraction of a line of single hydrogen atoms parallel and perpendicular to the dimer rows of the (2×1) reconstruction, respectively, creating so-called dangling bonds. The dangling-bond wires show for each direction a different electric behavior due to the different intra-dimer and inter-dimer coupling as well as a distinct dependency on the local chemical setting. Dangling-bond wires parallel to the dimers of the reconstruction reveal a metal-like electron transport and are insusceptible to local surface changes, whereas in the perpendicular arrangement the conductivity is lower and the dependence on the local chemical setting is high. This leads to the possible application of perpendicular dangling-bond wires as atomic switches. Their conductivity changes dramatically by changing the position of a few dangling bonds, for instance by passivating or depassivating dangling bonds next to the atomic wire using a molecule. Atomic logic gates can be build from inverter and followers that could replace existing devices of today's semiconductor industry. At the end of the Chapter 2, a short overview is given for the technical realization of such switches using interconnection machines.

For the development of planar atomic-scale electronics, the use of a scanning tunneling microscope (STM) proves to be essential. Therefore, Chapter 3 showed the theoretical basics of STM as well as the different mechanisms behind tip-induced manipulation on conductive surfaces.

The experimental setup as well as the used ultra-high vacuum system used in this thesis was described in Chapter 4. The UHV system has a base pressure below $7\cdot10^{-11}$ mbar, has a coolable manipulator and the STM is operated at 5 K. These present optimal parameters to prepare clean metallic and semiconducting surfaces with sub-monolayer coverage of functional molecules. Moreover, the low-temperature operation allows single-molecule manipulation.

From just being preliminary preparation tests for the candidates of molecular latches, ABP showed interesting and relevant results on the Au(111) surface. The molecules self assembled on this surface into groups of three or four molecules. The predominant structure of the tetramers was windmill-like, whereas the trimer groups could be observed as a Y-like, windmill-like or triangular structure. All structures were non-covalently bond. Due to the fragile nature of non-covalently bound supramolecular structures traditional lateral manipulation

is not preferable. Therefore, as shown in Chapter 5, supramolecular assemblies were moved controllably by applying voltage pulses. All but the triangular structure could be moved, when a voltage pulse was applied above one of the molecules within the structure. Depending on the tip polarity, the assemblies moved towards to or away from the tip. The statistical analysis proved an underlying one-electron process as well as a yield contingent on the electronic structure of the nanostructures. These findings represent a novel procedure to gently and purely electronically manipulate individual nanostructures to desired positions on the surface. Therefore, a new route for the construction of artificial molecular devices could be opened. As in the bottom-up approach, devices have to be built by self assembly the order and complexity is confined by chemistry. With the procedure shown in this thesis, small, well ordered structures can be self assembled and then brought together with the help of STM. This is useful especially for future nanoelectronics, where uniformly covered or patterned surfaces are not feasible. In this scenario molecular devices can be transported to their respective contact points. Another application of the tetramer nanostructures can be for a molecular motor to transport single atoms or small molecules.

Moving towards a possible implementation of devices within the present information technology, Chapter 6 showed the development of a standard procedure for the preparation of Si(100) within the used UHV system. In addition, the resulting (2×1) reconstructed Si surfaces were characterized topographically and spectroscopically. The next step would be the development of a procedure for hydrogen passivation of silicon. Passivated silicon is less susceptible to contamination and the perfect basis for in-built nanowires or dangling-bond wires.

In Chapter 7, the switching of ABP was proven on Si(100). One conformation of the molecule could be observed on the surface. By applying voltage pulses on top of the molecule, a second conformation was created. Reproducible switching was observed between both conformations. Density functional theory and nudged elastic band method confirmed two conformations, where one is covalently bound to the surface via the acetyl group and the first phenyl ring and the second conformation is in addition bound to the second phenyl ring. The statistical analysis of the switching process reveals an inelastic electron process for the conformational change. The yield analysis indicates different dependencies for the two transitions. The shown experiments represent the first reproducible molecular switch on the Si(100) surface. As the molecule adsorbs along the dimer rows, it exhibits the perfect geometry for the latching of a dangling-bond wire perpendicular to the (2×1). The described experimental work opens new ways to develop atomic-scale logic gates and circuits, which can be an alternative to existing microelectronic devices. Further experiments are now needed to combine the ABP switch with dangling-bond wires and logic gates on hydrogen-passivated Si(100). Thereby, the latching effect could be demonstrated on a complete dangling-bond circuit.

The lateral manipulation of a double-wheel molecule with nitrogen tags on Au(111) was shown in Chapter 8. Whereas in most cases the subphthalocyanine molecules can be moved rigidly, in some cases rolling could be observed. The rolling motion was deduced from the change of the position of the nitrogen tags on the wheels. By measuring the apparent height

of the corresponding wheel in the topographic STM images the position of the tags could be monitored. A further evidence for the rolling can be found in the manipulation curves. Whereas the rigid movements can be assigned to the well known pulling, pushing, and sliding modes, the curve is characteristically different. As these experiments are carried out on the flat and inert Au(111) surface, future experiments should be carried out on corrugated surfaces which would favor intramolecular rotation. After the prove of principle of the subphthalocyanine nanowheels, new nanovehicles can be designed with an underbody of this wheels. The ultimate goal is to assemble nanorobots able to transport single atoms or atomic groups to predestined places on a surface.

Publications

Publications in peer-reviewed journals

A. Nickel, R. Ohmann, J. Meyer, M. Grisolia, C. Joachim, F. Moresco, and G. Cuniberti, *Moving Nanostructures: Pulse-Induced Positioning of Supramolecular Assemblies*, ACS Nano **7**, 191-197 (2013)

A. Nickel, J. Meyer, R. Ohmann, H.-P. Jacquot de Rouville, G. Rapenne, F. Ample, C. Joachim, G. Cuniberti, and F. Moresco, *STM manipulation of a subphthalocyanine double-wheel molecule on Au(111)*, Journal of Physics: Condensed Matter **24**, 404001 (2013)

J. Meyer, *A. Nickel*, R. Ohmann, Lokamani, C. Toher, D. A. Ryndyk, Y. Garmshausen, S. Hecht, F. Moresco, and G. Cuniberti, *Tuning the formation of small coordination nanostructures on a gold surface*, Chemical Communications **51**, 12621-12624 (2015)

R. Ohmann, J. Meyer, *A. Nickel*, J. Echeverria, M. Grisolia, C. Joachim, F. Moresco, G. Cuniberti, *A supramolecular motor at work: Rotation and translation of single atoms*, ACS Nano, doi: 10.1021/acsnano.5b03131

R. Ohmann, C. Toher, J. Meyer, *A. Nickel*, F. Moresco, and G. Cuniberti, *Quantum coherence of bulk electrons on metals revealed by scanning tunneling microscopy*, Physical Review B **89**, 205433 (2014)

H.-P. Jacquot de Rouville, H. Garbage, F. Ample, *A. Nickel*, J. Meyer, F. Moresco, C. Joachim, and G. Rapenne, *Synthesis and STM Imaging of Symmetric and Dissymmetric Ethynyl-Bridged Dimers of Boron-Subphthalocyanine Bowl-Shaped Nanowheels*, Chemistry- A European Journal **18**, 8925-8928 (2012)

J. Meyer, *A. Wadewitz*, Lokamani, C. Toher, R. Gresser, K. Leo, M. Riede, F. Moresco, and G. Cuniberti, *Molecules for organic electronics studied one by one*, Physical Chemistry - Chemical Physics **13**, 14421-14426 (2011)

Other Publications

F. Moresco, *A. Nickel*, R. Ohmann, J. Meyer, M. Grisolia, C. Joachim, G. Cuniberti, *Electron tunneling manipulation of self-assembled molecular nanostructures*, Enano Newsletters **28**, 5- 12 (2013)

Conferences

A. Nickel, J. Meyer, R. Ohmann, C. Joachim, G. Cuniberti, F. Moresco, *Switching single molecules by STM voltage pulses on the Si(100) surface*, Frühjahrstagung der DPG, Dresden, Germany, March 2014, *talk*

A. Nickel, R. Ohmann, J. Meyer, C. Joachim, G. Cuniberti, and F. Moresco, *Electrically inducedcontrolled manipulation of supramolecular structures*, International Conference on Nanoscience + Technology 2012, Paris, France, July 2012, *talk*

A. Nickel, R. Ohmann, J. Meyer, M. Grisola, C. Joachim, G. Cuniberti, and F. Moresco, *Pulse induced manipulation of supramolecular nanostructures*, Berlin Symposium on Surface Science, Berlin, Germany, September 2012, *poster*

A. Nickel, J. Meyer, R. Ohmann, G. Rapenne, H.-P. Jacquot, C. Joachim, G. Cuniberti, and F. Moresco, *STM measurements on subphthalocyanine nanowheels*, 493. Wilhelm und Else Heraeus Seminar on Latest Developements in Scanning Probe Techniques focused on Nanotechnology, Bad Honnef, Germany, December 2011, *poster*

A. Nickel, J. Meyer, R. Ohmann, G. Cuniberti, and F. Moresco, *STM investigation of 4-Acetyl-Biphenyl molecules on Au(111)*, 2nd Consortium meeting of the European project "Atomic scale and single molecule logic gate technologies" (AtMol), Krakow, Poland, October 2011, *talk*

A. Wadewitz, J. Meyer, F. Moresco, G. Rapenne, H.-P. Jacquot, C. Joachim, and G. Cuniberti, *First STM measurements on a new class of nanowheels*, Frühjahrstagung der DPG, Dresden, Germany, March 2011, *poster*

R. Ohmann, *A. Nickel*, J. Meyer, J. Echevarria, M. Grisolia, C. Joachim, G. Cuniberti, F. Moresco, *A supramolecular motor at work: Rotation and translation of single atoms*, Frühjahrstagung der DPG, Berlin, Germany, March 2015

J. Krüger, F. Eisenhut, J. Meyer, *A. Nickel*, G. Cuniberti, and F. Moresco, *STM study of molecular n-dopants for organic electronics*, Frühjahrstagung der DPG, Berlin, Germany, March 2015

R. Ohmann, *A. Nickel*, J. Meyer, F. Moresco, G. Cuniberti, *Atomic Force Microscopy: The qPlus sensor applied to molecules on metal surfaces*, Frühjahrstagung der DPG, Dresden, Germany, March 2014

J. Meyer, *A. Nickel*, R. Ohmann, Lokamani, C. Toher, D. Ryndyk, F. Moresco, G. Cuniberti, *Interaction of a Kondo impurity with its molecular ligand*, Frühjahrstagung der DPG, Dresden, Germany, March 2014

J. Meyer, *A. Nickel*, R. Ohmann, C. Toher, F. Moresco, G. Cuniberti, *Nanostructure formation of hexphenylnitril*, Frühjahrstagung der DPG, Regensburg, Germany, March 2013

R. Ohmann, C. Toher, J. Meyer, *A. Nickel*, F. Moresco, G. Cuniberti, *Electronic structure of Ag(100) revisited by STS*, Frühjahrstagung der DPG, Regensburg, Germany, March 2013

Lokamani, C. Toher, J. Meyer, *A. Nickel*, R. Ohmann, F. Moresco, G. Cuniberti, *Investigations of PEEB adsorbed on metallic surfaces*, Frühjahrstagung der DPG, Regensburg, Germany, March 2013

R. Ohmann, J. Meyer, *A. Nickel*, C. Toher, F. Moresco, and G. Cuniberti, *Spatially mapping the Kondo resonance across a magnetic molecule by scanning tunneling spectroscopy*, European Conference on Surface Science, Edinburgh, Great Britain, September 2012

R. Ohmann, L. Vitali, K. Kern, *A. Nickel*, J. Meyer, F. Moresco, and G. Cuniberti, *Imaging and manipulation of molecular orbitals on metal surfaces with scanning tunneling microscopy*, Workshop: Imaging and manipulating molecular orbitals, Berlin, Germany, September 2012

J. Meyer, *A. Nickel*, R. Ohmann, C. Toher, F. Moresco, and G. Cuniberti, *Spin crossover effect in single aza-BODIPY molecule*, Frühjahrstagung der DPG, Berlin, Germany, March 2012

C. Toher, J. Meyer, *A. Nickel*, R. Ohmann, F. Moresco, and G. Cuniberti, *Organometallic opto-electronically active magnetic molecules on metallic surfaces*, Frühjahrstagung der DPG, Berlin, Germany, March 2012

C. Toher, J. Meyer, *A. Nickel*, Lokamani, R. Ohmann, F. Moresco, and G. Cuniberti, *SPM studies of organic solar cell components*, 493. Wilhelm und Else Heraeus Seminar on Latest Developements in Scanning Probe Techniques focused on Nanotechnology, Bad Honnef, Germany, December 2011

J. Meyer, *A. Nickel*, R. Ohmann, C. Toher, Lokamani, G. Cuniberti, and F. Moresco, *STM-experiments on Aza-Bodipy*, 493. Wilhelm und Else Heraeus Seminar on Latest Developements in Scanning Probe Techniques focused on Nanotechnology, Bad Honnef, Germany,

December 2011

J. Meyer, *A. Wadewitz*, C. Toher, Lokamani, F. Moresco, and G. Cuniberti, *STM-investigations on aza-BODIPYs at low temperatures*, Frühjahrstagung der DPG, Dresden, Germany, March 2011

Lokamani, C. Toher, J. Meyer, *A. Wadewitz*, F. Moresco, and G. Cuniberti, *Investigations of Aza-Bodipy adsorped on metallic surfaces*, Frühjahrstagung der DPG, Dresden, Germany, March 2011

C. Toher, J. Meyer, Lokamani, *A. Wadewitz*, F. Moresco, and G. Cuniberti, *Opto-electronically active block copolymers on metallic surfaces*, Frühjahrstagung der DPG, Dresden, Germany, March 2011

J. Meyer, *A. Wadewitz*, C. Toher, F. Moresco, and G. Cuniberti, *STM-experiments on Aza-Bodipy*, 5th International Meeting on molecular electronics, Grenoble, France, December 2010

Bibliography

[1] International Technology Roadmap for Semiconductors, *Progress Integration, Devices, and Structures Summary*, 2013.

[2] B. D. Sierawski et al., *Muon-Induced Single Event Upsets in Deep-Submicron Technology*, IEEE Transactions on Nuclear Science **57**, 3273 (2010).

[3] D. G. Feitelson, *Optical Computing: A Survey for Computer Scientists*, MIT Press, Cambridge, MA, 1988.

[4] J. Stolze and D. Suter, *Quantum Computing: A short Course from Theory to Experiment*, Physics Textbooks, Wiley-VCH, Weinheim, 2004.

[5] A. Aviram and M. A. Ratner, *Molecular rectifiers*, Chemical Physics Letters **29**, 277 (1974).

[6] C. Celle et al., *Self-assembled monolayers for electrode fabrication and efficient threshold voltage control of organic transistors with amorphous semiconductor layer*, Organic Electronics **10**, 119 (2009).

[7] A.-S. Hallbäck, B. Poelsema, and H. J. W. Zandvliet, *Rectification behaviour of molecular layers on Si(111)*, Solid State Communications **141**, 645 (2007).

[8] C. Joachim, J. K. Gimzewski, and A. Aviram, *Electronics using hybrid-molecular and mono-molecular devices*, Nature **408**, 541 (2000).

[9] F. Ample, I. Duchemin, M. Hliwa, and C. Joachim, *Single OR molecule and OR atomic circuit logic gates interconnected on a Si (100) H surface*, Journal of Physics: Condensed Matter **23**, 125303 (2011).

[10] W.-H. Soe et al., *Manipulating molecular quantum states with classical metal atom inputs: demonstration of a single molecule NOR logic gate*, ACS Nano **5**, 1436 (2011).

[11] Y. Sugimoto et al., *Chemical identification of individual surface atoms by atomic force microscopy*, Nature **446**, 64 (2007).

[12] L. Gross, F. Mohn, N. Moll, P. Liljeroth, and G. Meyer, *The chemical structure of a molecule resolved by atomic force microscopy*, Science **325**, 1110 (2009).

[13] L. Gross et al., *High-resolution molecular orbital imaging using a p-wave STM tip*, Physical Review Letters **107**, 086101 (2011).

[14] M. A. Reed, C. Zhou, C. J. Muller, T. P. Burgin, and J. M. Tour, *Conductance of a molecular junction*, Science **278**, 252 (1997).

[15] S. H. Choi, B. S. Kim, and C. D. Frisbie, *Electrical resistance of long conjugated molecular wires*, Science **320**, 1482 (2008).

[16] L. Lafferentz et al., *Conductance of a single conjugated polymer as a continuous function of its length*, Science **323**, 1193 (2009).

[17] W. Wang et al., *Manipulating Localized Molecular Orbitals by Single-Atom Contacts*, Physical Review Letters **105**, 126801 (2010).

[18] C. Joachim, J. K. Gimzewski, and H. Tang, *Physical principles of the single-C 60 transistor effect*, Physical Review B **53**, 16407 (1998).

[19] F. Ample and C. Joachim, *The chemisorption of polyaromatic hydrocarbons on Si (100) H dangling bonds*, Surface Science **602**, 1563 (2008).

[20] Y. Wada, T. Uda, M. Lutwyche, S. Kondo, and S. Heike, *A proposal of nanoscale devices based on atom/molecule switching*, Journal of Applied Physics **74**, 7321 (1993).

[21] H. Kawai et al., *Dangling-bond logic gates on a Si(100)-(2x1)-H surface*, Journal of Physics: Condensed Matter **24**, 095011 (2012).

[22] H. Kawai, Y. K. Yeo, and M. Saeys, *Conductance decay of a surface hydrogen tunneling junction fabricated along a Si(001)- (2x1)-H atomic wire*, Physical Review B **81**, 195316 (2010).

[23] Y. Wada, *Proposal of atom/molecule switching devices*, Journal of Vacuum Science and Technology A **17**, 1399 (1999).

[24] L. Soukiassian, A. J. Mayne, M. Carbone, and G. Dujardin, *Atomic wire fabrication by STM induced hydrogen desorption*, Surface Science **528**, 121 (2003).

[25] W. Ye et al., *Scanning tunneling spectroscopy and density functional calculation of silicon dangling bonds on the Si(100)-2x1:H surface*, Surface Science **609**, 147 (2013).

[26] T. Hitosugi et al., *Scanning tunneling microscopy/spectroscopy of dangling-bond wires fabricated on the Si(100)-2x1-H surface*, Applied Surface Science **130**, 340 (1998).

[27] M. Kolmer et al., *Construction of atomic-scale logic gates on a surface of hydrogen passivated germanium*, Microelectronic Engineering **109**, 262 (2013).

[28] S. Hosaka et al., *Fabrication of nanostructures using scanning probe microscopes*, Journal of Vacuum Science and Technology B **13**, 2813 (1995).

[29] J.-H. Cho and L. Kleinman, *Nature of lattice distortion in one-dimensional dangling-bond wires on Si and C*, Physical Review B **66**, 235405 (2002).

[30] P. Doumergue, L. Pizzagalli, C. Joachim, A. Altibelli, and A. Baratoff, *Conductance of a finite missing hydrogen atomic line on Si(001)-(2 x 1)-H*, Physical Review B **59**, 15910 (1999).

[31] H. Raza, *Theoretical study of isolated dangling bonds, dangling bond wires, and dangling bond clusters on a H:Si(001)-(2x1)surface*, Physical Review B **76**, 045308 (2007).

[32] S. Watanabe, Y. A. Ono, T. Hashizume, and Y. Wada, *Theoretical study of atomic and electronic structures of atomic wires on an H-terminated Si(100)2x1 surface*, Physical Review B **54**, 17308 (1996).

[33] M. Lundstrom, *Fundamentals of Carrier Transport*, Cambridge University Press, Cambridge, 2nd Edition, 2000.

[34] S. Kirchhoff, *Ueber den Durchgang eines elektrischen Stromes durch eine Ebene, insbesondere durch eine kreisförmige*, Annalen der Physik **64**, 497 (1845).

[35] J. L. Pitters, L. Livadaru, M. B. Haider, and R. A. Wolkow, *Tunnel coupled dangling bond structures on hydrogen terminated silicon surfaces*, The Journal of Chemical Physics **134**, 064712 (2011).

[36] G. P. Lopinski, D. J. Moffatt, and R. A. Wolkow, *Benzene/Si (100): metastable chemisorption and binding state conversion*, Chemical Physics Letters **282**, 305 (1998).

[37] C. Joachim et al., *Multiple atomic scale solid surface interconnects for atom circuits and molecule logic gates*, Journal of Physics: Condensed Matter **22**, 084025 (2010).

[38] P. Gupta, V. L. Colvin, and S. M. George, *Hydrogen desorption kinetics from monohydride and dihydride species on silicon surfaces*, Physical Review B **37**, 8234 (1988).

[39] J. Yang, J. Deng, N. Chandrasekhar, and C. Joachim, *Ultrahigh vacuum scanning tunneling microscope manipulation of single gold nanoislands on MoS[sub 2] for constructing planar nanointerconnects*, Journal of Vacuum Science and Technology B **25**, 1694 (2007).

[40] E. W. Müller and T. T. Tsong, *Field ion microcopy / principles and applications*, American Elsevier Publishing, New York, 1969.

[41] M. d. Rezeq, J. Pitters, and R. A. Wolkow, *A Well Defined Electron Beam Source Produced by the Controlled Field Assisted Etchingof Metal Tips to < 1 nm Radius*, Journal of Scanning Probe Microscopy **2**, 1 (2007).

[42] M. H. T. Lwin et al., *Silicon on insulator nanoscale backside interconnects for atomic and molecular scale circuits*, Journal of Vacuum Science and Technology B **28**, 978 (2010).

[43] M. Kolmer et al., *Atomic scale fabrication of dangling bond structures on hydrogen passivated Si(001) wafers processed and nanopackaged in a clean room environment*, Applied Surface Science **288**, 83 (2014).

[44] *Brockhaus Enzyklopädie*, Bibliographisches Institut & F. A. Brockhaus AG, 2005.

[45] R. Young, J. Ward, and F. Scire, *The Topografiner: An Instrument for Measuring Surface Microtopography*, Review of Scientific Instruments **43**, 999 (1972).

[46] G. Binning, H. Rohrer, C. Gerber, and E. Weibel, *Surfaces studies by scanning tunneling microscopy*, Physical Review Letters **49**, 57 (1882).

[47] G. Binnig, H. Rohrer, C. Gerber, and E. Weibel, *7x7 Reconstruction on Si(111) Resolved in Real Space*, Physical Review Letters **50**, 120 (1983).

[48] Nobelprize.org, Press release: The 1986 nobel prize in physics, `http://www. nobelprize.org/nobel_prizes/physics/laureates/1986/press.html`.

[49] D. M. Eigler and E. K. Schweizer, *Positioning singe atoms with a scanning tunneling microscope*, Nature **344**, 524 (1990).

[50] L. Bartels, G. Meyer, and K.-H. Rieder, *Basic steps of lateral manipulation of single atoms and diatomic clusters with a scanning tunneling microscope tip*, Physical Review Letters **79**, 697 (1997).

[51] F. Moresco, *Manipulation of large molecules by low-temperature STM: model systems for molecular electronics*, Physics Reports **399**, 175 (2004).

[52] L. Gross et al., *Trapping and moving metal atoms with a six-leg molecule*, Nature Materials **4**, 892 (2005).

[53] G. Rapenne, *Synthesis of technomimetic molecules: towards rotation control in single-molecular machines and motors*, Organic & biomolecular chemistry **3**, 1165 (2005).

[54] C. Manzano et al., *Step-by-step rotation of a molecule-gear mounted on an atomic-scale axis*, Nature Materials **8**, 576 (2009).

[55] F. Chiaravalloti et al., *A rack-and-pinion device at the molecular scale*, Nature Materials **6**, 30 (2007).

[56] N. Koumura, R. W. Zijlstra, R. A. van Delden, N. Harada, and B. L. Feringa, *Light-driven monodirectional molecular rotor*, Nature **401**, 152 (1999).

[57] G. S. Kottas, L. I. Clarke, D. Horinek, and J. Michl, *Artificial Molecular Rotors*, Chemical Reviews **105**, 1281 (2005).

[58] T. Kudernac et al., *Electrically driven directional motion of a four-wheeled molecule on a metal surface*, Nature **479**, 208 (2011).

[59] L. Grill et al., *Imaging of a molecular wheelbarrow by scanning tunneling microscopy*, Surface Science **584**, L153 (2005).

[60] G. Vives and J. M. Tour, *Synthesis of Single-Molecule Nanocars*, Accounts of Chemical Research **42**, 473 (2009).

[61] A. A. Tseng, K. Chen, C. D. Chen, and K. J. Ma, *Electron beam lithography in nanoscale fabrication: recent development*, IEEE Transactions on Electronics Packaging Manufacturing **26**, 141 (2003).

[62] J. V. Barth, G. Costantini, and K. Kern, *Engineering atomic and molecular nanostructures at surfaces*, Nature **437**, 671 (2005).

[63] U. Schlickum et al., *Metal-Organic Honeycomb Nanomeshes with Tunable Cavity Size*, Nano Letters **7**, 3813 (2007).

[64] M. Stöhr et al., *Controlling Molecular self assembly in two dimensions: the concentration dependance of thermally induced 2D aggregation of molecules on a metal surface*, Angewandte Chemie - International Edition **44**, 7394 (2005).

[65] J. I. Urgel, D. Écija, W. Auwärter, and J. V. Barth, *Controlled Manipulation of Gadolinium-Coordinated Supramolecules by Low-Temperature Scanning Tunneling Microscopy*, Nano Letters **14**, 1369 (2014).

[66] A. Nickel et al., *Moving Nanostructures: Pulse-Induced Positioning of Supramolecular Assemblies*, ACS Nano **7**, 191 (2012).

[67] R. Wiesendanger, *Scanning Probe Microscopy and Spectroscopy - Methods and Applications*, Cambridge University Press, 1994.

[68] J. Bardeen, *Tunneling from a many-particle point of view*, Physical Review Letters **6**, 57 (1961).

[69] J. Tersoff and D. R. Hamann, *Theory of the scanning tunneling microscope*, Physical Review B **31**, 805 (1985).

[70] P. Sautet and C. Joachim, *Calculation of the benzene on rhodium STM images*, Chemical Physics Letters **185**, 23 (1991).

[71] S.-W. W. Hla, *Scanning tunneling microscopy single atom/molecule manipulation and its application to nanoscience and technology*, Journal of Vacuum Science and Technology B **23**, 1351 (2005).

[72] U. Dürig, O. Züger, and D. W. Pohl, *Observation of Metallic Adhesion Using the Scanning Tunneling Microscope*, Physical Review Letters **65**, 349 (1990).

[73] B. N. J. Persson, *Inelastic vacuum tunneling*, Physica Scripta **38**, 282 (1988).

[74] B. C. Stipe et al., *Single-molecule dissociation by tunneling electrons*, Physical Review Letters **78**, 4410 (1997).

[75] S. Tikhodeev and H. Ueba, *How Vibrationally Assisted Tunneling with STM Affects the Motions and Reactions of Single Adsorbates*, Physical Review Letters **102**, 246101 (2009).

[76] K. Besocke, *An Easily Operable Scanning Tunneling Microscope*, Surface Science **181**, 145 (1987).

[77] H. Ibach and H. Lüth, *Solid-State Physics*, Springer, Berlin Heidelberg, 4 Edition, 2009.

[78] J. V. Barth, H. Brune, G. Ertl, and R. J. Behm, *Scanning tunneling microscopy observations on the reconstructed Au (111) surface: Atomic structure, long-range superstructure, rotational domains, and surface defects*, Physical Review B **42**, 9307 (1990).

[79] Y. Hasegawa and P. Avouris, *Manipulation of the reconstruction of the Au (111) surface with the STM*, Science **258**, 1763 (1992).

[80] J. A. Stroscio and D. M. Eigler, *Atomic and Molecular Manipulation with the Scanning Tunneling Microscope*, Science **254**, 1319 (1991).

[81] M. Parschau, H. J. Hug, K.-H. Rieder, and K.-H. Ernst, *Hopping, turning and flipping of single molecules during lateral manipulation with a scanning tunneling microscope*, Surface and Interface Analysis **42**, 1629 (2010).

[82] D. M. Eigler, C. P. Lutz, and W. E. Rudge, *An atomic switch realized with the scanning tunnelling microscope*, Nature **352**, 600 (1991).

[83] L. Bartels, G. Meyer, and K.-H. Rieder, *Controlled vertical manipulation of single CO molecules with the scanning tunneling microscope: A route to chemical contrast*, Applied Physics Letters **71**, 213 (1997).

[84] D. Keeling et al., *Bond Breaking Coupled with Translation in Rolling of Covalently Bound Molecules*, Physical Review Letters **94**, 146104 (2005).

[85] G. Dujardin et al., *Vertical manipulation of individual atoms by a direct STM tip-surface contact on Ge(111)*, Physical Review Letters **80**, 3085 (1998).

[86] J. Repp, G. Meyer, S. Paavilainen, F. E. Olsson, and M. Persson, *Imaging bond formation between a gold atom and pentacene on an insulating surface*, Science **312**, 1196 (2006).

[87] Y.-Q. Xu et al., *Electric Field Assisted Hopping of tert-Butylamine on Cu (111) Surface*, Acta Physico - Chimica Sinica **26**, 2686 (2010).

[88] T. Sonnleitner, I. Swart, N. Pavliček, A. Pöllmann, and J. Repp, *Molecular Symmetry Governs Surface Diffusion*, Physical Review Letters **107**, 186103 (2011).

[89] I. Swart, T. Sonnleitner, J. Niedenführ, and J. Repp, *Controlled lateral manipulation of molecules on insulating films by STM*, Nano Letters **12**, 1070 (2012).

[90] T. Komeda, Y. Kim, M. Kawai, B. N. J. Persson, and H. Ueba, *Lateral Hopping of Molecules Induced by Excitation of Internal Vibration Mode*, Science **295**, 2055 (2002).

[91] M. Böhringer, K. Morgenstern, W.-D. Schneider, and R. Berndt, *Separation of a Racemic Mixture of Two-Dimensional Molecular Clusters by Scanning Tunneling Microscopy*, Angewandte Chemie - International Edition **38**, 821 (1999).

[92] F. Vidal et al., *Chiral Phase Transition in Two-Dimensional Supramolecular Assemblies of Prochiral Molecules*, Journal of the American Chemical Society **127**, 10101 (2005).

[93] S. Horowitz and R. C. Trievel, *Carbon-Oxygen Hydrogen Bonding in Biological Structure and Function*, Journal of Biological Chemistry **287**, 41576 (2012).

[94] S. J. Knak Jensen, T.-H. Tang, and I. G. Csizmadia, *Hydrogen-Bonding Ability of a Methyl Group*, The Journal of Physical Chemistry A **107**, 8975 (2003).

[95] J. Bernstein, R. E. Davis, L. Shimoni, and N. L. Chang, *Patterns in Hydrogen Bonding: Functionality and Graph Set Analysis in Crystals*, Angewandte Chemie-International Edition English **34**, 1555 (1995).

[96] J. V. Barth et al., *Building Supramolecular Nanostructures at Surfaces by Hydrogen Bonding*, Angewandte Chemie - International Edition **39**, 1230 (2000).

[97] D. Kühne et al., *Rotational and constitutional dynamics of caged supramolecules*, Proceedings of the National Academy of Sciences USA **107**, 21332 (2010).

[98] H. L. Tierney et al., *Experimental demonstration of a single-molecule electric motor*, Nature Nanotechnology **6**, 625 (2011).

[99] R. D. Astumian, *Thermodynamics and kinetics of a Brownian motor*, Science **276**, 917 (1997).

[100] B. C. Stipe, M. A. Rezaei, and W. Ho, *Inducing and Viewing the Rotational Motion of a Single Molecule*, Science **279**, 1907 (1998).

[101] W.-H. Soe, C. Manzano, A. De Sarkar, N. Chandrasekhar, and C. Joachim, *Direct observation of molecular orbitals of pentacene physisorbed on Au (111) by scanning tunneling microscope*, Physical Review Letters **102**, 176102 (2009).

[102] M. Ohara, Y. Kim, and M. Kawai, *Electric field response of a vibrationally excited molecule in an STM junction*, Physical Review B **78**, 201405 (2008).

[103] R. E. Schlier and H. E. Farnsworth, *Structure and Adsorption Characteristics of Clean Surfaces of Germanium and Silicon*, The Journal of Chemical Physics **30**, 917 (1959).

[104] K. Takayanagi, Y. Tanishiro, M. Takahashi, and S. Takahashi, *Structural analysis of Si(111)-7X7 by UHV-transmission electron diffraction and microscopy*, Journal of Vacuum Science and Technology A **3**, 1502 (1985).

[105] R. M. Tromp, R. J. Hamers, and J. E. Demuth, *Si(001) Dimer Structure Observed with Scanning Tunneling Microscopy*, Physical Review Letters **55**, 1303 (1985).

[106] M. B. Haider et al., *Controlled coupling and occupation of silicon atomic quantum dots at room temperature*, Physical Review Letters **102**, 046805 (2009).

[107] W.-H. Soe et al., *Demonstration of a NOR logic gate using a single molecule and two surface gold atoms to encode the logical input*, Physical Review B **83**, 155443 (2011).

[108] D. J. Chadi, *Atomic and Electronic Structures of Reconstructed Si(100) Surfaces*, Physical Review Letters **43**, 43 (1979).

[109] C. Manzano, W.-H. Soe, H. Kawai, M. Saeys, and C. Joachim, *Origin of the apparent (2x 1) topography of the Si (100)-c (4x2) surface observed in low-temperature STM images*, Physical Review B **83**, 201302 (2011).

[110] R. M. Tromp, R. J. Hamers, and J. E. Demuth, *Quantum States and Atomic-Structure of Silicon Surfaces*, Science **234**, 304 (1986).

[111] R. A. Wolkow, *Direct Observation of an Increase in Buckled Dimers on Si(001) at Low-Temperature*, Physical Review Letters **68**, 2636 (1992).

[112] J. J. Boland, *Scanning tunneling microscopy of the interaction of hydrogen with silicon surfaces*, Advances in Physics **42**, 129 (1993).

[113] Institute of Electronic Materials Technology, `http://www.itme.edu.pl/products-642.html`, 133 Wolczynska, 01-919 Warsaw, Poland.

[114] B. S. Swartzentruber, Y. W. Mo, M. B. Webb, and M. G. Lagally, *Scanning tunneling microscopy studies of structural disorder and steps on Si surfaces*, Journal of Vacuum Science and Technology A **7**, 2901 (1989).

[115] J. A. Kubby and J. J. Boland, *Scanning tunneling microscopy of semiconductor surfaces*, Surface Science Reports **26**, 61 (1996).

[116] R. J. Hamers and U. K. Köhler, *Determination of the local electronic structure of atomic-sized defects on Si (001) by tunneling spectroscopy*, Journal of Vacuum Science and Technology A **7**, 2854 (1989).

[117] J. A. Stroscio, R. M. Feenstra, and A. P. Fein, *Electronic Structure of the Si(111) 2x1 Surface by Scanning Tunneling Microscopy*, Physical Review Letters **57**, 2579 (1986).

[118] M. Z. Hossain, H. S. Kato, and M. Kawai, *Self-Directed Chain Reaction by small Ketones with the Dangling Bond Site on the Si(100)-(2x1)-H Surface: Acetophenone, A Unique Example*, Journal of the American Chemical Society **130**, 11518 (2008).

[119] S. R. Schofield et al., *Phenyl Attachment to Si (001) via STM Manipulation of Acetophenone*, The Journal of Physical Chemistry C **117**, 5736 (2013).

[120] H. Mehdipour, *Single-Hydrogen Dissociation Paths for Upright and Flat Acetophenone Adsorbates on the Si(001) Surface*, Journal of Physical Chemistry C **118**, 23682 (2014).

[121] V. A. Ukraintsev and J. T. Yates, *The role of nickel in Si(001) roughening*, Surface Science **346**, 31 (1996).

[122] P. Hohenberg and W. Kohn, *Inhomogeneous Electron Gas*, Physical Review **136**, B864 (1964).

[123] W. Kohn and L. J. Sham, *Self-Consistent Equations Including Exchange and Correlation Effects*, Physical Review **140**, A1133 (1965).

[124] S. N. Patitsas, G. P. Lopinski, O. Hul'ko, D. J. Moffatt, and R. A. Wolkow, *Current-induced organic molecule-silicon bond breaking: consequences for molecular devices*, Surface Science **457**, L425 (2000).

[125] G. Henkelman, B. P. Uberuaga, and H. Jónsson, *A climbing image nudged elastic band method for finding saddle points and minimum energy paths*, The Journal of Chemical Physics **113**, 9901 (2000).

[126] P. A. Sloan and R. E. Palmer, *Two-electron dissociation of single molecules by atomic manipulation at room temperature*, Nature **434**, 367 (2005).

[127] T. Komeda, Y. Kim, Y. Fujita, Y. Sainoo, and M. Kawai, *Local chemical reaction of benzene on Cu(110) via STM-induced excitation*, The Journal of Chemical Physics **120**, 5347 (2004).

[128] H. J. Lee and W. Ho, *Single-bond formation and characterization with a scanning tunneling microscope*, Science **286**, 1719 (1999).

[129] S.-W. W. Hla, L. Bartels, G. Meyer, and K.-H. Rieder, *Inducing all steps of a chemical reaction with the scanning tunneling microscope tip: towards single molecule engineering*, Physical Review Letters **85**, 2777 (2000).

[130] C. Joachim, *The driving power of the quantum superposition principle for molecule-machines*, Journal of Physics: Condensed Matter **18**, S1935 (2006).

[131] A. Carella, J.-P. Launay, R. Poteau, and G. Rapenne, *Synthesis and Reactivity of [Penta (4-halogenophenyl) cyclopentadienyl][hydrotris (indazolyl) borato] ruthenium (II) Complexes: Rotation-Induced Fosbury Flop in an Organometallic Molecular Turnstile*, Chemistry - A European Journal **14**, 8147 (2008).

[132] E. R. Kay, D. A. Leigh, and F. Zerbetto, *Synthetic Molecular Motors and Mechanical Machines*, Angewandte Chemie - International Edition **46**, 72 (2007).

[133] G. Vives, H.-P. J. de Rouville, A. Carella, J.-P. Launay, and G. Rapenne, *Prototypes of molecular motors based on star-shaped organometallic ruthenium complexes*, Chemical Society Reviews **38**, 1551 (2009).

[134] L. Grill et al., *Rolling a single molecular wheel at the atomic scale*, Nature Nanotechnology **2**, 95 (2007).

[135] G. Rapenne and G. Jimenez-Bueno, *Molecular machines: synthesis and characterization of two prototypes of molecular wheelbarrows*, Tetrahedron **63**, 7018 (2007).

[136] G. Vives, J. Kang, K. F. Kelly, and J. M. Tour, *Molecular machinery: synthesis of a "nanodragster"*, Organic Letters **11**, 5602 (2009).

[137] F. Moresco et al., *Recording intramolecular mechanics during the manipulation of a large molecule*, Physical Review Letters **87**, 088302 (2001).

[138] M. Alemani et al., *Recording the intramolecular deformation of a 4-legs molecule during its STM manipulation on a Cu (211) surface*, Chemical Physics Letters **402**, 180 (2005).

[139] C. Joachim, H. Tang, F. Moresco, G. Rapenne, and G. Meyer, *The design of a nanoscale molecular barrow*, Nanotechnology **13**, 330 (2002).

[140] F. Ample and C. Joachim, *A semi-empirical study of polyacene molecules adsorbed on a Cu(110) surface*, Surface Science **600**, 3243 (2006).

[141] H.-P. Jacquot de Rouville et al., *Synthesis and STM Imaging of Symmetric and Dissymmetric Ethynyl-Bridged Dimers of Boron–Subphthalocyanine Bowl-Shaped Nanowheels*, Chemistry - A European Journal **18**, 8925 (2012).

[142] N. Jiang et al., *Polymorphism and chiral expression in two-dimensional subphthalocyanine crystals on Au(111)*, Physical Chemistry Chemical Physics **12**, 1318 (2010).

Acknowledgements